Use of mouse models to establish genotype-phenotype correlations in Williams-Beuren syndrome

Maria Segura Puimedon

DOCTORAL THESIS UPF / 2012

THESIS SUPERVISORS

Dr. Maria Victoria Campuzano Uceda

Prof. Luis Alberto Pérez Jurado

Departament de Ciències Experimentals i de la Salut

UNIVERSITAT POMPEU FABRA

Science is an imaginative adventure of the mind seeking truth in a world of mystery.

Sir Cyril Herman Hinshelwood

Als meus pares,

al Toni i a l'Enric

ACKNOWLEDGEMENTS

Durant els anys de la tesi he compartit moments amb persones que m'han ensenyat a ser millor persona i espero que millor científica i, sense l'esforç i la contribució de les quals aquest capítol que ara arriba a la fi no hauria estat possible. Per aquest motiu, us vull agrair a tots la vostra aportació.

A la Mariví per haver-me acceptat primer per les pràctiques de 5è de carrera i després com a estudiant de doctorat. Per haver estat sempre al despatx del costat per ensenyar-me i orientar-me, contestar preguntes i discutir resultats.

Al Luis també per haver-me acceptat al laboratori, per la supervisió, per les idees i els consells.

A totes les persones que són o han passat pel laboratori de genètica durant aquests anys: Ivon, Raquel, Olaya, Benja, Cris, Anna, Marco, Andreu, Tina, Marta, Débora, Clara, Aïda, Gaby, Verena, Armand, Eva, Thais, Judith... Pels moments compartits al laboratori o als sopars de la Paradeta!

A la Ivon per les nostres xerrades teatrals i musicals, per estar sempre disponible per respondre les preguntes dels predocs.

A la Raquel per l'alegria que aporta al laboratori, per estar sempre allà per qualsevol cosa que li demanes. Pels viatges en cotxe.

A la Olaya i al Benja per ser grans companys, tot i que ara s'hagin canviat al "lado oscuro".

A la Cris per les discussions de l'hora de dinar i per convidar-nos a un gran cap de setmana a Segovia.

A la Verena per ser una gran companya de projecte als inicis, per totes les extraccions de DNA compartides.

A la Tina per ser la meva companya de projecte a la part final, per les rialles tot endreçant mostres al -80ºC.

A l'Aïda per la seva visió sempre positiva de les coses, també pels moments compartits i les sortides.

A la Clara per haver compartit un camí comú, per SEAGen, per les quantis, per les nostres xerrades abans d'anar a dormir.

A la Gaby per tantes hores compartides, al bus, al màster, a Vall d'Hebrón, a la taula del costat, al bàsquet i al volley. Per aguantar les classes de català.

Als qGenomics, el Manel, Lluís, el Xavi, la Sònia, la Cristina, la Mª Jesús. Perquè compartir el laboratori amb ells és un plaer i per deixar-me robar les pipetes i la centrífuga de tant en tant.

A l'Ignasi per la seva ajuda en la part de comportament.

Obrigada to all the Portugal people: Nuno, Ana, Carinha, Bárbara, Sonia, Joana, John, Shilan, Magda, Andreia, Ze Miguel... Especially to Nuno for accepting me and to Ana João for being a wonderful supervisor! Obrigada to all of you for helping me with the microscope and for all the jantares!

Als Gens Bojos pels entrenaments i els partidets a la platja. I per les nostres dues copes!

A la junta de SEAGen per totes les estones compartides que al final tenen el seu fruit. I a Magma per totes les reunions i Exporecerques compartides.

A l'Anna i el Xavi per l'amistat des de la facultat i als sopars del divendres per mantenir-nos al dia!

A tots els EMPEs, els de tota la vida i les noves incorporacions per tots els moments compartits al llarg dels anys per diferents punts de Catalunya, per sopars, dinars, concerts, atacs de riure, per ser sempre allà! En especial a les nenes, per tots els anys que portem aguantant-nos.

Al Toni per tot el que hem compartit a casa, a Puigcerdà i voltant pel món, per estar sempre disposat a ajudar-me en tot. Perquè et trobo a faltar. I a la Lenka, per ser una gran incorporació a la família.

Als meus pares, per ensenyar-me a ser bona persona, per ajudar-me i animar-me en tots els punts del camí, hagin estat bons o dolents. Pel seu amor incondicional.

I a l'Enric, per ser com ets, pel que compartim, per ser sempre amb mi, per entendre'm i ajudar-me en totes les facetes de la vida. Per les noves aventures. Per tot.

Gràcies!

ABSTRACT

Williams-Beuren syndrome (WBS) is a neurodevelopmental disorder caused by the common deletion of 26-28 contiguous genes in the 7q11.23 region, which poses difficulties to the establishment of genotype-phenotype correlations. The use of mouse models would broader the knowledge of the syndrome, the role of deleted genes, affected pathways and possible treatments. In this thesis project, several mouse models, tissues and cells have been used to define the phenotypes at different levels, the deregulated genes and pathways, and to discover modifying elements leading to novel treatments for the cardiovascular phenotype. In addition, a new binding motif has been described for *Gtf2i*, a deleted gene encoding a transcription factor with a major role in WBS, providing new target genes from deregulated pathways. The obtained results confirm the utility of mouse models for the study of WBS, becoming essential tools for unraveling the pathogenetic mechanism of the disease as well as new therapeutic options.

RESUM

La síndrome de Williams-Beuren és una malaltia del neurodesenvolupament causada per una deleció comú d'entre 26 i 28 gens contigus a la regió 7q11.23, dificultant enormement l'establiment de relacions genotip-fenotip. L'ús de models de ratolí pot augmentar el coneixement sobre la malaltia, el paper dels gens delecionats, les vies moleculars afectades i els futurs tractaments. En aquesta tesi, s'han usat diversos models de ratolí, les seves cèl·lules i teixits per tal de descriure i definir fenotips, gens i vies moleculars desregulades i per descobrir elements modificadors i nous tractaments. Per últim, s'ha definit un nou motiu d'unió i nous gens diana per *Gtf2i*, uns dels gens delecionats que codifica per un factor de transcripció amb un rol central en la síndrome. Els resultats obtinguts revelen el paper essencial dels models de ratolí per a l'estudi de la síndrome de Williams-Beuren, proporcionen noves opcions terapèutiques i defineixen nous gens i vies moleculars afectades que podrien suposar noves dianes terapèutiques.

PROLOGUE

The study of Williams-Beuren syndrome has been an active field of research since the discovery of this clinical entity five decades ago, and has attracted the attention of multiple groups for the characteristic combination of physical and cognitive abnormalities in these patients. Clinical and molecular investigations in human patients along with several mouse models have already established some genotype-phenotype correlations, but more knowledge is needed to better understand all the peculiarities of the syndrome.

The aim of this thesis project has been to contribute to the genotype-phenotype correlations and physiopathology of the syndrome through the use of mouse models, defining existent phenotypes and their relation with human symptoms. Deregulated genes and pathways were also studied and a new binding motif for a candidate gene was discovered.

The thesis is organized in several parts:

The introduction provides a general overview of the clinical features of the syndrome, the molecular causes, physiopathology and the current knowledge on genotype-phenotype correlations.

The articles define the main part of the thesis project presenting in detail the methodology and main results, organized in different chapters.

The discussion aims to integrate and interpret all the obtained results relating them to previous existing knowledge. The final part of the thesis includes the main conclusions of the project.

CONTENTS

LIST OF FIGURES

INTRODUCTION

CHAPTER 1

CHAPTER 2

CHAPTER 3

CHAPTER 4

CHAPTER 5

DISCUSSION

LIST OF TABLES

CHAPTER 1

CHAPTER 2

CHAPTER 3

CHAPTER 4

CHAPTER 5

INTRODUCTION

1. WILLIAMS-BEUREN SYNDROME CLINICAL DESCPRIPTION

Williams-Beuren syndrome (WBS, OMIM 194050) is a neurodevelopmental disorder with an incidence of 1/7500 newborns [1].

WBS was first described in clinical reports of children with infantile hypercalcemia, short stature, and variable congenital malformations [2]. Williams and Beuren published papers at the beginning of the 60's about a condition with supravalvular aortic stenosis, dysmorphic features and mental retardation [3-4]. In 1964, the characteristic behavioral phenotype of WBS was described associated with loquacity, anxiety and friendliness [5]. WBS produces affectation of several organs and systems and a wide range of phenotypic variability exists in patients, although they all show the characteristic facies (Figure 1).

Figure 1. Typical facial features of WBS in a 3-year-old boy. Broad brow, bitemporal narrowing, epicanthal folds, periorbital fullness, stellate iris pattern, strabismus, short nose with anteverted nares, full nasal tip, full cheeks, malar hypoplasia, long philtrum, full lips, small, widely spaced teeth, malocclusion, wide mouth, small jaw, and prominent ear lobes. From [6].

1.1. Infancy, growth and puberty

WBS infants present some common conditions in higher frequency, such as colic, feeding problems, gastroesophageal reflux, vomiting, chronic constipation and recurrent ear infections. They are hypotonic and have developmental delay [7]. Patients also present an abnormal pattern of growth, already in the prenatal stage where the growth deficiency is around 50-70%. Growth disturbance is maintained during infancy and childhood with 70% of patients present failure to thrive. Adults are in 70% of the cases

below the 3rd percentile for mid parental height [7]. Puberty typically occurs early and is associated with a briefer growth spurt, both in boys and girls [8].

1.2. Cardiovascular phenotype

The hallmark of WBS is the cardiovascular disease (CV). The prevalence of any CV is around 84%, males being more affected than females and many of them suffering from multiple CV findings. Supravalvular aortic stenosis (SVAS) is the most frequent symptom (70% of patients on average) (Figure 2), followed by pulmonary aortic stenosis (34% of the cases) [9]. Approximately 30% of individuals require surgical repair of SVAS, with a perioperative mortality rate of 3–7% [10]. If untreated, the resultant increase in arterial resistance leads to elevated left heart pressure, cardiac hypertrophy, and cardiac failure [11].

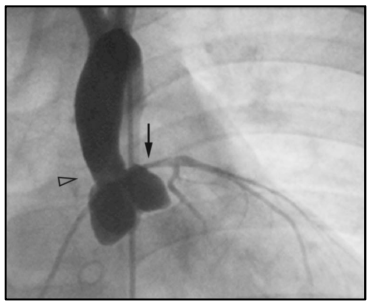

Figure 2. Aortogram in a 4-year-old with WBS. SVAS (arrowhead) and mild narrowing of the proximal left main coronary artery (arrow) are shown. From [12].

Systemic hypertension increases with age and is normally found in adults, but it can also appear during infancy. Studies have shown the presence of hypertension in 40-42% of WBS patients. After controlling for age, sex, and weight, the diagnosis of WBS adds approximately 10 mmHg to mean daytime and nighttime blood pressure. In one of the published studies, there is a significant association of hypertension and a history of infantile hypercalcemia [13-14].

Other less common findings are mitral valve disease, coarctation of the aorta, aortic hypoplasia, pulmonary valve disease and aortic valve disease [10, 12, 15-16]. Cerebral infarction has also been reported in a few cases [17].

A higher risk of sudden death exists in WBS, the frequency being 25 to 100 times higher than in age matched control population, with some associated

risk factors, such as the use of anesthesia, biventricular outflow obstruction, biventricular hypertrophy or coronary artery obstruction [18].

1.3. Endocrinological phenotype

WBS patients present several endocrine abnormalities: hypercalcemia, hypercalciuria, hypothyroidism, diabetes or glucose intolerance and early puberty [19].

Infantile hypercalcemia was historically important in the diagnosis of the syndrome, being one of the keys features that lead to diagnosis in the first reports. It is present in up to 50% of the cases and is particularly relevant during childhood, but the averaged prevalence is 15%. Hypercalciuria can appear in up to 30% of cases, sometimes related to hypercalcemia, but also isolated [6, 9].

Diabetes and glucose intolerance are remarkably high in WBS patients, appearing in 75-90% of studied patients on standard 2-h oral glucose tolerance test [19-20]. Thyroid abnormalities are present in an average of 10% of patients. Subclinical hypothyroidism is diagnosed in 15 to 30% of screened patients and is often accompanied by mild thyroid hypoplasia on ultrasonography [9, 21].

Regarding other endocrine issues, a study with adult male and female patients showed a high degree of osteopenia or osteoporosis, diagnosed in 60% of individuals [19].

1.4. Neurological and craniofacial phenotype

Neurological problems in adult WBS patients include coordination difficulties, hyperreflexia, hypertonia and signs of cerebellar dysfunction, such as ataxia and dysmetria, resulting in difficulties with balance, tool use and motor planning [22]. The joint and postural abnormalities in combination with the cerebellar dysfunction often lead to a stiff, awkward gait, especially in adults [21, 23]. In young patients, hypotonia is present in the majority of cases and cerebellar signs are also frequent, although ataxia in walking is rare. The number of mild extrapyramidal signs increase with age [24].

The neurological phenotype is here divided in cognitive profile, behavioral phenotype, structural and functional brain abnormalities and craniofacial phenotype.

1.4.1. Cognitive profile

WBS is characterized by mild to moderate intellectual disability, with an intelligence quotient (IQ) average of 55, ranging from 40 to 100 [25]. Many studies report a higher verbal than performance IQ [26]. WBS has a definite cognitive profile including strengths and weaknesses. The typical strength is the preservation of the language and the non-verbal reasoning, although language acquisition is delayed. Other relatively conserved areas are auditory rote memory, facial recognition and discrimination and social and interpersonal skills. The most important weakness is in visuospatial construction, understood as the ability to visualize an object (or picture) as a set of parts and construct a replica of the object from those elements. It is usually measured by either drawing or pattern construction (Figure 3) [25-26].

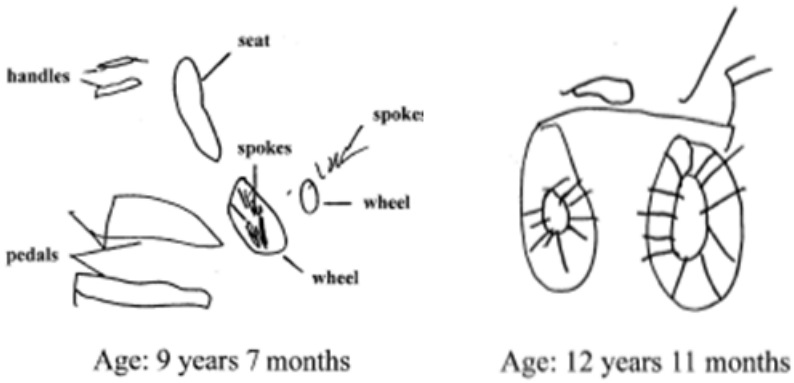

Figure 3. Two drawings of a bicycle by a girl with WBS. In both cases, the child was given a blank piece of paper and asked to draw the best bicycle that she could. From [27].

1.4.2. Behavioral phenotype

One of the most noticed characteristics of WBS patients is their distinct social-affective profile, showing high sociability, even with strangers, disinhibition, over-friendliness and strong empathy. However, up to 80% of patients present anxiety, preoccupations or obsessions, distractibility, and irritability. 50 to 60% of patients present generalized and anticipatory anxiety

and more than 90% show persistent and marked fears classified as specific phobias [19, 28-29]. Attention deficit–hyperactivity disorder is also a common psychiatric disorder present in WBS with 67% of children showing attention deficits [22].

1.4.3. Structural and functional brain abnormalities

Initial post-mortem neuroanatomical studies pointed to a reduced brain size in WBS patients [30-31]. Posterior studies using both volumetric and neuroimaging techniques have confirmed the total reduction in the volume of the intracranial content (11-13%) as a consequence of the reduction in white (20%) and grey matter and cerebrospinal fluid [32-34]. The posterior brain is more affected in WBS patients producing shape changes by the reduction in grey matter which is confined to the parietal and occipital lobes. Gyrification alterations with an increase in occipital cortex have also been reported [35-36].

Several magnetic resonance imaging studies have been performed in the past 15 years in different WBS population to dissect which are the brain anomalies presents in patients [37]. These studies differ in the population used, as well as in the methods and posterior analysis and, as a consequence, different or even contradictory results have been obtained. The most interesting and replicated findings are the reduction (20%) of the basal ganglia and brain stem, the relative preservation of cerebellum, superior temporal gyrus, prefrontal and orbitofrontal cortex and anterior cingulate [38-39].

Amygdala is the brain structure in charge of the coordination of behavioral, autonomic and endocrine responses. It is necessary for fear-motivated learning, coordinates the responses to stress and anxiety and has a modulatory effect on memories that evoke emotional content. It has been related to the social and emotional symptoms of WBS and has been the object of several reports. A relative increase in amygdala volume in WBS compared with healthy controls was reported, that likely reflects abnormal neurodevelopmental processes of midline brain structures [33]. WBS patients exposed to threatening, non-socially relevant and to socially irrelevant stimulus showed an increase in the amygdala reactivity [40]. Phobias are also increased in WBS which could also point to the role of the amygdala as a possible explanation for the high rate of non-social anxiety. Deficits in the structural integrity of prefrontal–amygdala white matter pathways have been

reported and might underlie the increased amygdala activity and extreme non-social fears observed in patients [41].

The orbitofrontal cortex has also been related with the social phenotype of patients. Several studies point to differences in volume of this area in patients, although others found no differences. It has been found that the orbitofrontal cortex does not interact with the amygdala in WBS but it does in controls through a negative correlation [38, 42-44]. A functionally abnormal orbitofrontal cortex is in good agreement with the social disinhibition and impairments in adjusting behavior according to social cues that are found in individuals with WBS [37].

The hippocampus is crucial for the processing of spatial navigation and integration of visual elements. It also controls corticosteroid production and is involved in declarative memory. Normally, ventral hippocampus is activated by faces and houses, but not in WBS patients, pointing to a primary hippocampal dysfunction. Reduction of the regional cerebral blood flow along with a depression of hippocampal energy metabolism and synaptic activity is also present. Finally, reduced NAA (cellular integrity marker and measure of synaptic abundance) is described, especially in the left ventricle of the hippocampus. Problems in hippocampus are hypothesized to arise as a consequence of a functional impairment of neurons in the region [37].

Recently, another brain region has been associated with WBS, the insula. This brain region is implicated in mediating social emotional response. A reduction in the grey matter volume of the insula as a whole has been found. The reduction is especially important in the dorsal anterior area of the insula, which is associated with affective-cognitive integration. However, an increase has been reported in the ventral anterior region of the insula, implicated in the social/emotional processes. The insula is also found to be functionally disturbed, in addition to having structural anomalies. A reduction in the regional cerebral blood flow is found in the dorsal anterior region and an increase in the ventral anterior [45].

Regarding the visual areas, histological general examinations have shown differences in neuronal cell size, coarseness, packing density, and organization in the primary visual cortex of patients, suggesting abnormal neuronal development and connectivity [31]. The visual system also shows hypofunction in the dorsal stream (occipito-parietal lobes), which is the one involved in the spatial processing in WBS patients [46].

1.4.4. Craniofacial phenotype

WBS subjects present a characteristic and distinctive facies described in childhood as cute or pixielike, with broad forehead, flat nasal bridge, short upturned nose, periorbital puffiness, long philtrum, strabismus, wide mouth, full cheeks, small jaw and delicate chin, whereas older patients have slightly coarse features, with full lips, wide smile, dental malocclusion, full nasal tip and long neck. [6]

Regarding the cranial phenotype, the largest differences are seen in the middle and posterior parts of the neurocranium, which is the relation between the development of brain tissue and the bones surrounding the brain. Results point to a reduced height of the neurocranium, a flattening of the parietal bone, and a greater prominence of the occipital bone. The frontal and occipital bones are considerably thicker compared to controls. Differences are found in young patients and are maintained through age [47]. A retrognathic or a micrognathic mandible and a deficient chin have been described in WBS patients [48].

1.5. Other frequent symptoms

Visual and audiologic phenotype: visual problems include strabismus, hyperopia, myopia, presbyopia, cataracts and chronic conjunctivitis [19]. Auditory testing has revealed the presence of hyperacusia in 90% of patients. Mild to moderate progressive sensorineural hearing loss is also present [49].

Dental anomalies: the most common problem in WBS regarding dental anomalies is malocclusion, occurring in 85% of the cases [6].

Gastrointestinal anomalies: 25%-40% of the patients present constipation since infancy as well as feeding problems. A common feature in adolescents and adults is chronic abdominal pain [6, 19, 21].

Muscoloskeletal anomalies: affect up to 80% of patients and include scoliosis, lordosis, radioulnar synostosis and feet problems.

Genitourinary anomalies: 50% of the subjects report urinary frequency anomalies as the most common problem and 30% of adults have recurrent

urinary tract infections. Other defects include bladder diverticule and nephrocalcinosis [6, 19].

Connective tissue: the connective tissue abnormalities include a hoarse/deep voice, hernias, bladder/bowel diverticulae, soft/lax skin, joint laxity or limitation [6].

2. WILLIAMS-BEUREN SYNDROME CRITICAL REGION (WBSCR)

2.1. Region Structure

WBSCR is located at the chromosomal band 7q11.23. The region structure was described in 2000 by two different groups reporting the existence of segmental duplications or low-copy repeat (LCRs) elements [50-51]. LCRs are defined as DNA fragments >1 kb in size and of >90% DNA sequence identity [52]. The region consists of three large region-specific LCRs: centromeric (cen), medial (med), and telomeric (tel), each with a size of approximately 320kb and composed of three differentiated blocks A, B, and C. The LCRs are flanking a single-copy gene region of 1.2Mb. Remarkably, the blocks of the centromeric and medial LCRs are in the same orientation (in tandem) but with different order, whereas the third segmental duplication lies more telomeric, with the same order as the centromeric LCR but in the opposite orientation (Figure 4) [53].

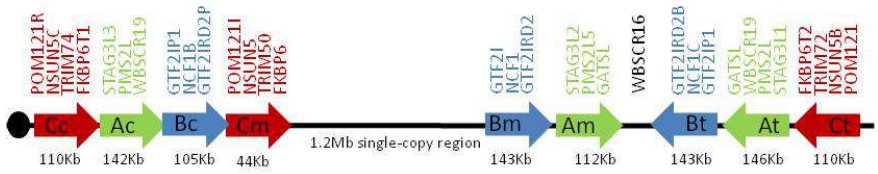

Figure 4. Schematic representation of the 7q11.23 region. The centromeric, middle, and telomeric LCRs are shown as colored arrows with their relative orientation to each other. Modified from [54].

2.2. Mutational mechanisms

2.2.1. Deletion

WBS is caused by a continuous heterozygous deletion containing 26-28 genes [51]. 90% of the patients present a ~1,55Mb deletion, and an atypical deletion of 1,84Mb is found in 5% of the cases (Figure 5) [55]. It is a *de novo* occurrence in most cases, although autosomal dominant transmission has been described in families [56]. Deletions occur regardless of the parental origin of the disease-transmitting chromosome. The deletion arises as a consequence of non allelic homologous recombination (NAHR) between the segmental duplications that flank the region, followed by unequal crossing over [57].

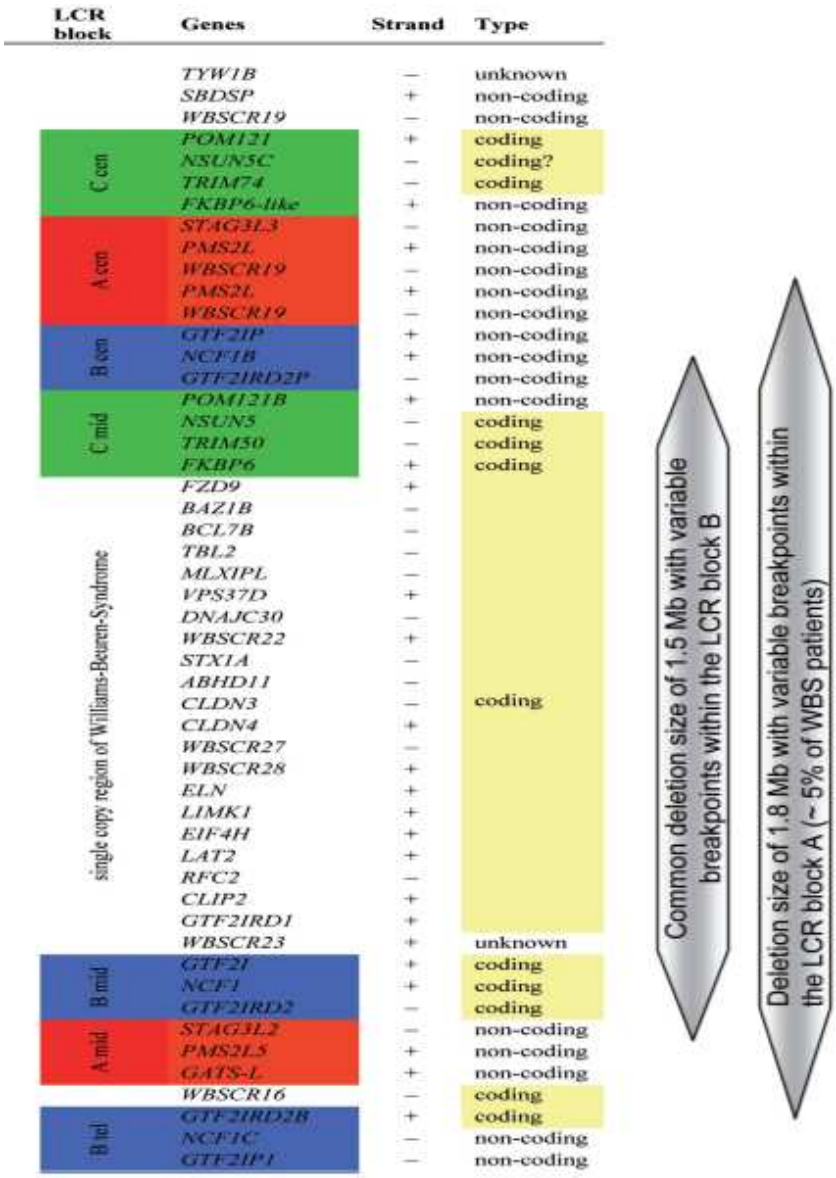

Figure 5. Summary of the genes within the WBS region. Displayed are the gene name, transcription direction and gene type. In vertical arrows, the common deletion size of ~1.5 Mb and the more rare deletion size of ~1.8 Mb in WBS patients are depicted. These NAHR events affect 26 coding genes that are invariably deleted. In addition to these 26 genes, *NCF1* and *GTF2IRD2* can be variable deleted depending on the NAHR locus within block B or A. Modified from [53].

The 1,5Mb deletion displays different possible breakpoints in the B cen and B med blocks, which have a sequence identity of 99,6%. In a study by Del Campo et al, four different breakpoints are defined, implicating different copy number for *NCF1* and *GTF2IRD2* genes (Figure 6) [58]:

- B1: Deletion proximal to the *NCF1* gene that does not affect the number of copies of *NCF1*.
- B2-B3: Deletion causing the loss of one copy of *NCF1*.
- B4: Inversion-mediated deletion with the loss of one copy of *NCF1*.

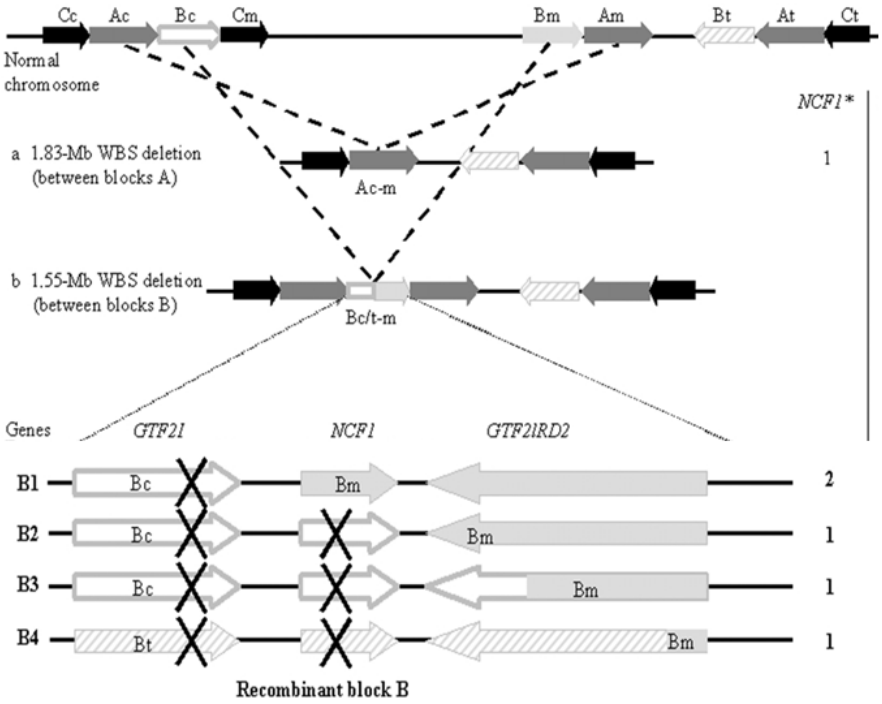

Figure 6. Schematic representation of the common deletions associated with WBS and the characterization of deletion breakpoints. *Top,* Scheme of the 7q11.23 genomic region, and the two common deletions. *Bottom,* Genomic structure and resulting recombinant block B in patients with the 1.55-Mb deletion. The resulting chromosomes, depending on deletion breakpoints, are shown with arrows corresponding to functional genes or pseudogenes (marked with an X) indicating their transcriptional direction. The numbers of functional copies of corresponding to each rearrangement are displayed at the right of the figure. The asterisk (*) indicates that the possibility of additional *NCF1* copies due to polymorphism is not shown in the figure. Modified from [58]

The presence of *NCF1* in the segmental duplications blocks predisposes to gene conversion events, so the number of functional copies of Ncf1 can increase up to 4 copies. Generally, the *NCF1* pseudogenes have a GT deletion at the beginning of exon 2 which predicts the lack of function of these copies. However, in an analysis by Bayés et at, 9% of the analyzed patients are detected to have more than two copies of the functional *NCF1* gene variant [57]. The reason for this difference in the copy number is the lack of the GT deletion in *NCF1* pseudogenes, as a gene conversion consequence, converting them into functional copies [59]. As a result, WBS patients have been identified carrying from 1 to 4 functional copies of *NCF1*.

The 1,8Mb deletion involves the A cen and A med block, which have an identity rate of 98,2%. This deletion includes the deletion of the whole B cen and B med blocks, with the loss of one of the functional copies of *NCF1* [53].

2.2.2. Duplication and triplication

The duplication for the WBS region was first described in 2005 associated to a severe-expressive language delay [60]. The duplication occurs between the B med and the B cen blocks, being the exact reciprocal of the common WBS deletion and pointing to the same mechanism of unequal meiotic recombination as a cause [53, 61]. Moreover, duplication patients can present attention deficit hyperactivity disorder, autism, mild mental retardation and no deficits in visuospatial integration, although the phenotype is variable. In 2009, a facial phenotype for the duplication syndrome was described including straight and neatly placed eyebrows, a high broad nose and thin upper lip. Some of the features are in direct contrast with the ones found in the deletion [62].

It was recently published the first case report of a patient with a triplication of the WBSCR with an underlying mechanism that is different from non-allelic homologous recombination [63]. The patient has developmental delay with a severe retardation in language and speech, behavioural problems, features of autism and mild dysmorphic features resembling the ones present in the duplication.

The symptoms in the triplication are at the severe end of the spectrum seen in duplication patients, pointing to a dosage-effect for the genes in the WBSCR.

2.2.3. Predisposing factors

A report published in 2001 identified a genomic polymorphism in families with WBS, consisting in a paracentric inversion of the critical region encompassing the 1,5Mb. Heterozygosity for the inversion may lead to unequal chromosome pairing in meiotic prophase and predispose to the WBS deletion. The inversion is found in 25-30% of the chromosome transmitting parents and only in 5% of the non-WBS population [64]. A parent with the inversion has a ~1/1750 chance of having a child with WBS, whereas without the inversion the risk is ~1/9500 [65].

Another predisposing factor to WBS are copy number variants. In 2008, Cuscó et al described the presence of a CNV in 4,4% of the WBS-transmitting parents who display a chromosome with large deletions of LCRs. The CNV is only in 1% of the non-transmitting progenitors [66].

3. GENOTYPE-PHENOTYPE CORRELATIONS IN WILLIAMS-BEUREN SYNDROME

First insights on the contribution of one or several genes to the WBS phenotype have been a consequence of the existence of patients with atypical, smaller deletions [67]. Secondly, information has arisen from the function of the deleted genes, which can give an idea of the consequences of its loss in the disease. In third place, several expression studies have been performed in order to identify which are the expression levels of some of the WBS genes in different tissues and determine which the targets of these genes are. Finally, the entire WBSCR is conserved at the chromosomal band 5G2 in mice, although in reverse orientation with respect to the centromere (Figure 7) [68].

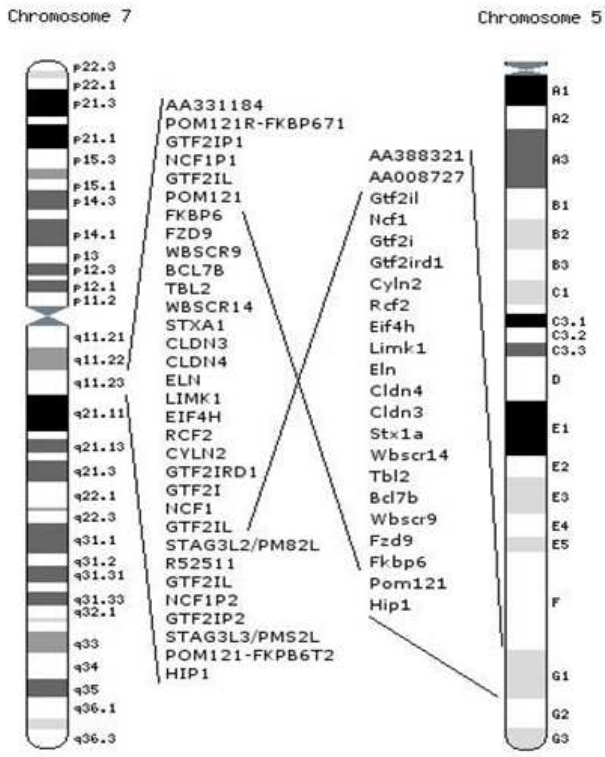

Figure 7. Comparative representation of the genomic organization of human chromosome 7q11.23 (**left**) and the syntenic region in mouse chromosome 5G1 (**right**). An inversion is observed in human with respect to mouse with the breakpoints located exactly at the sites of the LCR. Modified from [50].

Mouse also lacks the low copy repeats that predispose to the rearrangement in humans, due to an evolutionary inversion with chromosomal breakpoints at the sites where human LCR are located [50]. Animal models have proved to be useful tools to obtain a greater knowledge about genes and related pathways.

Traditionally and based in patients with smaller deletions, WBSCR distal deletion (DD) region in mice (from *LimK1* to *Trim50*) has been related with the medical history of WBS phenotype [54, 69], while the WBSCR proximal deletion (PD) region (from *Gtf2i* to *Limk1*) has been more correlated with neural-cognitive-behavioral phenotype (Figure 8) [70-72].

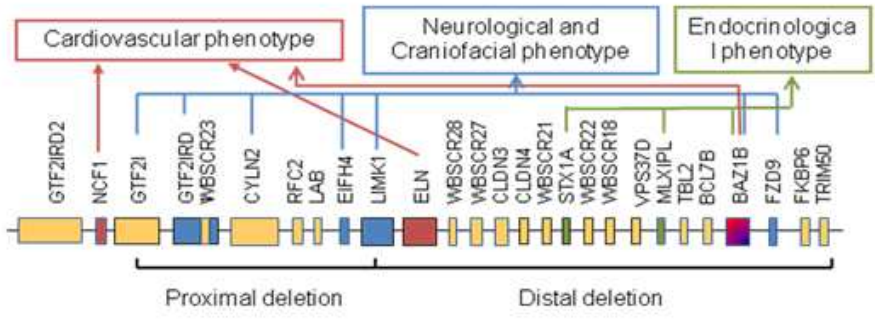

Figure 8. Genotype-phenotype correlations in WBS and candidate genes for phenotypes based on function and mouse models.

Partial mouse models point to some phenotypes, like reduced body weight and skull abnormalities, as being more severe in the distal and partial (D/P) model than in the partial ones. D/P model is the combination of both partial models and these results indicate a summation effect of the two half deletions. However, other phenotypes show a main contribution of a specific gene region. Neural anomalies and abnormal sociability phenotypes provide evidence for PD region gene(s) being the main contributor(s), in accordance with what is described in patients [73].

Sensory and motor function tests show that both DD and PD region genes appear to regulate sensorimotor processing in different ways, depending on the nature of the stimulus. Learning and memory tests indicate that DD animals have impaired learning and/or memory performance [73].

Cardiovascular phenotype has been studied in DD and D/P mice. DD mice present hypertension, but not the D/P mouse model. Aorta anterior and posterior wall motions are reduced in DD and D/P. When analyzing the aorta, stenosis is not observed in any of the mice but disorganized and fragmented elastin sheets are present in both models. However, none have an increase in the number of elastin sheets [74].

3.1. Cardiovascular phenotype

The cardiovascular phenotype of WBS has been specially associated with two genes, *ELN* and *NCF1*, but *BAZ1B* could also contribute to the cardiovascular phenotype.

3.1.1. Elastin (*ELN*)

Elastin was the first gene to be clearly associated with one of the symptoms of the disorder. Elastin hemizygosity in WBS was described in 1993 [75] and that same year a patient report was published showing a family with SVAS carrying a translocation that disrupted the elastin gene [76]. Elastin being the cause of SVAS and some connective abnormalities was confirmed, and several types of causing mutations leading to hemizygosity of the gene were identified [77].

Elastin is the principal component of the elastic fibers of the extracellular matrix of connective tissue throughout the body and has an essential function in the arterial morphogenesis [78]. This protein induces actin stress fiber organization, signals via a nonintegrin, heterotrimeric G-protein-coupled pathway and stabilizes the arterial structure by inducing a quiescent contractile state in vascular smooth muscle cells [79].

The mouse model for the elastin gene was created in 1998, achieving both the $Eln^{+/-}$ and $Eln^{-/-}$. $Eln^{-/-}$ mice die at postnatal day 4.5 due to the thickening and obliteration of the vascular lumen of the aorta. The change is caused by the subendothelial accumulation of arterial smooth muscle cells [78]. Regarding the $Eln^{+/-}$ mice, an increase in the number of lamellar units is observed, both in the ascending and descending aorta. The extensibility of the aorta is reduced in $Eln^{+/-}$ animals at elevated blood pressures [69]. Heterozygous mice are hypertensive from birth and have a moderate cardiac hypertrophy although they do not present SVAS [80].

3.1.2. Neutrophil Cytosolic Factor 1 (*NCF1*)

NCF1 is a gene present in the segmental duplications surrounding the WBS deleted area. This gene is variably deleted on WBS, as analyzed in the mutational mechanisms of WBS, depending on the breakpoints and gene conversion events [58].

NCF1 encodes p47phox, a cytosolic subunit of the NADPH (Nicotinamide Adenin Dinucleotide Phosphate) oxidase (NOX) complex (Figure 9). This complex is composed by proteins that transfer electrons across biological membranes. Their final function is the generation of reactive oxygen species (ROS), normally by transferring an electron from NADPH to oxygen, creating the superoxide product. The *Ncf1*$^{-/-}$ mouse model shows an undetectable ROS response, enhanced autoimmunity, arthritis and encephalomyelitis [81].

ROS are produced physiologically to maintain vascular integrity and vascular contraction-relaxation process. An increased activity of ROS leads to endothelial dysfunction, increased contractility, vascular smooth muscle cells growth and monocyte invasion, which are important factors in hypertensive damage. Several experiments, both in animal models and human patients, corroborate an important increase of ROS in hypertension. An increased activity of the NADPH complex has been detected in spontaneously hypertensive rats (SHR) producing higher amount of O_2^-. Interestingly, an increased expression of *Ncf1* in several vascular tissues has been reported in the same SHR rats, providing a link between the NADPH activity and the development of hypertension. Moreover, treatment of the rats with antioxidants like Ang II type-1 receptor blockers or NADPH oxidase inhibitors decreases ROS production and ameliorates hypertension [82-84].

Human essential hypertensive patients show an increase in ROS production and activation of the renin-angiotensin system, which could be the mediator of the process through the action of the NADPH oxidase complex [83].

NCF1 has been described as a protective factor in developing hypertension in WBS patients. Reduced AngII-mediated oxidative stress in the vasculature is the proposed mechanism behind this protective effect [58]. Patients with a sole copy of *NCF1* present a reduced expression and activity of the protein and, as a result, reduced activity of the NADPH complex producing lower oxidative stress and reducing the risk of developing hypertension. Decreased

p47phox protein, superoxide anion production, and protein nitrosylation levels are also observed in cell lines from hemizygous patients for *NCF1*.

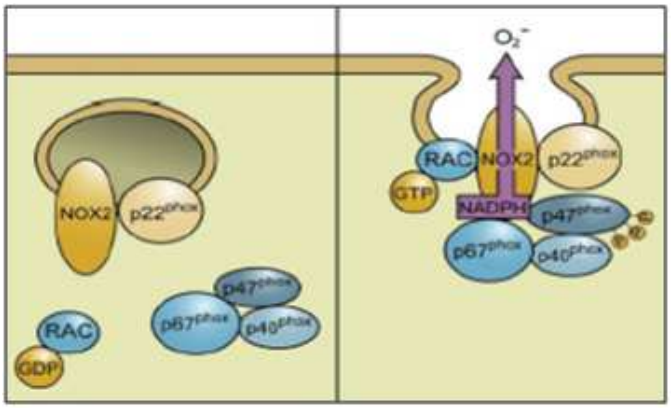

Figure 9. Assembly of the phagocyte NADPH oxidase NOX2. In resting neutrophil granulocytes, NOX2 and p22phox are in the membrane of intracellular vesicles. Upon activation, there is an exchange of GDP for GTP on RAC leading to activation. Phosphorylation of the cytosolic p47phox subunit leads to conformational changes allowing interaction with p22phox. The movement of p47phox brings p67phox and p40phox, to form the active NOX2 enzyme complex which fusions with the plasma membrane or the phagosomal membrane. The active enzyme complex transports electrons from cytoplasmic NADPH to extracellular or phagosomal oxygen to generate superoxide. Obtained from [82].

3.1.3. Bromodomain Adjacent to Zinc Finger Domain, 1B *(BAZ1B)*

BAZ1B is a component of the ATP-dependent chromatin remodelling complexes *WSTF* including the nucleosome assembly complex (WINAC). It is involved in many functions such as transcription, replication and chromatin maintenance. Haploinsufficiency of this gene possibly leads to an increased chromosomal condensation and an overall impaired transcriptional activity of cells producing diverse abnormalities, like abnormal vitamin D metabolism and hypercalcaemia. It is also important in the developing heart, and is required for normal function of cardiac transcriptional regulators [53, 85-86].

Baz1b mouse model shows cardiovascular abnormalities in 10% of the *Baz1b*$^{+/-}$ and in all knockout animals, leading in the last case to neonatal death. Some of the detected defects are dilation of ventricles, ventricular

septal defects, heart hypertrophy or infantile coarctation of the aorta, reminding the cardiac defects found in WBS. Through gene expression studies, *Baz1b* was determined to be crucial for normal gene cascades in developing heart [87].

3.1.4. Expression Arrays

Array studies have also given some insights in the genotype-phenotype correlations of WBS. Expression arrays performed in *Gtf2i* $^{-/-}$ mouse embryos show a high number of deregulated genes, especially downregulated. Most of the genes functions are related to oxidative metabolism, transcription, translation and other core biological processes. Interestingly, these embryos present important cardiovascular anomalies, embryonic lethality and a significant downregulation of *Vegfr2*, a gene which is the primary mediator of vascular endothelial growth factor [88].

3.2. Neurological and craniofacial phenotype

Several genes of the deleted region have been related with the neurological and craniofacial phenotype, with the genes of the TFII-I family being the most studied and representative ones. Other genes which could have a role in these phenotypes are *Limk1*, *Eif4h*, *Fzd9*, *Clip2* and *Baz1b*.

3.2.1. Transcription Factor II-I family (TFII-I): *GTF2I* and *GTF2IRD1*

TFII-I family of transcription factors is composed by *GTF2I*, *GTF2IRD1* and *GTF2IRD2*. The first two genes are invariably lost in WBS and the loss of GTF2IRD2 depends on the deletion breakpoints. It is a gene family implicated in several important biological functions in the cell, between them, cell cycle, TGFβ and calcium signaling [89] [54].

Genes in the TFII-I family, specially *GTF2I* and *GTF2IRD1* have an important role in WBS. This role was first known thanks to several atypical deletion cases, all of them including the loss of *GTF2I* and *GTF2IRD1* and showing the cognitive and behavioural symptoms of WBS [70]. The opposite situation happens in another patient with a smaller deletion (~1Mb) not including *GTF2I* and *GTF2IRD1* genes whose symptoms propose a role for the TFII-I family genes in facial dysmorphism and specific motor and cognitive defects [90]. As a result of all these partial deletions patients, an important role of *GTF2I* and *GTF2IRD1* has been proposed for the

cognitive profile of WBS, specially in visuospatial and craniofacial defects [72].

Mouse models have also contributed to clarify the role of *GTF2I* and *GTF2IRD1* in WBS. More than one mouse model for both genes has been published, with some different phenotypic consequences. The complete loss of *Gtf2i* is lethal embryonically presenting brain and neural tube defects [88]. Haploinsuficiency of *Gtf2i* has also been related to an increase in social interactions in mouse, a phenotype that recalls what happens in human patients [91]. Loss of *Gtf2ird1* in different mouse models presents a phenotype in accord with the typical findings of WBS including hypersociability and some neurological deficits. In three of the models, growth retardation and craniofacial abnormalities are present. Other symptoms found are abnormal motor coordination and motor activity, increased anxiety, a novel audible vocalisation phenotype and increased use of both audible and ultrasonic vocalisations in response to swim stress [92-94].

A general characterization of the expression in mouse embryo brain shows a uniform and widespread pattern in brain and spinal cord. In adult animals, the expression is specially high in cerebellar Purkinje cells, piramidal neurons, interneurons of the hippocampus and large neurons in the cerebral cortex, all of them regions known to be affected in human WBS patients [95]. *Gtf2i* is also proposed as a candidate gene for tooth anomalies in WBS, as its expression is found to be higher in the developing teeth than in surrounding tissues throughout tooth development [96].

Cellular models point to *Gtf2i* regulating the expression of marker genes for osteoblast differentiation and craniofacial development. All of them suffer significant decreases in the expression upon inactivation of *Gtf2i* [48, 97].

GTF2I structure is formed by six direct reiterated I-repeats (R1-R6), each with a putative helix-loop-helix motif acting as a protein-protein interaction module, and a basic region before R2. It also contains a functional nuclear localization signal and a N-terminal leucine zipper involved in dimerization [89]. TFII-I was discovered for its capacity of binding to and functioning via the Initiator element (Inr). Apart from its interaction with the Inr element, TFII-I also interacts with an upstream E-box element that is generally recognized by HLH proteins [98]. Efforts have also been directed to the

identification of new binding sites and target genes for *Gtf2i* which may have a role in the pathophysiology of WBS. GATT was originally indentified as a binding sequence for *Gtf2i*, later extended to BRGATTRBR. Target genes related to some interesting pathways have been identified. Among them genes related to chromatin remodeling, cell cycle and neural tube closure [99-100].

3.2.2. LIM Kinase 1 *(LIMK1)*

LIMK1 is a serine protein kinase which is prominently expressed in the developing brain and localized in the neuromuscular synapse. *LIMK1* controls actin dynamics via phosphorylation of cofilin and has been implicated in the control of growth cone motility in cultured neurons [101]. The role in actin remodeling could be crucial for the existence of dendritic spines modifications, which make the synaptic connections in the hippocampus and are associated with the formation and maintenance of memory and learning [102].

Controversial results implicate *LIMK1* in the impaired visuospatial construction of WBS [71, 103-105]. Finally, the accepted idea is that *LIMK1* alone is not sufficient to cause the impairment of visuospatial problems [70, 106].

Knockout mice models suggest a role of *Limk1* in synaptic structure and spine morphology in pyramidal neurons and functions related to the actin network. In concordance with the WBS phenotype, mice show behavioral anomalies, including impaired fear conditioning and spatial learning. [107].

3.2.3. Eukaryotic Initiation Factor 4H (*EIF4H*)

EIF4H is ubiquitously expressed and it is suggested to be involved in translation initiation and RNA duplex unwinding [108]. The role of *EIF4H* has not been studied in patients with partial deletions. However, a knockout mouse model was created and it has reduced fertility, reduced body weight and length and craniofacial abnormalities, all of these characteristics reminding of WBS. Brain volume is reduced, with a significant reduction in posterior areas and there is also a reduction in dendritic complexity, spine number and branching in cortical neurons. Mice also present behavioral impairments affecting fear related learning and associative memory formation [109].

3.2.4. Frizzled 9 *(FZD9)*

The *FZD9* gene is widely expressed in testis, brain, skeletal muscle and kidney and selectively expressed in hippocampus [54, 110]. The role of *FZD9*, was considered not responsible for the major features of WBS, as two patients with smaller deletions not including *FZD9* show the full WBS phenotype [111]. However, the knockout mouse model shows some characteristics which point to an interesting role of the gene in WBS. *Fzd9* null and heterozygous mice have increased apoptotic cell death and increased precursor proliferation during hippocampal development. These evidences suggest that *Fzd9* has an important role in hippocampal development. The model also displays a higher seizure predisposition and in the null mice defects in visuospatial learning tasks are found [112]. However, in another study, no WBS development and morphologic features abnormalities are observed in *Fzd9* knockout mice but they present immune and hematologic abnormalities of B cells in the bone marrow as well as splenomegaly and thymus atrophy [113].

3.2.5. CAP-Gly Domain-Containing Linker Protein 2 (*CLIP2, CYLN2*)

CLIP2 belongs to a family of membrane–microtubule interacting proteins that is highly enriched in neurons of the hippocampus, piriform cortex, olfactory bulb, and inferior olive [114]. It has also been implicated in regulation of microtubule dynamics [115].

As in the case of *LIMK1,* studies in patients with partial deletions generated controversial data on contribution of *CLIP2* to the cognitive deficits of WBS [70, 116-117]. The mouse model shows brain abnormalities, behavior anomalies and reduced synaptic plasticity in CA1 region of the hippocampus confirming a role of this gene in correct brain development and function [118].

3.2.6. Bromodomain Adjacent to Zinc Finger Domain, 1B *(BAZ1B)*

BAZ1B has not only been related with the cardiovascular abnormalities of WBS patients. Mouse models analysis also related this gene to craniofacial abnormalitie,s as reduced levels of the protein produce craniofacial abnormalities [119].

3.2.7. Expression Arrays

Array studies have also help to identify some possible targets in the neurological phenotype. Lymphoblastoid cell lines from patients with common and atypical deletions have been used to perform a comparative transcriptome profiling study. One of the most affected pathways is neuronal migration, as well as some genes involved in microtubule formation. Interesting genes which could be used as targets in the future include *MAP1B, KIF14, SNX4, USO1* and *CCDC88A,* all of them part of the neuronal migration pathway which could be related to the visual impairments in WBS [120].

In another array study performed using skin fibroblasts, gene ontology categories have been obtained related to extracellular matrix genes and class I MHC as well as postsynaptic membrane genes. A module approach in this study has identified genes related to DNA binding and transcription, vasculature development and regulation with involved genes that can be related to the WBS pathophysiology, such as metabolic phenotypes (*UCP2*), dental anomalies (*SPON1*), neurological features, cognition or brain development (*HSPB2, ABHD14A* and *GABRE*) [121].

3.3. Endocrinological phenotype

Only two genes inside the WBSCR have been related to the endocrinological phenotype observed in human patients.

3.3.1. Max-Like Protein Interacting Protein-Like (*CHREBP, MLXIPL)*

MLXIPL is a member of the basic-helix-loop-helix leucine family of transcription factors and binds to carbohydrate responsive element motifs in the promoter region of some glucose-regulated and lipogenic genes activating their expression. *MLXIPL* is maintained in an inactive, phosphorylated status in the cytosol. Conversely, high glucose levels result in dephosphorylation, nuclear translocation, and transcriptional activation of the gene [54]. *MLXIPL* is involved in the regulation of expression of carbohydrate responsive enzymes in the liver, which in turn control glucose metabolism and synthesis of fatty acids and triglycerides [122]. Both glycolisis and lipogenesis are affected in the knockout mouse [122-123].

3.3.2. Syntaxin 1A *(STX1A)*

STX1A encodes for a plasma membrane protein abundantly expressed in neurons and plays an essential role in exocytosis of neuronal and neuroendocrine cells, forming a complex with the 25-kDa synaptosomal-associated protein (*SNAP-25*) and vesicle-associated membrane protein 2 (*VAMP-2*). It is also related to neurotransmitter release and vesicle fusion processes. A role in modulating ion channels in exocrine and muscular cells has also been reported for this gene [53, 124-125].

As in *FZD9*, the role of *STX1A* has been considered not responsible for the major features of WBS, as two patients with smaller deletions excluding this gene show the full WBS phenotype [111]. However, studies in mice relate this gene to the endocrinological phenotype. The mouse model with a 30% of *Stx1a* overexpression displays fasting hyperglycemia and a more sustained elevation of plasma glucose levels after an intraperitoneal glucose tolerance test, with correspondingly reduced plasma insulin levels. They also show increased fear conditioned memory [126]. The knockout model, presents no hyperglycemia but impairment in the glucose tolerance test with significant higher glucose levels when compared to wild-type animals. In agreement, the insulin levels are reduced [127]. As a conclusion, *STX1A* could be a good candidate for the glucose abnormalities in patients.

3.3.3. Bromodomain Adjacent to Zinc Finger Domain, 1B *(BAZ1B)*

Finally, *BAZ1B* has also been related with infantile hypocalcaemia present in infantile patients, from a mouse model showing calcium anomalies [128].

3.3.4. Expression Arrays

The same array study by Antonell *et al*, which has identified the neuronal migration pathway as affected, identified the glycolisis pathway as the most significant affected one in the group of WBS patients, but not in the patients with partial deletions not including the deletion of Gtf2i genes, pointing to a possible role of this gene in the endocrinological phenotype of WBS. Interesting genes in the glucose pathway include *PGAM1*, *ENO2* and *ALDOC* and could be target genes for the metabolic disturbances seen in the syndrome [120].

HYPOTHESIS

Mouse models are useful tools for the study of human disease. Several single and partial mouse models for WBS have been created so far, contributing to deepen in the knowledge of the disease and its phenotypes. A mouse model that mimics the most common deletion in WBS would show the same phenotype as human patients and would provide a model for the study of the syndrome and new possible treatments. Moreover, the establishment of genotype-phenotype correlations comparing our model to the previously described one could be performed.

One of the hallmarks of WBS is the cardiovascular phenotype, with a described role of elastin gene as the cause of supravalvular aortic stenosis and hypertension. *Ncf1*, a subunit of the NADPH-oxidase complex, has been described as a modifier for WBS cardiovascular phenotype. The characterization of the cardiovascular phenotype in mouse models for WBS would identify the abnormalities and causes of the phenotype. The reduction of the NADPH-oxidase complex activity by reduction of the *Ncf1* gene dosage or by pharmacological treatment would partially or totally rescue the cardiovascular phenotype in mouse models of WBS.

Several studies in mice with induced single or combined gene mutations and phenotypic studies of cases with atypical WBS deletions suggest that hemizygosity of *GTF2I* is involved in the intellectual disability associated with WBS. TFII-I expression is continuous in the embryo and the pattern of expression in adult mouse brain correlates with affected regions in the human brain. The creation and characterization of a mouse model lacking the N-terminal part of the protein would allow the identification of which is the role of this domain in disease and its relation with WBS phenotype. Moreover, the use of *Gtf2i* and WBS mutant embryonic stem cells to perform a transcriptome analysis would allow the identification of deregulated pathways and genes. The analysis will determine the differences and similarities of *Gtf2i* or complete deletion loss related to expression deregulation.

OBJECTIVES

1. Create a mouse model that mimics the most common deletion found in WBS.

2. Fully characterize the cardiovascular, craniofacial, neurological, behavioural and endocrinological phenotype of the complete deletion mouse model (CD)

3. Define the functions of the N-terminal part of the TFII-I protein and its relation with the WBS phenotype.

4. Identify new target genes for TFII-I using differential expression of affected brain tissues and ES cell lines.

5. Compare observed phenotypes among the available mouse models in our group and in literature.

6. Establish the effect of the *Ncf1* expression and gene dosage reduction in the cardiovascular phenotype of mouse models.

7. Establish the efficacy and safety of two different pharmacological treatments that reduce the NAPDH-oxidase complex activity in the cardiovascular phenotype of the distal deletion mouse model.

8. Determine the deregulated genes and pathways related to the WBS phenotypes in ES cells models for *Gtf2i* and WBS using expression arrays.

CHAPTER 1

Reduction of NADPH-Oxidase Activity Ameliorates the Cardiovascular Phenotype in a Mouse Model of Williams-Beuren Syndrome

Victoria Campuzano, Maria Segura-Puimedon, Verena Terrado, Carolina Sánchez-Rodríguez, Mathilde Coustets, Mauricio Menacho-Márquez, Julián Nevado, Xosé R. Bustelo, Uta Francke, Luis A. Pérez-Jurado

PLoS Genet. 2012; 8(2): e1002458.

doi:10.1371/journal.pgen.1002458

One of the main characteristics of WBS is a generalized arteriopathy leading to hypertension and other cardiovascular complications. Previous studies have related the deletion of a functional copy of the *NCF1* gene with a reduced risk of hypertension.

In this project we characterized the cardiovascular phenotype of the distal deletion (DD) mouse model, carrying a heterozygous deletion including the *Eln* gene, known cause of the cardiovascular problems. The model presented generalized arteriopathy, hypertension, and cardiac hypertrophy, associated with elevated angiotensin II, oxidative stress parameters, and *Ncf1* expression.

Genetic and pharmacological strategies were applied to rescue the cardiovascular abnormalities in the model obtaining the reduction of NOX activity and the normalization of the biochemical parameters and blood pressure levels and improved cardiovascular histology. We provide strong evidence for implication of the redox system in the pathophysiology of the cardiovascular disease in a mouse model of WBS.

Victoria Campuzano, Maria Segura-Puimedon, Verena Terrado, Carolina Sánchez-Rodríguez, Mathilde Coustets, Mauricio Menacho-Márquez, Julián Nevado, Xosé R. Bustelo, Uta Francke, Luis A. Pérez-Jurado.

Reduction of NADPH-Oxidase Activity Ameliorates the Cardiovascular Phenotype in a Mouse Model of Williams-Beuren Syndrome

PLoS Genet. 2012; 8(2): e1002458.

Campuzano, V; Segura-Puimedon, M; Terrado, V; Sánchez-Rodríguez, C; Coustets, M; Menacho-Márquez, M; Nevado, J; Bustelo, XR; Francke, U; Pérez-Jurado, LA. Reduction of NADPH-oxidase activity ameliorates the cardiovascular phenotype in a mouse model of Williams-Beuren Syndrome. Supporting information. PLoS Genet. 2012 Feb;8(2):e1002458.

CHAPTER 2

Essential role of the N-terminal region of TFII-I in viability and behavior

Jaume Lucena, Susana Pezzi, Ester Aso, Maria C Valero, Candelas Carreiro, Pierre Dubus, Adriana Sampaio, Maria Segura, Isabel Barthelemy, Marc Y Zindel, Nuno Sousa, José L Barbero, Rafael Maldonado, Luis A Pérez-Jurado, Victoria Campuzano

BMC Med Genet. 2010 Apr 19;11:61

Gtf2i is a transcription factor from the TFII-I family which is deleted in Williams-Beuren syndrome, a neurodevelopmental disorder caused by a 1,5Mb deletion at 7q11.23. *Gtf2i* has been related to both cranial and cognitive abnormalities found in patients.

We have created a mouse model lacking the first 140 aminoacids of the protein and have performed a characterization at several levels. Cell cultures have shown a reduced growth in the heterozygous cells. The homozygous model presents reduced viability and both homozygous and heterozygous animals present craniofacial abnormalities. The behavioral characterization shows increased anxiety and sound intolerance in the heterozygous mice.

We have demonstrated the essential role of the N-terminal region of TFII-I in cell growth and in some behavioral characteristics that can be linked to WBS.

Jaume Lucena, Susana Pezzi, Ester Aso, Maria C Valero, Candelas Carreiro, Pierre Dubus, Adriana Sampaio, Maria Segura, Isabel Barthelemy, Marc Y Zindel, Nuno Sousa, José L Barbero, Rafael Maldonado, Luis A Pérez-Jurado, Victoria Campuzano.

Essential role of the N-terminal region of TFII-I in viability and behavior

BMC Med Genet. 2010 Apr 19;11:61.

Lucena J, Pezzi S, Aso E, Valero MC, Carreiro C, Dubus P, Sampaio A, Segura M, Barthelemy I, Zindel MY, Sousa N, Barbero JL, Maldonado R, Pérez-Jurado LA, Campuzano V. Essential role of the N-terminal region of TFII-I in viability and behavior. Additional files. BMC Med Genet. 2010 Apr 19;11:61.

CHAPTER 3

Deletion of the entire 1.3Mb orthologous region in mouse recapitulates most of the WBS phenotypes

Maria Segura-Puimedon, Ignasi Sahún, Carmen Valero, Emilie Velot, Pierre Dubus, Cristina Borralleras, Ana João Rodrigues, Nuno Sousa, Yann Herault, Mara Dierssen, Luis A Pérez-Jurado, Victoria Campuzano

In preparation

Williams-Beuren syndrome is a compelling disease for the combination of physical and cognitive characteristics that includes. It is caused by a 1,5Mb deletion of 26 to 28 continuous genes at chromosomal band 7q11.23. We have, for the first time, created a mouse model mimicking the most common deletion in WBS, from *Gtf2i* to *Fkbp6*. The mouse model has been characterized following all the phenotypes affected human patients. The homozygous deletion is lethal and heterozygous animals are viable, fertile and with a preserved survival. Males and females present a reduced body weight and the model lacks the characteristic cardiovascular phenotype of the disease, which may be a consequence of reduced *Ncf1* expression. The model presents endocrinological characteristics reminding of diabetic patients and a reduced mandible, which is present in human patients. The neurological phenotype can in some cases correlate the definite anomalies affecting some of the described brain areas with the behavior of the model.

The complete deletion mouse model is a useful tool for future studies regarding genotype-phenotype correlations and future treatments.

Deletion of the entire 1.3Mb orthologous region in mouse recapitulates most of the WBS phenotypes

Segura-Puimedon M, Sahún I, Velot E, Dubus P, Borralleras C, Rodrigues AJ, Sousa N, Herault Y, Dierssen M, Pérez-Jurado LA, Campuzano V

ABSTRACT

Williams-Beuren syndrome is a rare neurodevelopmental disorder caused by a 1.5 Mb hemizygous deletion of ~26 contiguous genes on chromosome band 7q11.23. WBS symptoms include physical abnormalities with cardiovascular, endocrinological and craniofacial abnormalities and neurological, cognitive and behavioral anomalies. To dissect genotype-phenotype correlations we have created a cell line and a mouse model with the complete WBS typical deletion, from *Gtf2i* to *Fkbp6*. The homozygous deletion is lethal and heterozygous mice are viable, fertile, have a reduced body and brain weight and present no differences in survival. Consistent with gene dosage, a reduced expression of genes inside the deletion is found. The model presents no cardiovascular phenotype probably as a consequence of the reduction in the Nfc1 expression. A reduction in the area of Langerhans islets is found, although no differences appear in the glucose levels. A reduced mandible is present and neurological abnormalities are found in the amygdala, orbitofrontal cortex and hippocampus. CD model shows motor problems and behavioral tendencies to greater interest in novelty and an inhibited behavior. Comparison with partial and single models allows the establishment of genotype-phenotype correlations. CD model recapitulates most of the physical and cognitive features present in WBS patients, becoming the best model to unravel the molecular causes of disease as well as the tool to evaluate new therapeutic approaches.

INTRODUCTION

Williams-Beuren syndrome (WBS, OMIM 194050) is a rare neurodevelopmental disorder with an incidence of 1/7500 newborns, which usually occurs sporadically [1]. It is caused by the hemizygous deletion of 26-28 contiguous genes on chromosome band 7q11.23 [2]. The common deletion size (90% of the patients) is 1,5 Mb and is mediated by large region-specific low copy repeats elements (LCR) that flank the WBS critical region. Misalignment of the LCRs leads to non allelic homologous recombination (NAHR) [3-4].

WBS is a very intriguing disease, as it includes a wide variety of symptoms and phenotypes in patients. One of the hallmarks of the disease is the cardiovascular phenotype, present in 84% of patients and characterized by supravalvular aortic stenosis and hypertension [5-6]. Physical abnormalities also include a dysmorphic face with craniofacial abnormalities, growth retardation and a high prevalence of glucose intolerance, present in up to 75% of patients. Hyperacusis and infantile hypercalcemia are also frequent [7-9].

Patients present mild to moderate intellectual disability and a characteristic cognitive profile including preserved verbal skills, gregarious personality and deficient visuospatial abilities [10-11]. Neurological problems have also been described including hypotonia and motor impairment [12-13]. A reduced brain volume is also reported, as well as structural and functional abnormalities in many brain areas, especially in regions related to the social phenotype, amygdala, insula and orbitofrontal cortex and with the visuospatial anomalies, hippocampus [14-15].

One of the main difficulties in this syndrome, as there are many deleted genes, is the establishment of genotype-phenotype correlations. The use of patients with atypical deletions and the studies in mouse models have established some correlations. The clearest one is the role of *ELN* and *NCF1* in cardiovascular disease and hypertension [16-18]. A double heterozygote (D/P) model has been created from a combination of two partial deletions models, the proximal deletion (PD) and distal deletion (DD). The D/P model contains the WBS common deletion but the two halves are *in trans* and there is the complete loss of *Limk1* [19]. The PD (from *Gtf2i* to *Limk1*) has been more related to the cognitive abnormalities, as it includes the deletion of the TFII-I family genes, mostly associated to the intellectual disability and visuospatial problems [20-21]. On the contrary, the DD model (from *Limk1* to *Trim50*), has been more related to the physical abnormalities because, besides including *Eln*, it also contains the deletion of *Stx1a* and *Mlxipl*, which have been related to the endocrinological phenotype [22-23].

Here we present a mouse model that presents the most common deletion found in WBS patients, with the loss of the genomic region between *Gtf2i* and *Fkbp6* genes. This model recapitulates most of the physical and cognitive features present in WBS patients, becoming the best model to unravel the molecular causes of disease as well as the tool to evaluate new therapeutic approaches.

RESULTS

Generation and characterization of the ESSP9 cell line

To generate ESSP9, carrying the most common deletion of WBS (WBSCR), we first produced *2loxP* ES cells with a *loxP* site in *Gtf2i* [24] and the second one in *Fkbp6* (Fig 1A). After Cre-recombinase expression, positive clones were selected and the genotype was confirmed by MLPA (Fig 1B). mRNA from ESSP9 undifferentiated cell line in cultured conditions was used to carry out microarray expression analysis. As expected, the majority of the WBSCR genes (12 out of the 15) were downregulated in ESSP9 respect the wild-type (WT) R1 cell line, although only 6 out of this 12 were significantly downregulated (Table 1). We analyzed the global expression of the WBSCR genes and also ten genes at both the centromeric (expanding 5Mb due to lower gene density) and the telomeric regions (expanding 1.5 Mb). We did not find significant expression changes in these genes in the ESSP9 cell line when compared with two other genomic regions used as external controls (chromosome 2 and 11), although the centromeric region was slightly downregulated (Fig 1C).

Genes in WBSCR	ESSP9/R1		
	adj.P.Val	B	Fold Chg
Gtf2i	0,15150	-5,06	-0,12
Limk1	0,06896	-3,79	-0,36
Rfc2	0,00017	6,16	-0,70
Gtf2ird1	0,02264	-1,94	-0,26
Fkbp6	0,00006	8,14	-1,11
Baz1b	0,32868	-6,17	-0,26
Tbl2	0,00178	2,38	-0,64
Wbscr22	0,00142	2,75	-0,52
Wbscr27	0,26734	-5,88	-0,15
Cldn3	0,54133	-6,78	-0,10
Cldn4	0,00044	4,53	-1,13
Eln	0,01604	-1,34	0,63
Mlxipl	0,87565	-7,22	0,04
Abhd11	0,00128	2,90	-0,50

Table 1. Adjusted p value, B value and fold change for the genes in the array present in the WBS deleted region. Significantly downregulated genes in dark grey.

To identify gene expression differences among ESSP9 and R1, we performed microarray expression analysis under the same conditions. We have applied highly stringent and restrictive parameters of significance for the processing and selection of the data. We used several algorithms that

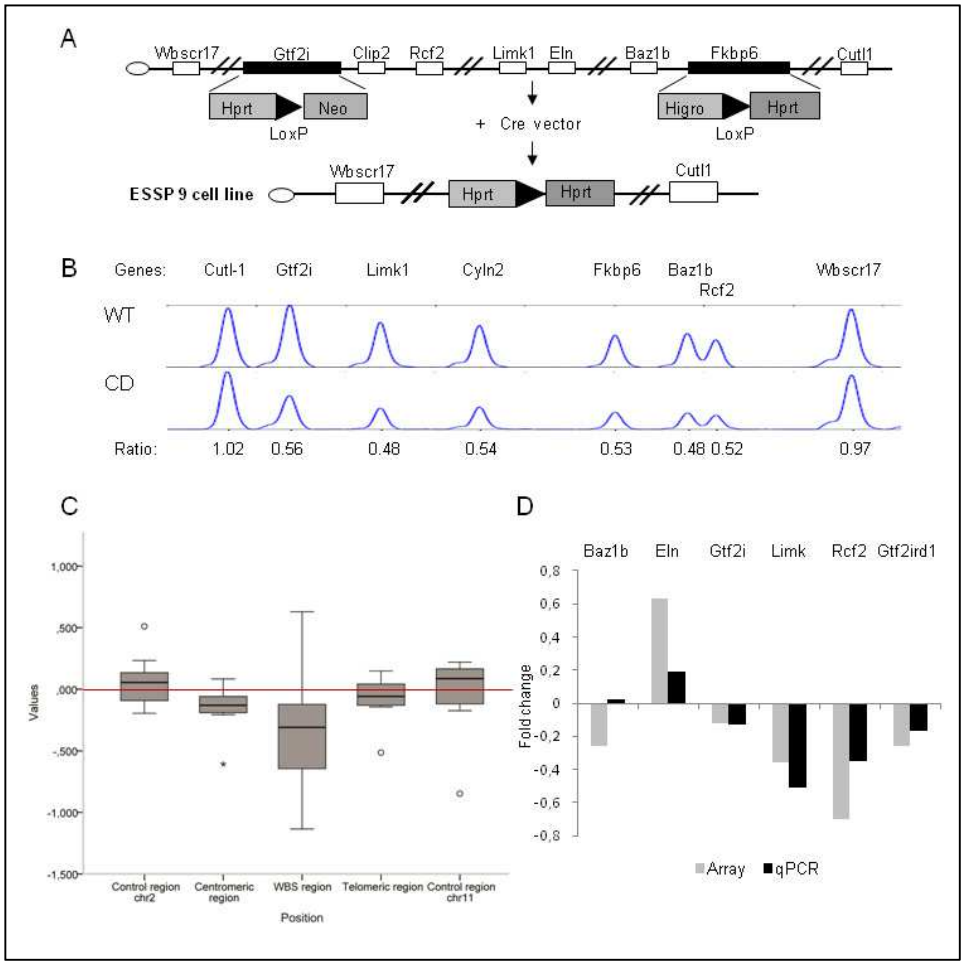

Figure 1. Generation and characterization of ESSP9 cell line. A: Schematic genomic diagram of the targeting strategy. B: MLPA experiment in F0 mouse, using Cutl-1 and Wbscr17 as external genes and Gtf2i, Limk1, Cyln2, Fkbp6, Baz1b and Rcf2 as genes inside the deletion. The ratios are around 1 for the external genes and 0,5 for the genes in the deletion indicating the copy loss. C: Box plots of array expression in different regions for ESSP9 cell line. Two external control regions in chromosomes 2 and 11 are used. Centromeric and telomeric regions of WBS deletion region are analysed as well as the WBS deleted region. D: Expression array validation of the ESSP9 cell line.

allowed us to minimize the background noise and to maximize the statistical significance of the data. We did not observe large expression changes (>3 fold) for any of the genes. By carrying out hierarchical clustering of the microarray data, we found a very good correlation between replicates. Differentially expressed genes (DEG) were selected for B>0 and p<0.01, obtaining 599 differently expressed genes among the ESSP9 and R1 cell lines. Of these, 394 were downregulated and 205 upregulated in the WBS cell line. In order to validate the microarray data, we selected 6 genes inside the WBSCR. Real time quantitative RT-PCR (qRT-PCR) using the same RNA data source corroborated microarray expression for all the genes except *Baz1b* (Fig 1D).

To perform the bioinformatic pathway definition, Affimetrix identification number

(IDs) were transformed to Ensembl, obtaining 571 correct IDs. 548 out of the 571 genes were correctly identified by the CPDB software to perform the over-representation analysis. The most significant deregulated pathway was smooth muscle contraction followed by the presence of several pathways related to cardiomyopathy. Other interesting pathways for WBS pathology appeared deregulated, like aldosterone regulated sodium reabsorption, vitamin D metabolism, various lipid metabolism pathways and axon guidance (Table 2). The complete list of deregulated pathways can be consulted at Supp table 1.

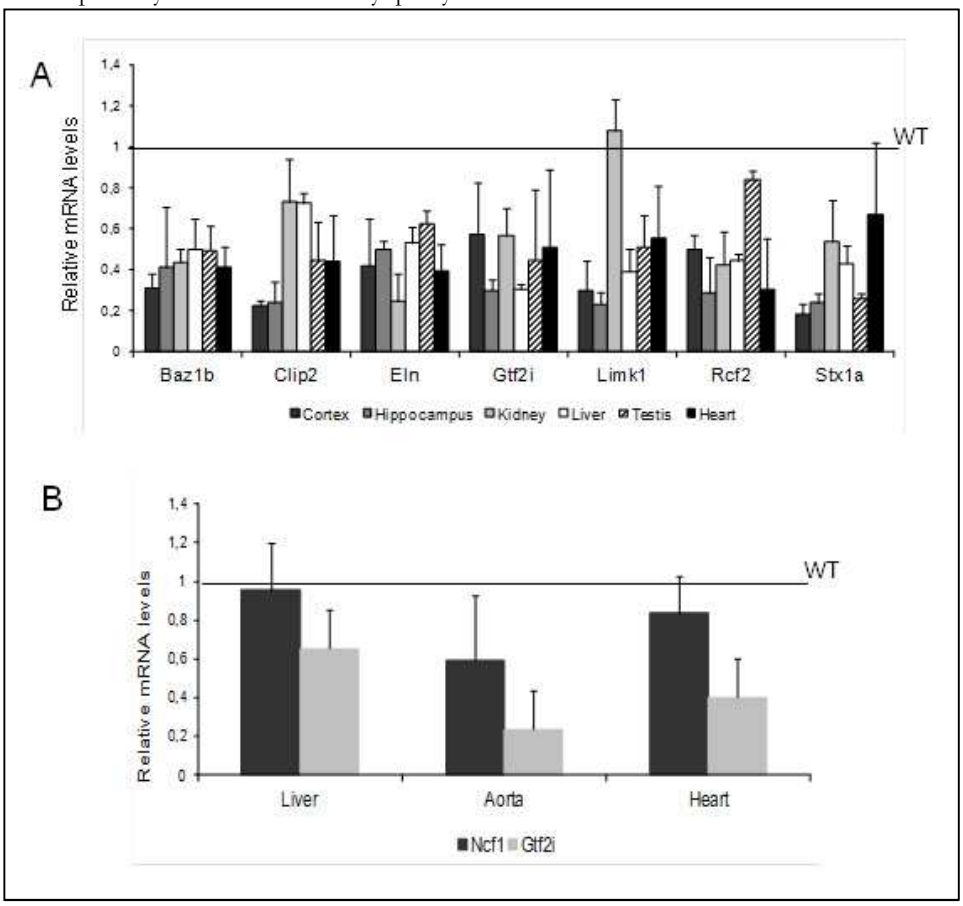

Figure 2. RT-qPCR analysis in CD mouse model. A: Relative gene transcript levels of seven deleted genes in 6 different tissues. Data was normalized so the mean of the wild-type group was 1.0 represented as the black line. Results represent the mean ± SD (n=3 animals per group). B: Relative gene transcript levels of the Ncf1 gene and Gtf2i as a control in aorta, heart and liver tissue of CD mouse. Data was normalized so the mean of the wild-type group was 1.0 represented as the black line. Results represent the mean ± SD (n=5 animals per group).

Generation of the complete deletion (CD) mouse model

Complete deletion (CD) mouse model was obtained following two strategies. In the first, ESSP9 cell line was used to generate chimeric mice and animals were crossed until the deletion was germinally transmitted. In the second one, *2loxP* mice were directly mated with TgPGK-Cre mice obtaining CD mice. To corroborate the copy loss seen in the MLPA with a reduction in the gene expression, qRT-PCR

p-value	Pathway	Genes
1,44E-04	Smooth Muscle Contraction	Cals1, Myl9, Itgb5, Myh11, Actg2, Tpm2, Acta2
5,90E-04	Dilated cardiomyopathy	Igf1, Tgfb2, Itga8, Tpm1, Adcy7, Dmd, Tgfb3, Itga9, Tpm2, Itgb5, Itga6
0,00066	Hypertrophic cardiomyopathy (HCM)	Igf1, Tgfb3, Itga8, Tgfb2, Dmd, Tpm1, Itga9, Itgb5, Tpm2, Itga6
0,01049	Aldosterone-regulated sodium reabsorption	Nedd4l, Igf1, Nr3c2, Atp1b1, Irs1
0,01384	Vitamin D (calciferol) metabolism	Lrp2, Cubn
0,02042	Lipid digestion, mobilization, and transport	Apoe, Cubn, Abhd5, Lpl, Mgll
0,03478	Axon guidance	Dpysl3, Crmp1, Col5a1, Lama1, Myl9, Ncam1, Myh11, Slit2, Nrcam, Sema4d, Itga9, Col1a1

Table 2. Most interesting deregulated pathways and genes of the over representation analysis in the ESSP9 cell line.

analysis of representative genes inside the deletion in different affected tissues (cortex, hippocampus, kidney, liver, testis, heart) was performed. A reduction in the expression in all studied tissues was present, with the exception of *Limk1* in the kidney and *Rfc2* in testis (Fig 2A). Viability of the complete deletion heterozygous mice was normal. However, no homozygous mice were obtained, as expected for previous results from our group and other mouse models for deleted genes in WBS. No homozygous embryos were detected already at 12.5 days post coitum, indicating early lethality. Fertility was normal in the heterozygous mice and no gender genotype distribution differences were detected. WBS patients display an abnormal pattern of growth, present already in the prenatal stage and maintained into adulthood as 70% of patients are below the 3rd percentile for mid parental height [9]. Heterozygous animals did not show a reduction in the body weight at birth, but the significant difference in body weight was already present in the first month and maintained until 6 months of age, with a more accused difference in males than in females. The significant difference was lost from the 6 months of age, although wild-type animals tent to have an increased body weight during the whole studied period (Supp fig 1).

Macroscopic study of several tissues showed no differences in the general tissue organization at 16 weeks old (data not shown). No differences were found regarding the age at death (Supp fig 2). Death causes were varied and mostly due to tumors in both genders and genotypes. Pathology examination of several tissues in the animals indicated that the most common death cause for both genotypes was lymphoma B (follicular type) in a variety of organs, especially in liver, kidney and lung, according to what is known in the C57BL/6 background. Even if they did not

Parameter	Wild-type	CD
Systolic BP (mmHg)	108,26 ± 14,21	125,06 ± 7,56
Dyastolic BP (mmHg)	82 ± 12,47	97,8 ± 6,59
Mean BP (mm Hg)	90,46 ±12,95	106,6 ± 6,68
Heart rate (bpm)	630 ± 37,44	569,4 ± 81,51
Body weight (g)	42,19 ± 3,24	38,74 ± 2,91
Heart weight (g)	0,196 ± 0,0075	0,184 ± 0,0097
%Heart weight/ Body weight	0,474 ± 0,04	0,477 ± 0,017
Aorta wall thickness (μm)	62,87 ± 2,81	69,63 ± 3,99
Lamellar units in aorta	7,16 ± 0,58	7,83 ± 0,58

Table 3. Cardiovascular parameters of 16 and 32 weeks old mice. 32 weeks old mice used for pressure, heart rate and %heart/body weight and 16 weeks old mice used for the aorta wall thickness and lamellar units. Results represent mean ± SD (n=5-6 per group).

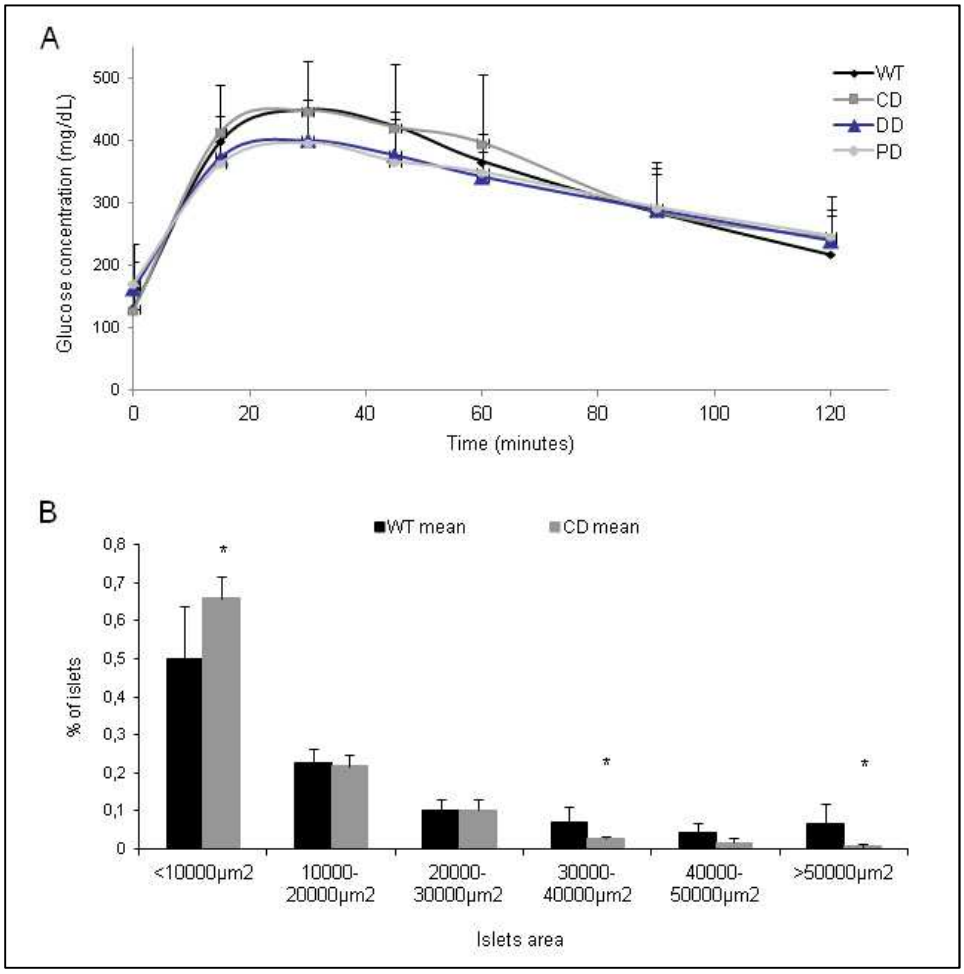

Figure 3. Endocrinological analysis. A: Intraperitoneal glucose tolerance test. Results represent the mean ± SD (N=8-16). B: Langerhans islets area analysis. Results represent the mean ± SD (N=3-6).

reach significant differences, a wider variety of tumors and a higher prevalence of steatosis were more present in the CD animals (Supp table 2).

Additionally, 10 independent mouse embryonic fibroblasts cultures were established from 12.5 embryos and characterized following the 3T3 protocol and no differences were obtained regarding the immortalization passage, growth curves, or the saturation curves (Supp fig 3).

Cardiovascular phenotype

Heart weight from animals at different ages was annotated to search for cardiac hypertrophy and measured as the heart wet-weight relative to the body weight. No significant differences were found in the heart to body ratio weight in young (3-4 months) or old animals (9-12 months) (Supp table 3). We studied the systolic, diastolic and mean blood pressure as well as the heart rate in both genotypes at 32 weeks of age. No significant differences in blood pressure were found for any of the studied

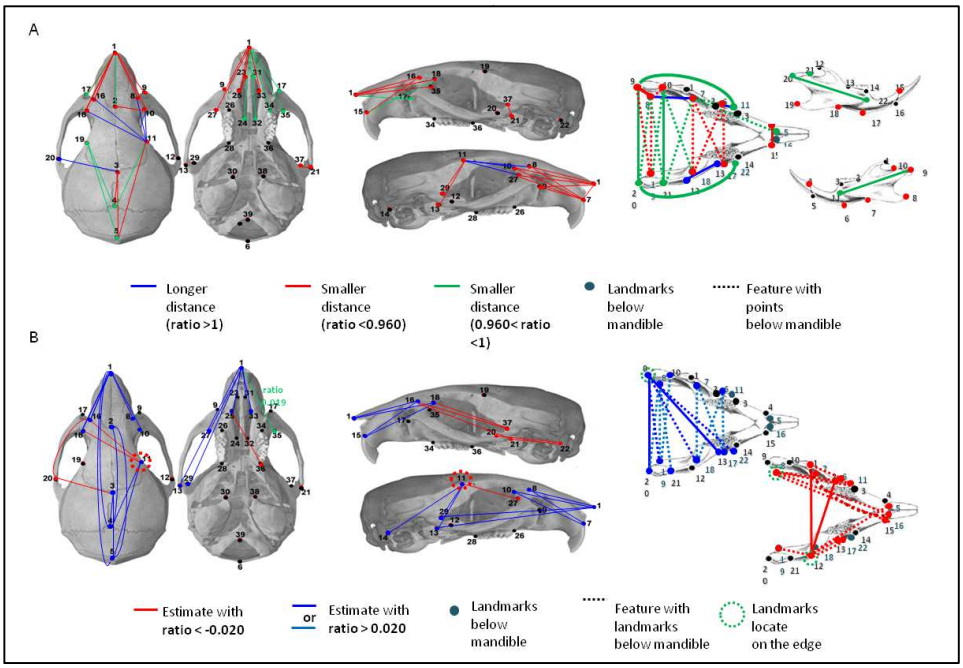

Figure 4. Craniofacial analysis of the CD model. A: Size analysis. B: Shape analysis. N=15 females per group.

parameters, although there was a 17% increase in the CD mice mean arterial pressure. Post-mortem evaluation at 32 weeks of age showed no differences in body weight, as expected from the growth curves, and no differences in heart weight (Table 3). The structure of the aorta was examined with vascular histological and morphological methods. CD mice showed no differences in arterial wall thickness or in the number of lamellar units of the aorta, although a tendency to an increase in both parameters was present (Table 3).

NCF1 is a modulator of blood pressure and cardiovascular phenotype in WBS [16, 18]. In view of the results, we decided to study whether the expression of *Ncf1* was affected in different tissues of the CD mice. An expression level comparable to the wild-type was found in heart and liver of the CD animals but a reduction was found in the aorta of the same animals (Fig 2B).

Endocrinological phenotype

The most prevalent endocrine abnormalities in WBS are glucose intolerance or diabetes [8]. To analyze the presence of anomalies in the glucose metabolism, glucose curves were performed in WT, CD, PD and DD animals (Figure 3A). The glucose basal levels were importantly increased in the PD and DD animals, although the differences did not reach significance. Regarding the glucose curve, no differences were observed among genotypes, although PD and DD models did not reach the same levels as WT and WBS. Further steps were made in order to analyze the morphology of the Langerhans islets in our model. CD animals showed a significant increased number of smaller Langerhans islets, correlating with a reduction of bigger islets (66% of smaller islets versus 49,8% in the wild-type and 0,51% of bigger islets versus 6,51% in wild-type) (figure 3B).

	Inferior			Superior		
	Length	Neurones	Neurones/Length	Length	Neurones	Neurones/Length
WT	1253,6	65,74	0,056	1344,65	66,21	0,0509
CD	962,3	49,94	0,055	1175,07	81,41	0,0716
PD	954,85	53,77	0,059	1187,53	70,91	0,0583
P value WT- CD	0,025	0,063	0,89	0,120	0,089	0,001
P value WT- PD	0,0003	0,068	0,69	0,032	0,480	0,206
P value CD-PD	0,790	0,540	0,54	0,860	0,190	0,041

Table 4. Analysis of the doublecortin positive cells in the hippocampus.

Craniofacial phenotype

To study the cranial phenotype in the mouse model, 3D data was collected from 39 cranial and 22 mandible landmarks and a posterior morphometric analysis of the cranial structure of CD and wild-type females was performed. The cranial analysis showed no global differences in the size of the skull of the CD females, although a tendency to smaller nose was observed. However, we could see a reduced size of the mandible in the CD model when compared to the wild-type ($p=0.028$) (Fig 4A). Regarding the shape of the skull and mandible, no global differences were observed, although tendencies were present trough a flatter nose (Fig 4B).

Neurological phenotype.

To define the neurological phenotype in our mouse model, we measured the brain weight in both CD and WT animals. Brain weight was reduced in CD mice, both in males and females, with an 11% and a 7.97% reduction respectively (Fig 5A). We wanted to determine if this reduction was confined to a determined brain region and to study several regions which have been related to WBS phenotype, especially the social pathway and the hippocampus. We obtained brains from wild-type, CD and PD mouse model. We performed a structural analysis to analyze the volume and the total number of cells of the amydgala, the hippocampal formation and the orbitofrontal cortex. A general non significant reduction of the different studied brain regions exists between the WT and the CD models, while a general increase is observed in the PD model.

In the amygdala, a significant reduction in volume of the CD versus the PD model was present in the lateral area, but without differences in the number of cells. No differences in volume were observed in the basolateral amygdala, although a reduction in the number of cells was observed when comparing CD to PD, and nearly significant difference with the WT. Differences in cell number and volume in the amygdala could have a relation with the functional and structural anomalies found in this region in human patients (Figure 5B) [25-28].

In the orbitofrontal cortex, the CD model had a reduction in the volume of both the ventral and lateral layer I, where no cells are found, when compared to the other two genotypes. No differences were found in the number of cells (Figure 5C).

Most striking differences were detected in the hippocampus (Figure 5D). In the dentate gyrus, the CD model had a volume reduction in the molecular layer compared to the WT, and no differences were found in other layers of the dentate gyrus. In the CA3 region, differences were found in the three defined layers. The PD model had a significant or nearly significant increase in all three layers when compared to the other two models and the number of cells in the pyramidal layer of the CA3 region was significantly increased. The CD model had a nearly significant reduction of the pyramidal layer when compared to the WT model. No differences were found in the CA1 region

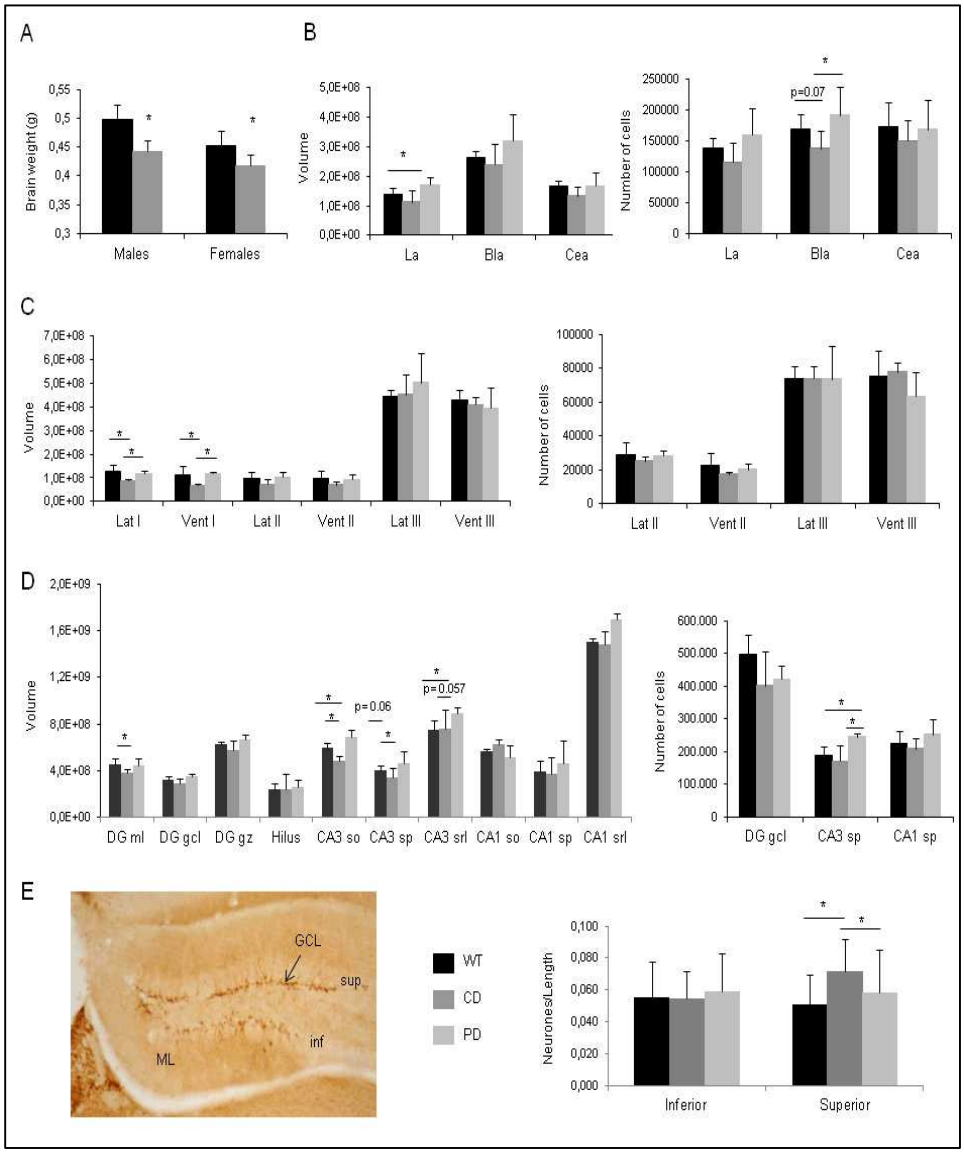

Figure 5. Neurological analysis of CD, PD and WT animals. A: Comparison of adult brain weights of CD and WT. N=9 males and 7 females. B: Volume and number of cells analysis of the amygdala. La: lateral, Bla: basolateral, Cea: central. C: Volume and number of cells analysis of the orbitofrontal cortex. Lat: lateral, Vent: ventral. D: Volume and number of cells analysis of the hippocampus. DG ml: dentate gyrus molecular layer, DG gl: dentate gyrus granular layer, DG gz: polimorphic layer, CA3/CA1 so: stratum oriens, CA3/CA1 sp: piramidal layer, CA3/CA1 srl: radiatum and lucidum layers. N= 4-5 per group. E: Doublecortin immunohistoquemistry. Density of doblecourtin positive neurones in the subgranular zone of the hippocampus. N= 2-3. Results represent the mean ± SD in all cases.

of the hippocampus in volume or number of cells for any of the models. To study the neurogenesis in the hippocampus, we performed an immunohistochemistry analysis with Doublecortin (Dcx), a marker for neurons in early differentiation stages, in the three models (Figure 5E). We found a significant increase in the density of immature neurons in the superior region of the subgranular zone of the hippocampus of CD animals compared to the two other groups. In the inferior region, a significant length reduction and a nearly significant decrease in the number of neurons was present in the CD and the PD mice compared to the WT, but the density in this region showed no differences (Table 4). Results pointed to an increased neurogenesis in the CD model and an increased volume and number of cells in the CA3 region of the PD model.

Behavioral characterization

A general behavioral characterization including neurosensorial (Shirpa protocol), motor and learning and attention tests was performed in our mouse model to determine which characteristics in the CD model were shared with other WBS models and with human patients.

It is known that motor problems exists in patients, showing hypotonia and cerebellar signs [13]. In an initial approach to the motor phenotype, we obtained significant results in the wire maneuver with CD model showing worst performance ($p=0.01$) and a reduction in the hindlimb tone ($p=0.01$) (Supplemental table 4). However, no differences were obtained in grip strength, geotaxis or equilibrium. To further analyze possible motor problems, the rotarod test was used and a significant difference was obtained in the CD model, with a reduction in the latency to fall ($p=0.016$) (Figure 6A). Finally, the treadmill test showed no significant differences among the two genotypes.

Anxiety is present in half of WBS patients and we used the open-field test to analyze the exploratory activity and anxiety. No differences were obtained in the time spent in the center or the periphery of the arena and no differences were present in the rearing at the center or periphery in the CD model compared to the WT model (data not shown).

The reaction to a marked toe pinch ($p=0.024$) was decreased in the CD model, but not in other less marked stimulus such as tail pinch or slight toe pinch, suggesting a possible reduction in pain sensitivity in the model.

To evaluate learning, memory and attention we used the object recognition test, the water maze test, the conditioned fear test and the startle response. The object recognition test is a visual discrimination test for memory and attention. No significant differences were observed among the two genotypes, although a tendency for a better discrimination existed in the CD model, tending to spend more time in the novel object than the wild-type animals (Figure 6B).

The water maze test is a spatial navigation test where animals have to find the hidden platform using visual cues in the space. It is used to investigate spatial learning, which is affected in patients as they present important visuospatial problems. No differences were found in the pre-training, the acquisition or the cued sessions regarding latency to escape, distance or average speed. Both groups showed comparable levels of cognitive flexibility in the removal session. No vision or motor problems were observed, as all animals were perfectly able to find the platform using the visual cues and no floating was observed. Both groups comprehended the platform localization and no differences were found regarding the time spent in the four different quadrants. However, we could see significant differences in the time spent in the center or the periphery of the pool in

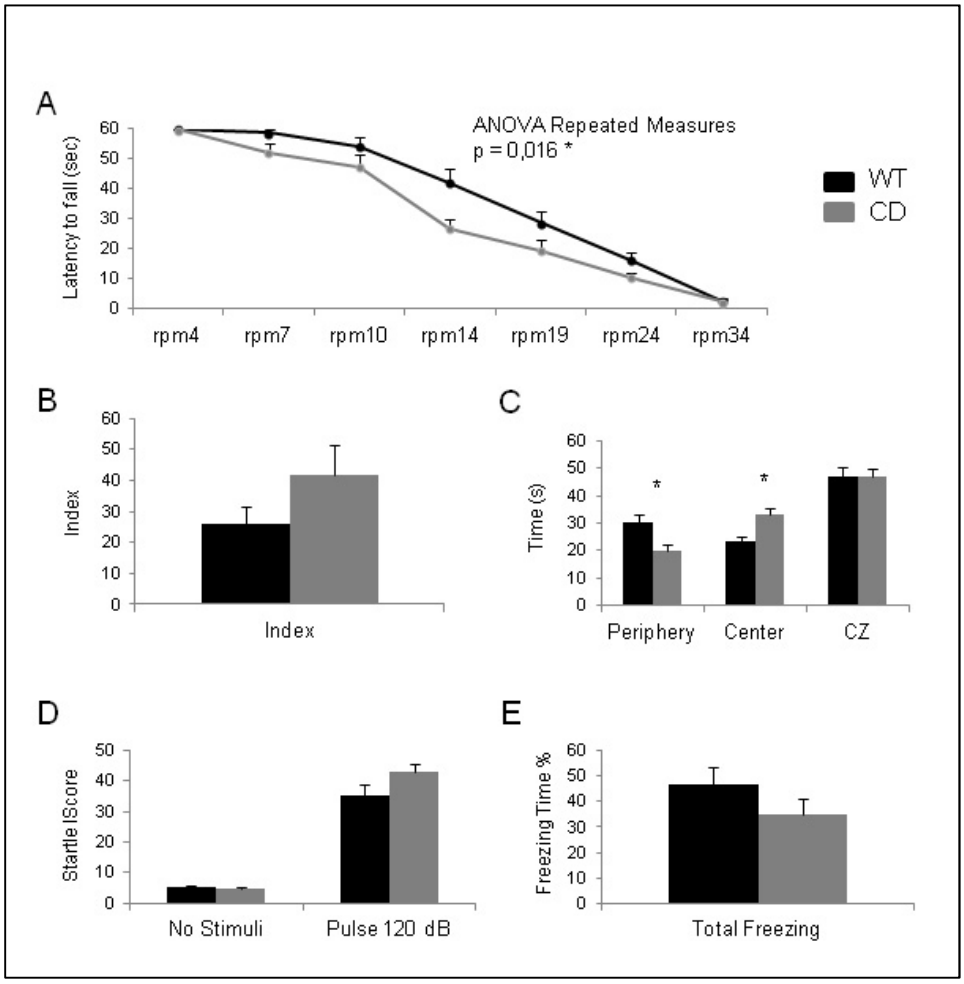

Figure 6. Behavioral analysis of the CD model. A: Rotarod test, latency to fall. B: Cued session of the Water Maze test. C: Object recognition test, index of discrimination D: Startle response test, startle score. E: Fear conditioning test. Results represent the mean ± SD in all cases (N= 15).

the cued session , with CD animals showing a reduced thigmotaxic behavior spending more time in the center or the critical zone of the pool (Figure 6C). The same tendency was observed in the Gallagher measure and the Whishaw corridor test (data not shown), where the CD animals have a better searching strategy with a reduced distance and an increased permanence in the direct path to the platform, respectively, pointing to a reduction in the anxiety behavior.

We evaluated the auditory response using the startle response test, as hyperacusia is present in 90% of WBS patients [29]. We could see a tendency to an increased startle response in the CD mouse model at 120 dB, which could be related to a hyperacusia (Figure 6D). Finally, in the fear conditioning test, a tendency was found to a reduction in the freezing time after the conditionate stimulus in the CD model (Figure 6E).

DISCUSSION

Williams-Beuren syndrome is a complex neurodevelopmental disease which has been widely studied for the specific combination of physiological and cognitive deficits that includes. Symptoms include growth abnormalities, cardiovascular, neurological and endocrinological anomalies, as well as characteristic cognitive-behavioral profile [7].

Several strategies have been followed in order to dissect the molecular mechanisms underlying the disease, to establish genotype-phenotype correlations and to identify possible therapeutic targets. To achieve all these goals we have created for the first time a mouse model that mimics the most common deletion found in human patients.

ES cell line array analysis

We have used Affymetrix microarray to acquire a genome-wide view of the gene expression profile induced by altered gene dose of all the genes in the WBS deleted region. It is widely known that undifferentiated ES cells express the majority of genes in an organism. In order to identify altered expressed genes from initial developmental stages we chose an ES cell line from which we obtained the model. The findings are highly consistent among replicates and the rate of validation by qRT-PCR is also high. The Williams-Beuren deleted region in ESSP9 includes 26 genes, 14 of them were analysed in the array. As expected, hemizygously deleted genes at 5G2 presented a reduced expression in WBSCR ES cell with respect to controls, with the exception of *Elastin* and *Mlxipl* that were slightly up regulated.

Alterations in the expression of non-deleted genes in the 2 Mb flanking intervals of the WBS have been reported [30]. We analyzed the expression of both centromeric and telomeric areas of the deletion and found no differences in the expression of these flanking genes, in agreement with the expression results obtained in global expression studies of RNA from three mouse brain regions [19] and also from human lymphoblastoid cell lines [31].

The final number of deregulated genes was 599, 65,7% of them downregulated and the rest upregulated. The number of DEG was similar to the study of Antonell et al in WBS patients, where the total number of DEG was 683 [31].

The most important deregulated pathway was muscle contraction, including 9 DEG. Cardiomyopathy was also present in several pathways, as hyperthropic cardiomyopathy, including genes of the intregrin alpha family (*Itga*) and growth factors (*Tgfb2, Tgfb3* and *Ifg1*).

Early deregulation of these cardiomyopathy pathways could play a role in the increased although no significant cardiovascular parameters observed in the CD model and could relate to the phenotype of WBS patients. The metabolism of vitamin D was also deregulated and could be related to the infantile hypercalcemia present in patients [5]. Several pathways related to lipid digestion, mobilization and transport or fatty acid oxidation were also found, which could have a relation with the increased steatosis observed in the CD model. Finally, a pathway related to axon guidance, with most of the implicated genes presenting an upregulation, could be related to neurocognitive problems present in the model. *Sema4d* is one of the upregulated genes and when binded to its receptor *plexinB1* triggers an inhibitory cascade via *Pi3k* and *Akt* inhibiting microtubule assembly and axon elongation [32]. Moreover, the exposure of rat hippocampal neurons to *Sema4d* resulted in axonal growth cone collapse [33]. Other upregulated genes related to the semaphoring cascade are *Dpysl3*, needed for cytoskeleton remodeling and *Crmp1* expressed in the nervous system and also related to growth cone collapse. Other genes present in these deregulated pathways which could play a role in axon guidance are *Ncam1*, implicated in neurite outgrowth and

Slit2, essential for midline guidance in the forebrain by acting as repulsive signal preventing inappropriate midline crossing by axons. In fact, a previous report on a transcriptome analysis also identified genes involved in axon guidance, neurogenesis and cytoskeleton regulation in neurons as deregulated in WBS patients [31].

General characteristics

The CD mouse model shows reduced body weight from the first and up to 6 months of age, which can be in accordance to the growth delay present in human patient. The reduced body weight can also be found in the DD, PD and D/P mouse models, although in that models the reduced body weight is already significant in the first weeks of life [19]. Regarding the survival of the model, no differences at the age of death are found, as it happens in other published heterozygous models for WBS or in human patients [5, 19]. Most of the animals present lymphomas, accordingly with what is known in the C57BL/6 background [34]. However, differences exist among genotypes, in the CD model a wider variety of tumors exist, including lymphoma, angiosarcoma, lung carcinoma, myeloproliferation and histiocytic sarcoma. Hepatic steatosis is more prevalent, although not significantly, in the CD model, pointing to a possible deregulation in the insulin regulation in these animals. Enlarged endocrines islets are more present in wild-type animals, which is in concordance with the reduced size of the Langerhans islets in the CD model.

Cardiovascular phenotype

Cardiovascular manifestations are one of the hallmarks of WBS and appear in up to 84% of patients, particularly arteriopathy consisting of stenoses of large arteries [35]. Elastin is the gene responsible for the supravalvular aortic stenosis present in most human patients (70%) [36]. Loss of one copy of this gene causes vascular narrowing and chronic activation of the NADPH complex producing hypertension in 40% of patients [37]. The expression of the elastin gene is reduced in heart of the CD mouse model, with a 60% reduction respect the wild-type. However, our mouse model does not present hypertension, although an increase of 17% in the mean arterial pressure at 32 weeks of age is present. In the similar D/P model, also with a reduction in the elastin expression, the reported increase in the arterial pressure is 10.1% at the same age [38]. Previous results in our group reported a whole cardiovascular phenotype for the DD model, with a 47% increase in the arterial pressure at 32 weeks of age. The phenotype also includes cardiac hypertrophy with an increase in the arterial wall thickness and a disorganization and an small increase in the elastin sheets [18]. In the CD model, all these parameters were also studied, showing no significant differences when compared to the wild- type, although a tendency to an increase is present in all parameters, including mean arterial pressure.

NCF1, a gene coding for the p47phox subunit of the NADPH complex, is an important modifier of hypertension in WBS. Patients with a deletion including the loss of one copy of *NCF1* showed less risk of hypertension, via a reduction in the angiotensin II-mediated oxidative stress [16]. Studies in the DD mouse model have shown an increased expression of *Ncf1* by more than 2 fold respect the wild-type. The loss of one copy of the *Ncf1* gene, with the consequent reduction in expression, rescues the cardiovascular phenotype, reducing the arterial pressure and heart weight to wild-type values [18]. In our case, an important reduction of the expression of *Ncf1* exists when comparing our model to the DD model. The CD model presents values comparable to the wild-type or even reduced. Taking all the data into account, the lack of cardiovascular phenotype in the CD mouse could be attributed to the reduced expression of *Ncf1*, confirming the role of this gene as the main modifier for the cardiovascular phenotype in WBS. However, more studied will be needed to

identify which is the mechanism acting in the CD mouse model that reduces the *Ncf1* expression. Our hypothesis is that in the CD model there is the deletion of an enhancer element located in the proximal part of the deletion which reduces the expression of *Ncf1* on the CD model.

Endocrinological phenotype

The endocrinological phenotype in WBS is characterized by the presence of glucose intolerance or diabetes in 75% of patients [8, 39]. Using single knockout mouse models, the endocrinological phenotype has been linked to the distal part of the deletion, by results in two genes, *Mlxipl* and *Stx1a*. The knockout model for *Mlxipl* showed significantly increased basal glucose levels [22]. Moreover, a knockout model for the *Stx1a* gene, which has a role in the 1st phase of insulin release, showed no hyperglycemia but an impairment in the glucose tolerance test with significant higher glucose levels when compared to wild-type animals, and the overexpression of the same gene also presented high glucose levels [23, 40].

In our models, no differences among the genotypes are observed in the basal glucoses levels or the glucose tolerance test, although a nearly significant increase in the basal glucose levels of PD and DD was present. The fact that both the PD and DD levels behave equally, points to a non sufficient role of *Mlxipl* and *Stx1a* in heterozygosis to produce the endocrinological phenotype in WBS. We can hypothesize that genes in the two parts of the deletion contribute to the nearly significant increase of the glucose basal levels in PD and DD. In the DD region the role may belong to the two already known genes. In the PD region, *Gtf2i* may play a role, as glucose related pathways were deregulated in WBS patients but not in patients with partial deletion not including this gene. In addition, the partial deletion pacients did not present glucose intolerance [31]. Another possible implication of *Gtf2i* in glucose regulation comes from the fact that it interacts with DJ-1, a protein which is overexpressed in response to high glucose levels or oxidative stress, present in WBS, and has a role in the protection of the pancreatic beta cells. The presence of DJ-1 makes *Gtf2i* stay in the cytosol and could provoke a transcriptional repression [41]. A certain degree of compensation among the two parts occurs in the CD as it has the same basal levels as the WT.

Regarding the Langerhans islet size, CD animals present a reduced size of the islets compared to the WT animals. The same reduction in the islet area has been seen in diabetes type 2 patients compared to non diabetic subjects, with the concrete loss of alpha and beta cells [42-43]. Glucose and insulin levels in old animals should be studied to determine whether this reduction in the area has long term functional consequences. This reduction could also be related with the fact that the WT animals have a tendency to present enlarged endocrine islets at the end of their lives, as seen in the pathology examination.

Craniofacial phenotype

A characteristic facial appearance is present in all WBS patients as well as definite cranial abnormalities, with a shortened cranial base. Patients have a broad forehead, short upturned nose, strabismus, full cheeks, small jaw and a delicate chin [7, 44]. A retrognathic or a micrognathic mandible and a deficient chin have also been described [45].

In our analysis we used CD females to measure the size and shape of both the skull and the mandible in CD mouse model. We do not see significant differences in the skull, although a tendency to a smaller and flatter nose is present. But a smaller mandible is present in our model, which could recapitulate the micrognathic chin of the human patients. In the partial published models, a shorter skull is present in DD and D/P mouse model, mostly at the posterior and occipital cranial bases, and a normal size appears in PD females and even an

increase in PD males [19]. Differences between the CD and the D/P models could be attributed to the lack of *Limk1* gene in the D/P mouse model, as well as to *in cis* effects in our model that are not acting in the D/P model and could compensate the phenotype.

Neurological phenotype

First insights in the neurological phenotype of WBS came from studies were a reduction in the brain volume around 11-13% was reported [46-47]. Our mouse model recapitulates the reduction in brain weight with an 11% decrease in males and 8% in females. Moreover, multiple abnormalities both structural and functional have been observed in different brain areas, especially in the amygdala, the orbitofrontal cortex and the hippocampus, among others [14, 28, 48-49]. To study these regions, we decided to perform a structural analysis in volume and number of cells in the CD model and also in the PD model, as it has a deletion of the genes in the TFII-I family which have been related to the cognitive abnormalities [20, 24, 50].

A general non significant reduction in CD and increase in PD volumes were appreciated in all the areas, pointing to the role of one or more genes in the DD region which would produce a reduction in the brain volume, in agreement with the published results where the DD and CD models showed a brain reduction but not the PD males [19].

In the amygdala, differences in both volume and number of cells are found between the CD and the PD models. The amygdala is essential for social cognition and fear conditioned learning and studies in humans provide controversial results in this area, where preservation or increase of the volume has been reported as well as an increase in the reactivity [14, 28]. The found differences could impair the function of the amygdala in the CD and the PD models. In the orbitofrontal cortex, differences are observed in the ventral and lateral layer I volumes with a reduction in the CD compared to PD and WT. The orbitofrontal cortex has important connexions with the amygdala and reductions and increases of the volume have been described in human WBS patients, especially reductions in the grey matter [15, 48, 51]. The reduced volume found in the CD model could have a relation with functional abnormalities in the region.

In the hippocampus, differences in volume are found in the dentate gyrus and also in the number of cells in the CA3 region with a reduction of the CD compared to the PD and tendencies to a reduction when compared to the WT. However, an increase in the density of immature Dcx positive neurones was found in the CA3 region of the CD model when comparing with the PD and the WT and a reduction in the length in the CA1 region. The hippocampus presents functional abnormalities in humans with reduced blood flow and synaptic activity [14], which could have a relation with the reduced number of cells and increased number of immature neurons found in the CD model.

Results of increased immature neurons in the CA3 region could be due to a reduced number of mature neurones in the CD model or changes in neurone morphology or size and more studies of neurone morphology will be needed to define this phenotype. Moreover, they indicate a possible role in neurone density in the hippocampus for the genes in the DD region like *Fzd9*, as heterozygous mice for this gene in the DD region have increased apoptotic cell deaths and increased precursor proliferation during hippocampal development, suggesting a role in hippocampal development [52]. However, more studies regarding neuron morphology will be needed to further define the phenotypes in these cerebral regions as well as the relation with the functional abnormalities to establish genotype-phenotype correlations.

Behavioral phenotype

WBS patients present a characteristic behavioral phenotype including motor problems, visuospatial problems, hyperacusia, increased non social anxiety and a definite social phenotype [5, 53]. To evaluate these aspects in the CD model we used a wide battery of tests. Regarding the motor activity, both general and specific tests were performed showing different results. An impaired performance in the CD model was obtained in the Rotarod test, which could be initially related to different causes, including motivation, equilibrium, coordination, learning or muscular tone. Muscular tone could be excluded because of the results in the grip strength, which showed no differences. Equilibrium was also excluded as neurosensorial results in geotaxis and equilibrium were comparable among the genotypes. Results in the wire maneuver pointed to a coordination problem, as CD model performed worse in this test and a learning problem could be also considered. D/P model, which is similar to our model, also presents impaired motor coordination in the Rotarod test, giving more strength to this phenotype [19]. Other mouse models for genes in WBS show motor problems, a reduction in the latency to fall was found in a knockout model for *Gtf2ird1* and also in the PD model, indicating a necessary but not sufficient role of this gene in the motor anomalies [19, 54]. Cerebral areas related to motor coordination should be further studied to determine the origin of this motor difference.

Regarding the anxiety, no differences were found in the open field test in our model. This result is in disagreement with the results obtained in the D/P model were an increased anxiety-related behavior was found, as well as in the PD model [19]. However, no differences were found in other anxiety tests in that model, pointing to a controversial conclusion of the anxiety in WBS mouse models.

Learning and attention were evaluated with different tests and no significant results were obtained in any of them, although interesting tendencies were found. In the object recognition test, a tendency was found in the CD model to better discriminate the novel from the familiar object, pointing to a greater interest in novelty in the CD model. More tests regarding the social phenotype of the model should be performed to better study and define the observed tendency.

The water maze test showed no visuospatial deficits in the model and no differences in adquisition, speed or reversal sessions. However, a significantly different tigmotaxic behavior was found in the CD model, spending more time in the center of the pool, which could be related to the uninhibited behavior found in human patients.

Tendencies were found to a reduction of the freezing in the fear conditioning test. The same tendency to a reduction in fear conditioning was observed in the D/P model, although significance is only achieved in the DD model, indicating a possible compensatory role of the PD region in the test [19]. Interestingly, studies with rats presenting lesions in the basolateral amygdala showed a reduction in the freezing time [55] and studies in humans go in the same direction, pointing to a possible relation of the obtained results with the nearly significant reduction in the number of cells of the basolateral amygdala in the CD model.

Finally, a tendency to an increase in the startle response was found in CD model. In other models, no differences were found for this test in the D/P but a significant increase was found in the PD model [19]. A closer study at the hyperacusia should be performed to verify the phenotype.

In summary, the CD mouse model is the first mouse model presenting the most common WBS deletion and recapitulates most of the phenotypes present in human

patients. The CD model shows a reduced body and brain weight, changes in the Langerhans islets, characteristic changes in several brain regions, motor problems and other behavioral changes related to the human patients. The model lacks the cardiovascular phenotype probably as a consequence of the reduced *Ncf1* expression. This model will be useful for future studies to deepen in the phenotype and to test future possible treatments.

MATERIALS AND METHODS

The study has been performed in accordance with the ARRIVE guidelines, reporting of in vivo experiments (http://www.nc3rs.org/ARRIVE).

Ethics statement. Animal procedures were conducted in strict accordance with the guidelines of the European Communities Directive 86/609/ EEC regulating animal research and were approved by the local Committee of Ethical Animal Experimentation (CEEA-PRBB).

All mice were bred on a majority C57BL/6J background (97%). Tail clipping was performed within 4 weeks of birth to determine the genotype of each mouse using PCR and appropriate primers (Supplemental table 5).

ES cell line: generation, genotyping and cell culture. Vector p856 containing a *PGK-neo* cassette in *Gtf2i* and previously published was used as starting point [24]. *Fkbp6* genomic sequences were cloned by plate hybridization from a lambda genomic library. For insertion of a *loxP* site in the intron five of *Fkbp6* we subcloned upstream and downstream genomic fragments in a plasmid containing the PGK-*hygro* cassette. The resulting final targeting vector, p936, was linearized and electroporated into mouse G6 ES cells [24] and recombinant clones were selected in the presence of Hygromycin. Positive *2loxP* clones were screened for correct homologous recombination by Southern blot using an external probe that recognizes an 11Kb wild-type and 5.2 Kb homologous recombinant *EcoRI* bands. We used FISH analysis to select clones with *in cis* integration of both cassettes. Positive clones were again electroporated with a vector containing Cre-recombinase gene and *Puromicin* resistance gene. Puromicin resistant clones were selected and genotyped by MLPA (multiplex ligation amplification probe). The mix probes used were *Cult-1* and *Wbscr17* as external genes and *Limk1, Stx1a, Fkbp6* and *WBSCR22* from inside the deletion. WBSCR complete deleted clone ESSP9 was chosen for the analysis.

ESSP9 and R1 wild-type cell lines were cultured in standard conditions, Knockout DMEM medium (10829), supplemented with 20% Knockout Serum Replacement for ES cells (10828) both reagents obtained from the GIBCO company (Invitrogen). Penicillin/streptomycin, LIF, no essential aminoacids and β-mercaptoethanol were also added to the medium. Cells were always cultured in a monolayer of feeder cells and maintained at 37ºC in a humidified 5% CO2 chamber.

Mouse embryonic fibroblasts characterization. Mouse embryonic fibroblasts (MEFs) were obtained following the previous described protocol [56]. Briefly, embryos were collected at day E11,5-13,5 and mechanically and chemically disaggregated and genotyped. Cell lines were grown in DMEM+Glutamax 1x medium supplemented with 10% donor bovine serum, 1% penicillin /streptomycin and 0.5% de glutamine. Trypsin-EDTA .25% 1x. and DPBS 1x were used in the cell cultures. All products from Invitrogen. Spontaneous immortalization was carried out following a classical 3T3 protocol [57]. Cell lines characterization followed the established protocols [56] including immortalization, growth curve and saturation rate.

Generation of the complete deletion (CD) mice. *2LoxP* cells were injected into

CD1 morulae generating chimeric mice. Mice transmitting the modified chromosome in the germline were crossed with C57BL/6 mice expressing the Cre-recombinase enzyme. In a second strategy, ESSP9 cell line was used to generate chimeric mice. Animals were crossed until the deletion was germinally transmitted. First mice with the deletion in germinal line were considered F0 and submitted to genotyping by MLPA to confirm the deletion. Mix probes for *Cult-1* and *Whscr17* as external genes and *Gtf2i*, *Rcf2*, *Fkbp6, Stx1a*, *Baz1b* and *Limk1* inside the deletion.

mRNA preparations and microarray hybridizations. mRNA was extracted from ESSP9 and R1 (wild-type) cell lines by using TRIZOL reagent (Invitrogen, Carlsbad, CA, USA), followed by a second extraction using RNeasy (Qiagen) in both cases according to the manufacturer's instructions. Quality of all RNA samples was checked using an Agilent 2100 Bioanalyzer (Agilent Technologies). Only those samples with an RNA Integrity Number (RIN) >7 were used for hybridization. Samples of 500ng/μl were used to perform an Affymetric mouse 430_2 expression array. Images were processed with Microarray Analysis Suite 5.0 (Affymetrix). All samples demonstrated characteristics of high-quality cRNA (3'/5' ratio of probe sets for glyceraldehyde-3-phosphate dehydrogenase and beta-actin of <1.5) and were subjected to subsequent analysis. Raw expression values obtained directly from .CEL files were preprocessed using the RMA method [58], a three-step process which integrates background correction, normalization and summarization of probe values. These normalized values were the basis for all the analysis. Previous to any analysis, data were submitted to non-specific filtering to remove low signal genes (those genes whose mean signal in each group did not exceed a minimum threshold) and low variability genes (those genes whose standard deviation between all samples did not exceed a minimum threshold).

Statistical analysis. The selection of differentially expressed genes between conditions was based on a linear model analysis with empirical Bayes moderation of the variance estimates following the methodology developed by Smyth [59]. The method extends traditional linear model analysis using empirical Bayes methods to combine information from the whole array and every individual gene in order to obtain improved error estimates. These are very useful in microarray data analysis where sample sizes are often small what can lead to erratic error estimates and, in consequence, to untrustful p-values. The analysis yields standard tests statistics such as fold changes, (moderated)-t or p–values which can be used to rank the genes from most to least differentially expressed. In order to deal with the multiple testing issues derived from the fact that many tests (one per gene) are performed simultaneously, p–values were adjusted to obtain strong control over the false discovery rate using the Benjamini and Hochberg method [60].

Bioinformatic pathway definition. Transformation to Ensembl IDs using the DAVID software was performed obtaining 571 genes [61-62]. Over-representation analysis was performed using the CPDB softwares (Release MM8 (1 5.03.2012)) [29-31]. 547 of 599 gene IDs were recognized and pathways were selected for $p < 0.05$ and more than one gene per entity.

cDNA obtention, qPCR experiments and data analysis. To perform qPCR analysis to validate the expression results obtained in the array analysis, 2 μg of the same mRNA used for the array hybridization were used for first-strand cDNA synthesis with Superscript II (Invitrogen). For all the other expression studies, mRNA was extracted from the tissue of interest. Primers and probes were designed to span an intron in all cases using

the Primer3 software Version 0.4.0 [63] (Supplemental table 5). Real-Time PCR was performed using the SYBR Green Ready Master Mix according to the manufacturer's instructions in an ABI PRISM 7900HT Sequence Detection System (Applied Biosystems). The standard curve method was used for the analysis. The results were normalized respect to a housekeeping gene selected for its stable expression among the different cell lines. A reagent-only (no DNA) negative control sample was always included in each run. Experiments were performed a minimum of 2 times in 384-well plates with three replicates per sample. Raw data was obtained using SDS 2.3 software (Applied Biosystems).

Accesion number. The accession number for supporting microarray data is: http://www.ncbi.nlm.nih.gov/geo/query/acc.cgi?token=drstlicyasoiyro&acc=GSE23202

Growh and survival curves. 11 wild-type males, 10 CD males, 16 wild-type females and 16 CD females were used for growth curves. Weight was recorded every month, from 1st to 22nd months of age. 10 females and 12 males for each wild-type and CD groups were used for survival curves. Dead animals were recorded daily and organs were collected when possible for pathology analysis.

Blood pressure measurements. Systolic, mean, and diastolic blood pressure were measured in conscious male mice on three separate occasions by using a tail cuff system (Non-Invasive Blood Pressure System, PanLab), while holding the mice in a black box on a heated stage. In order to improve measurement consistency, multiple sessions were performed to train each mouse. At least 12 readings (4 per session) were made for each mouse (n= 5 per group).

Heart histopathology. Animals were sacrificed at 16-week-old. Immediately following sacrifice, heart and aorta were removed in block and fixed in 10% buffered formalin at 4ºC for 16 hours. Hearts and aorta were dissected, washed, and weighed (wet weight). Hearts and vessels were processed for paraffin embedding. Wall thickness and lamellar units were analyzed using 5 mm cross-sections of the ascending aorta (transected immediately below the level of the brachiocephalic artery) stained with Verhoeff-van Gieson (VVG) to visualize elastic lamina. Wall thickness at 8 different representative locations was measured and averaged by an observer blinded to genotype for each mouse. The number of medial lamellar units (MLUs) at 4 sites was assessed and averaged. These axial cross-sections were imaged with an Olympus BXS1 microscope with epifluorescence and phase-contrast optics equipped with the Olympus DP71 camera, and images were captured with the CellB Digital Imaging system software. MLUs counting and wall thickness were quantified using Adobe Photoshop CS (Adobe Systems).

Langerhans islets analysis. Pancreas from three wild-type and 6 CD mice were obtained after 4% PFA perfusion, embedded and tissues were sectioned at 6μm. Hematoxilin and Eosin staining was performed to illustrate the general islet morphology under light microscopy. All the Langerhans islets of every animal were counted and the area was analysed. Mean value for the islet was obtained when present in more than one section. Islet size was divided in 5 groups for statistical analysis.

Intraperitoneal glucose tolerance test IPGTT. Mice were fasted for 6 hours before experimental procedure were carried out to assay. A drop of tail blood was taken and assayed for basal glucose levels (t=0) using the Accu-Chek Aviva glucometer (Roche). A 2g D-glucose/kg fasting body dose of glucose was injected into the intraperitoneum of the mice and tail blood

was taken at t= 15, 30, 45, 60, 90, 120 min postinjection for glucose measurement

Craniofacial analysis. Craniums were obtained from 15 CD and 15 wild-type females and stored in 100% ethanol. 3D coordinates of 39 cranial and 22 mandible relevant landmarks were recorded using Landmark software and posterior comparisons were performed with the Euclidean distance matrix analysis (EDMA) with the software WinEDMA (version 1.0.1 beta). 3D data was converted into linear distances compiling into a matrix. Both the form difference matrix (FDM) and the size difference matrix (SDM) were analysed.

Histological procedures for brain analysis. Five controls, five CD and four PD mice were perfused transcardially with fixative (4% paraformaldehyde). Brains were removed and placed in fixative. Brains were processed for stereology embedded in glycolmethacrylate (Tecnovit 7100; Heraeus Kulzer, Werheim, Germany) and every other microtomecut section (30_m) was then collected on a noncoated glass slide, stained with Giemsa, and mounted with Entellan New (Merck, Darmstadt, Germany).

*Region and layer boundaries.*We analyzed the amygdala, the orbitofrontal cortex and the hippocampus. These regions were outlined according to the atlas of Paxinos and Watson 2nd edition (2001). The amygdala was further divided in three regions (lateral, basolateral and central), the orbitofrontal cortex in lateral and ventral and each of these in layer I-III based on cell packing and presence. The hippocampus was divided in three areas for the two major subdivisions CA1 and CA3 (stratum oriens, pyramidal layer and stratum radiatum and lucidum) and the dentate gyrus in four areas (granular layer, molecular layer, hilus and polymorphic layer).

Stereological procedures. Volume and neuronal number estimations were performed using StereoInvestigator software (Microbrightfield, Williston, VT) and a camera (DXC-390; Sony, Tokyo, Japan) attached to a motorized microscope Visiopharm Integrator System, Olympus BX51.

Cavalieri's principle was used to assess the volume of each region. Briefly, every second (for amygdala), 8th (for orbitofrontal cortex), and 10th (for hippocampus and dentate gyrus) section was used and its cross-sectional area was estimated by point counting at a final magnification x100. For this we randomly superimposed onto each area a test point grid in which the interpoint distance, at tissue level, was 150x150 for amygdala and hippocampus and 75x75 for orbitofrontal cortex. The volume of the region of interest was calculated from the number of points that fell within its boundaries and the distance between the systematically sampled sections. Average cell numbers were estimated using the optical fractionator method. Briefly, every selected section was measured and the beginning was chosen at a random starting position, a grid of virtual three-dimensional boxes (40x40x20 for amygdala and 20x20x20 for hippocampus, dentate gyrus and orbitofrontal cortex cell containing layers) that were equally spaced (same grid as for the volume estimations) was superimposed within the predefined borders; and neurons were counted whenever their nucleus came into focus within the counting box. Neurons were differentiated from other cells on the basis of nuclear size (larger in neurons than in glia cells), a prominent nucleolus, and the shape of their perikarya caused by dendritic emergence.

Immunohistochemistry. Three adult wild-type, two CD and three PD mice of 12 weeks of age were anesthetized and transcardially perfused with 4% paraformaldehyde in 0.1M phosphate buffer. Brains were removed and postfixed in the same buffer for 24 h at 4°C. Thereafter, they were cryoprotected in 30% sucrose, frozen on dry ice, and sectioned on

a cryostat. Serial coronal or sagittal (40 µm-thick) sections were collected in a cryoprotectant solution (30% glycerol, 30% ethylene glycol, 40% 0.1 M phosphate buffer [pH 7.4]), and every forth section was used. Immunohistochemistry was performed using the ImmunoCruz goat ABC Staining System, Santa Cruz Biotechnology INC (Santa Cruz, USA) following the manufacturer's instructions. Briefly, endogenous peroxidase was blocked with 3% H_2O_2 solution in PBS for 20 min at room temperature and after three rinses with PBS, sections were washed with three consecutive changes of a solution of 0.2% Triton X-100 in PBS for 5 min each time. Sections were blocked for an hour and a half in blocking solution (1.5% blocking serum in PBS) and incubated overnight at 4°C with a goat polyclonal antibody against Doublecortin, a marker of newly formed migrating neurons (Santa Cruz Biotechnology, INC) diluted (1:300) in 1.5% blocking solution. Sections were incubated with a biotinylated secondary antibody following manufacturer's instructions for an hour, and positive signals were developed with a diaminobenzidine substrate by using the avidin-biotin-peroxidase system according to the manufacturer's instructions.

Behavior testing. Behavior testing was performed in the PRBB mouse facility using males, 15 wild-type and 15 CD animals. Testing was performed from the least to the most aversive test: SHIRPA, Rotarod, Object Recognition, Water Maze, Fear Conditioning, Startle Response and Treadmill test.

Neurosensorial characterization (SHIRPA protocol). The Shirpa protocol was performed as previously described [64].

Rotarod. The Rotarod test evaluates motor coordination and balance. The ability of each mouse to maintain balance on a rotating rod (5 cm diameter and 10 cm long) with a plastic dowel surface was assessed with a commercially available rotarod apparatus (Rotarod LE8500, Panlab, Harvard Apparatus, Spain). The equipment consisted of a rotating spindle that is able to maintain a fixed rotational speed (FRS) of 7, 10, 14, 19, 24, or 34 rpm and starting at 4 rpm to accelerate at a constant rate to 40 rpm over a 5-min period. The apparatus is provided with magnetic plates to detect when a mouse has fallen off the rod. Mice were placed on the middle of the rotating rod, its body axis being perpendicular to the rotation axis, and its head against the direction of rotation. All animals were tested for acquisitions and maintenance of rotarod performance. The experimental design consisted of two training trials (criterion test) at the minimum speed (4 rpm) followed by the test session in which motor coordination and balance were assessed by measuring the latency to fall off the rod in consecutive trials with increasing FRS (4, 10, 14, 19, 24, and 34 rpm). Animals were allowed to stay on the rod for a maximum period of 1 min per trial and a resting period of 5 min was left between trials.

Treadmill. The treadmill (Panlab, Harvard Apparatus Spain) consisted of a belt (50 cm long and 20 cm wide) that was varying in terms of speed (5 to 150 cm/s) and slope (0°–45°). At the end of the treadmill, an electrified grid delivered a foot shock (0.6 mA) whenever the mice felt off the belt. The mice were evaluated for eight trials on a single day session, with a cut-off period of 1 min per trial. The order of presentation of the different belt speeds and inclinations was identical for all mice. In the first two trials (Training), the belt speed was set at 5 cm/s and the inclination at 0°. In the following trials (Test), the inclination was increased from 0° to 20° from the horizontal plane, and we applied different speeds (5, 10, 20, 30, 40 and 50 cm/sec). The mice were placed on the top of the already moving belt facing away from the electrified grid and in the direction opposite to the movement of the belt. Thus, to avoid the foot shocks, the mice had to locomote forward. Whenever an animal fell off the

belt, foot shocks were applied for a maximal duration of 1 s and with an interval of 2 s between every shock. After the shocks, the mice were retrieved and placed back on the still moving belt to facilitate the association between safety and the belt.

Object Recognition. The novel object recognition task is based on the innate tendency of rodents to differentially explore novel objects over familiar ones. The day before the experiment a 10 minutes session (the habituation phase) was performed in the open field box (OF) with two equal objects, but with the same preference. 24 h later, a testing session composed by two trials was carried out. In the first trial (the familiarization phase) the animals were presented with the same two objects until they had explored the objects during 20 sec, in a maximum period of 10 min. The exploration of the objects is considered as any investigative behaviour (head orientation, or sniffing occurring) or deliberate contact that occurred with each object in a distance < or = 2 cm or when touching with the nose. The animals that did not explore the object within 10 min were excluded from the experiment. In the second trial (the test phase), performed 1h later, one of the familiar objects was changed for another new, and the animals were left in the OF during 5 min. The exploration time for the familiar (TF) or the new object (TN) during the test phase was recorded. Memory was operationally defined by the discrimination index for the novel object (DI) as the proportion of time animals spent investigating the novel object minus the proportion spent investigating the familiar one in the testing period [Discrimination Index, DI = (Novel Object Exploration Time/Total Exploration Time) – (Familiar Object Exploration Time/Total Exploration Time) X 100]. We also register activity parameters such speed, distance and the time spent in the center and the periphery of the apparatus. To control for odour cues, the OF arena and the objects were thoroughly cleaned with 90% ethanol, dried, and ventilated for a few minutes between mice.

Water Maze performance. Animals were tested in a visuo-spatial learning acquisition paradigm in the Water Maze test (WM). In the WM mice have to form an allocentric map to find the position of the hidden platform, helped by external cues around the pool. Mice were tested over 10 days (4 trials/session, 10-min inter-trial intervals). The water maze consisted of a circular pool (diameter, 1.20 m; height, 0.25 m). It was filled with tepid water (24°C) opacified by the addition of non-noxious white ink (Abacus SCCL, Spain). A white escape platform (10 cm diameter, height 24 cm) was located 1 cm below the water surface in a fixed position (NE quadrant, 22 cm away from the wall). The maze was surrounded by white curtains with black patterns affixed, to provide an arrangement of spatial cues. First, we performed a pre-training session in which the platform was visible in the center (day 1), followed by 10 acquisition sessions during which the platform was submerged 2 cm below the water (days 2-11). The platform was placed in a fixed position in the center of the northeast quadrant. In each trial, mice were placed at one of the starting locations in random order [north, south, east, west (N, S, E, W), including permutations of the four starting points per session] and were allowed to swim until they located the platform. Mice failing to find the platform within 60 s were placed on it for 20 s (the same period of time as the successful animals). At the end of every trial the mice were allowed to dry for 15 min in a heated enclosure and returned to their home cage. The acquisition was followed by a removal session (day 12) in which the platform was removed and the retention of the task was measured, and by a cue session (day 13) in which the external cues was removed and an intra-cue was introduced above the water, in the platform location. Finally, we performed two reversal session (day 14 and 15) in which the position of the platform is changed to the opposite quadrant (SW) and

the mice have to forget the previous localization and learn a new one. Escape latencies, length of the swimming paths and swimming speed for each animal and trial were monitored and computed by a software tracking system SMART© (Panlab, Harvard Apparatus, Spain) connected to a video camera placed above the pool.

Pure Contextual Fear Conditioning. Pure contextual fear conditioning paradigm was performed by pairing an initially neutral context (CS, conditioned stimulus) with an aversive stimulus such as an electric foot shock (US, unconditioned stimulus) to elicit a freezing response, a reliable measure of conditioned fear in rodents. The experimental procedure was performed in a metal cage (20cm x 20cm x 25 cm) with a grid floor connected to a shock generator, inside a sound-attenuating box and freezing behavior, defined as lack of movement except for respiration for at least 2 sec, was automatically recorded by using Startlefreezing software (Panlab, Harvard Apparatus Spain). On the first day (day 0) animals were placed in the testing chamber for a 3 min habituation session. Twenty four hours later (day 1) they were trained in the same chamber in a single 5 min session composed of 2 min exploration, for basal freezing records, followed by 5 US presentations (foot shock: 2 sec, 0.2 mA), separated by a variable inter-trial interval, (ITI, 15-60 sec); mice remained in the chamber for 30 sec following the last US presentation. Freezing behavior was measured during 15 sec after each shock. Data are reported as percent of freezing time, dividing the absolute freezing time by the total time analyzed for each session, averaged for genotype. Data were analyzed with one-way ANOVA for genotype during each testing day and with repeated measures along the different days of test.

Acoustic Startle response. The acoustic startle response was measured with Panlab startle response apparatus (Panlab, Harvard Apparatus Spain). Each mouse was handled for 2 days before the experiment and was habituated to the equipment by being introduced to the restraint device associated with the apparatus. The mice were given 15 min habituation to the apparatus and then exposed to a single 120 dB pulse in a single session. The startle response was recorded for 65 ms.

ACKNOWLEDGEMENTS

The authors gratefully acknowledge Verena Terrado for technical assistance, Thais Freitas for her help in the brain doublecortin analysis and José Miguel Pêgo for the help with the microscope analysis. This work was supported by grants from the Spanish Ministry of Health (FIS 04/0433, to VC), and the VI Framework Programme of the European Union (LSHG-CT-2006-037627, to LAP-J). MS-P was supported by CIBERER and UPF Fellowships. VC is a FIS Investigator.

REFERENCES

1. Stromme, P., P.G. Bjornstad, and K. Ramstad, *Prevalence estimation of Williams syndrome.* J Child Neurol, 2002. 17(4): p. 269-71.
2. Schubert, C., *The genomic basis of the Williams-Beuren syndrome.* Cell Mol Life Sci, 2009. 66(7): p. 1178-97.
3. Bayes, M., et al., *Mutational mechanisms of Williams-Beuren syndrome deletions.* Am J Hum Genet, 2003. 73(1): p. 131-51.
4. Peoples, R., et al., *A physical map, including a BAC/PAC clone contig, of the Williams-Beuren syndrome--deletion region at 7q11.23.* Am J Hum Genet, 2000. 66(1): p. 47-68.
5. Pober, B.R., *Williams-Beuren syndrome.* N Engl J Med, 2010. 362(3): p. 239-52.
6. Wessel, A., et al., *[Arterial hypertension and blood pressure profile in patients with Williams-Beuren syndrome].* Z Kardiol, 1997. 86(4): p. 251-7.
7. Morris, C.A. and C.B. Mervis, *Williams syndrome and related disorders.* Annu Rev Genomics Hum Genet, 2000. 1: p. 461-84.
8. Pober, B.R., et al., *High prevalence of diabetes and pre-diabetes in adults with Williams syndrome.*

Am J Med Genet C Semin Med Genet, 2010. 154C(2): p. 291-8.
9. Morris, C.A., et al., *Natural history of Williams syndrome: physical characteristics.* J Pediatr, 1988. 113(2): p. 318-26.
10. Martens, M.A., S.J. Wilson, and D.C. Reutens, *Research Review: Williams syndrome: a critical review of the cognitive, behavioral, and neuroanatomical phenotype.* J Child Psychol Psychiatry, 2008. 49(6): p. 576-608.
11. Mervis, C.B., et al., *The Williams syndrome cognitive profile.* Brain Cogn, 2000. 44(3): p. 604-28.
12. Dilts, C.V., C.A. Morris, and C.O. Leonard, *Hypothesis for development of a behavioral phenotype in Williams syndrome.* Am J Med Genet Suppl, 1990. 6: p. 126-31.
13. Gagliardi, C., et al., *Evolution of neurologic features in Williams syndrome.* Pediatr Neurol, 2007. 36(5): p. 301-6.
14. Jackowski, A.P., et al., *Brain abnormalities in Williams syndrome: a review of structural and functional magnetic resonance imaging findings.* Eur J Paediatr Neurol, 2009. 13(4): p. 305-16.
15. Meyer-Lindenberg, A., et al., *Neural basis of genetically determined visuospatial construction deficit in Williams syndrome.* Neuron, 2004. 43(5): p. 623-31.
16. Del Campo, M., et al., *Hemizygosity at the NCF1 gene in patients with Williams-Beuren syndrome decreases their risk of hypertension.* Am J Hum Genet, 2006. 78(4): p. 533-42.
17. Metcalfe, K., et al., *Elastin: mutational spectrum in supravalvular aortic stenosis.* Eur J Hum Genet, 2000. 8(12): p. 955-63.
18. Campuzano, V., et al., *Reduction of NADPH-oxidase activity ameliorates the cardiovascular phenotype in a mouse model of Williams-Beuren Syndrome.* PLoS Genet, 2012. 8(2): p. e1002458.
19. Li, H.H., et al., *Induced chromosome deletions cause hypersociability and other features of Williams-Beuren Syndrome in Mice.* EMBO Molecular Medicine, 2009. 1: p. 50-65.
20. Antonell, A., et al., *Partial 7q11.23 deletions further implicate GTF2I and GTF2IRD1 as the main genes responsible for the Williams-Beuren syndrome neurocognitive profile.* J Med Genet, 2010. 47(5): p. 312-20.
21. Edelmann, L., et al., *An atypical deletion of the Williams-Beuren syndrome interval implicates genes associated with defective visuospatial processing and autism.* J Med Genet, 2007. 44(2): p. 136-43.
22. Iizuka, K., et al., *Deficiency of carbohydrate response element-binding protein (ChREBP) reduces lipogenesis as well as glycolysis.* Proc Natl Acad Sci U S A, 2004. 101(19): p. 7281-6.
23. Ohara-Imaizumi, M., et al., *Imaging analysis reveals mechanistic differences between first- and second-phase insulin exocytosis.* J Cell Biol, 2007. 177(4): p. 695-705.
24. Lucena, J., et al., *Essential role of the N-terminal region of TFII-I in viability and behavior.* BMC Med Genet, 2010. 11(1): p. 61.
25. Meyer-Lindenberg, A., et al., *Functional, structural, and metabolic abnormalities of the hippocampal formation in Williams syndrome.* J Clin Invest, 2005. 115(7): p. 1888-95.
26. Martens, M.A., et al., *Approachability and the amygdala: insights from Williams syndrome.* Neuropsychologia, 2009. 47(12): p. 2446-53.
27. Avery, S.N., et al., *White matter integrity deficits in prefrontal-amygdala pathways in Williams syndrome.* Neuroimage, 2012. 59(2): p. 887-94.
28. Capitao, L., et al., *MRI amygdala volume in Williams Syndrome.* Res Dev Disabil, 2011. 32(6): p. 2767-72.
29. Marler, J.A., et al., *Sensorineural hearing loss in children and adults with Williams syndrome.* Am J Med Genet A, 2005. 138(4): p. 318-27.
30. Merla, G., et al., *Submicroscopic deletion in patients with Williams-Beuren syndrome influences expression levels of the nonhemizygous flanking genes.* Am J Hum Genet, 2006. 79(2): p. 332-41.
31. Antonell, A., M. Vilardell, and L.A. Perez Jurado, *Transcriptome profile in Williams-Beuren syndrome lymphoblast cells reveals gene pathways implicated in glucose intolerance and visuospatial construction deficits.* Hum Genet, 2010.
32. Zhou, Y., R.A. Gunput, and R.J. Pasterkamp, *Semaphorin signaling: progress made and promises ahead.* Trends Biochem Sci, 2008. 33(4): p. 161-70.

33. Swiercz, J.M., et al., *Plexin-B1 directly interacts with PDZ-RhoGEF/LARG to regulate RhoA and growth cone morphology.* Neuron, 2002. 35(1): p. 51-63.
34. Blackwell, B.N., et al., *Longevity, body weight, and neoplasia in ad libitum-fed and diet-restricted C57BL6 mice fed NIH-31 open formula diet.* Toxicol Pathol, 1995. 23(5): p. 570-82.
35. Pober, B.R., M. Johnson, and Z. Urban, *Mechanisms and treatment of cardiovascular disease in Williams-Beuren syndrome.* J Clin Invest, 2008. 118(5): p. 1606-15.
36. Tassabehji, M., et al., *Elastin: genomic structure and point mutations in patients with supravalvular aortic stenosis.* Hum Mol Genet, 1997. 6(7): p. 1029-36.
37. Broder, K., et al., *Elevated ambulatory blood pressure in 20 subjects with Williams syndrome.* Am J Med Genet, 1999. 83(5): p. 356-60.
38. Goergen, C.J., et al., *Induced Chromosome Deletion in a Williams-Beuren Syndrome Mouse Model Causes Cardiovascular Abnormalities.* J Vasc Res, 2010. 48(2): p. 119-129.
39. Cherniske, E.M., et al., *Multisystem study of 20 older adults with Williams syndrome.* Am J Med Genet A, 2004. 131(3): p. 255-64.
40. Lam, P.P., et al., *Transgenic mouse overexpressing syntaxin-1A as a diabetes model.* Diabetes, 2005. 54(9): p. 2744-54.
41. Inberg, A. and M. Linial, *Protection of pancreatic beta-cells from various stress conditions is mediated by DJ-1.* J Biol Chem, 2010. 285(33): p. 25686-98.
42. Kilimnik, G., et al., *Altered islet composition and disproportionate loss of large islets in patients with type 2 diabetes.* PLoS One, 2011. 6(11): p. e27445.
43. Deng, S., et al., *Structural and functional abnormalities in the islets isolated from type 2 diabetic subjects.* Diabetes, 2004. 53(3): p. 624-32.
44. Axelsson, S., et al., *Neurocranial morphology and growth in Williams syndrome.* Eur J Orthod, 2005. 27(1): p. 32-47.
45. Mass, E. and L. Belostoky, *Craniofacial morphology of children with Williams syndrome.* Cleft Palate Craniofac J, 1993. 30(3): p. 343-9.
46. Galaburda, A.M., et al., *Williams syndrome: neuronal size and neuronal-packing density in primary visual cortex.* Arch Neurol, 2002. 59(9): p. 1461-7.
47. Reiss, A.L., et al., *An experiment of nature: brain anatomy parallels cognition and behavior in Williams syndrome.* J Neurosci, 2004. 24(21): p. 5009-15.
48. Chiang, M.C., et al., *3D pattern of brain abnormalities in Williams syndrome visualized using tensor-based morphometry.* Neuroimage, 2007. 36(4): p. 1096-109.
49. Hocking, D.R., J.L. Bradshaw, and N.J. Rinehart, *Fronto-parietal and cerebellar contributions to motor dysfunction in Williams syndrome: a review and future directions.* Neurosci Biobehav Rev, 2008. 32(3): p. 497-507.
50. Enkhmandakh, B., et al., *Essential functions of the Williams-Beuren syndrome-associated TFII-I genes in embryonic development.* Proc Natl Acad Sci U S A, 2009. 106(1): p. 181-6.
51. Eckert, M.A., et al., *To modulate or not to modulate: differing results in uniquely shaped Williams syndrome brains.* Neuroimage, 2006. 32(3): p. 1001-7.
52. Zhao, C., et al., *Hippocampal and visuospatial learning defects in mice with a deletion of frizzled 9, a gene in the Williams syndrome deletion interval.* Development, 2005. 132(12): p. 2917-27.
53. Morris, C.A., *The behavioral phenotype of Williams syndrome: A recognizable pattern of neurodevelopment.* Am J Med Genet C Semin Med Genet, 2010. 154C(4): p. 427-31.
54. Howard, M.L., et al., *Mutation of Gtf2ird1 from the Williams-Beuren syndrome critical region results in facial dysplasia, motor dysfunction, and altered vocalisations.* Neurobiol Dis, 2011.
55. Power, A.E. and J.L. McGaugh, *Cholinergic activation of the basolateral amygdala regulates unlearned freezing behavior in rats.* Behav Brain Res, 2002. 134(1-2): p. 307-15.
56. Pantoja, C. and M. Serrano, *Murine fibroblasts lacking p21 undergo senescence and are resistant to transformation by oncogenic Ras.* Oncogene, 1999. 18(35): p. 4974-82.
57. Todaro, G.J. and H. Green, *Simian virus 40 transformation and the period of cellular*

deoxyribonucleic acid synthesis. J Virol, 1967. 1(1): p. 115-9.
58. Irizarry, R.A., et al., *Exploration, normalization, and summaries of high density oligonucleotide array probe level data.* Biostatistics, 2003. 4(2): p. 249-64.
59. Smyth, G.K., *Linear models and empirical bayes methods for assessing differential expression in microarray experiments.* Stat Appl Genet Mol Biol, 2004. 3: p. Article3.
60. Benjamini Y., H.Y., *Controlling the false discovery rate: A practical and powerful approach to multiple testing.* Journal of the Royal Statistical Society. Series B (Methodological), 1995. 57(1): p. 289-300.
61. Huang da, W., B.T. Sherman, and R.A. Lempicki, *Systematic and integrative analysis of large gene lists using DAVID bioinformatics resources.* Nat Protoc, 2009. 4(1): p. 44-57.
62. Dennis, G., Jr., et al., *DAVID: Database for Annotation, Visualization, and Integrated Discovery.* Genome Biol, 2003. 4(5): p. P3.
63. Rozen, S. and H. Skaletsky, *Primer3 on the WWW for general users and for biologist programmers.* Methods Mol Biol, 2000. 132: p. 365-86.
64. Rogers, D.C., et al., *Behavioral and functional analysis of mouse phenotype: SHIRPA, a proposed protocol for comprehensive phenotype assessment.* Mamm Genome, 1997. 8(10): p. 711-3.

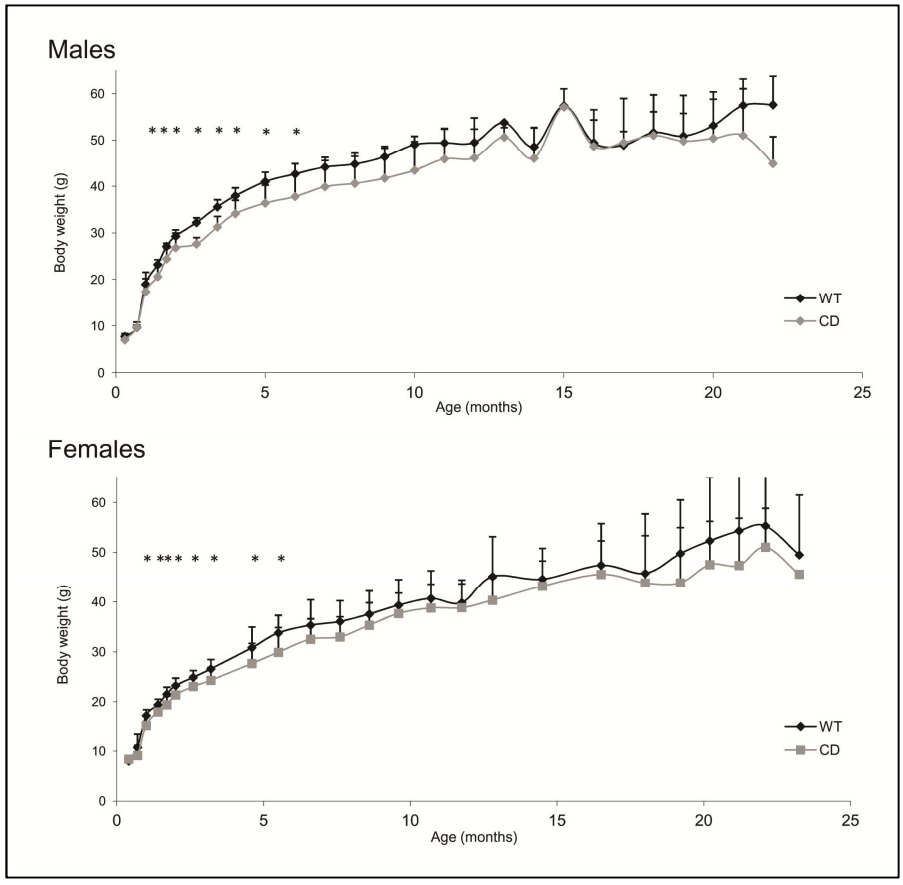

Supplemental figure 1. Growth curves of CD and WT animals indicating body weight reduction in males and females. *p=0.05 (N=4-16).

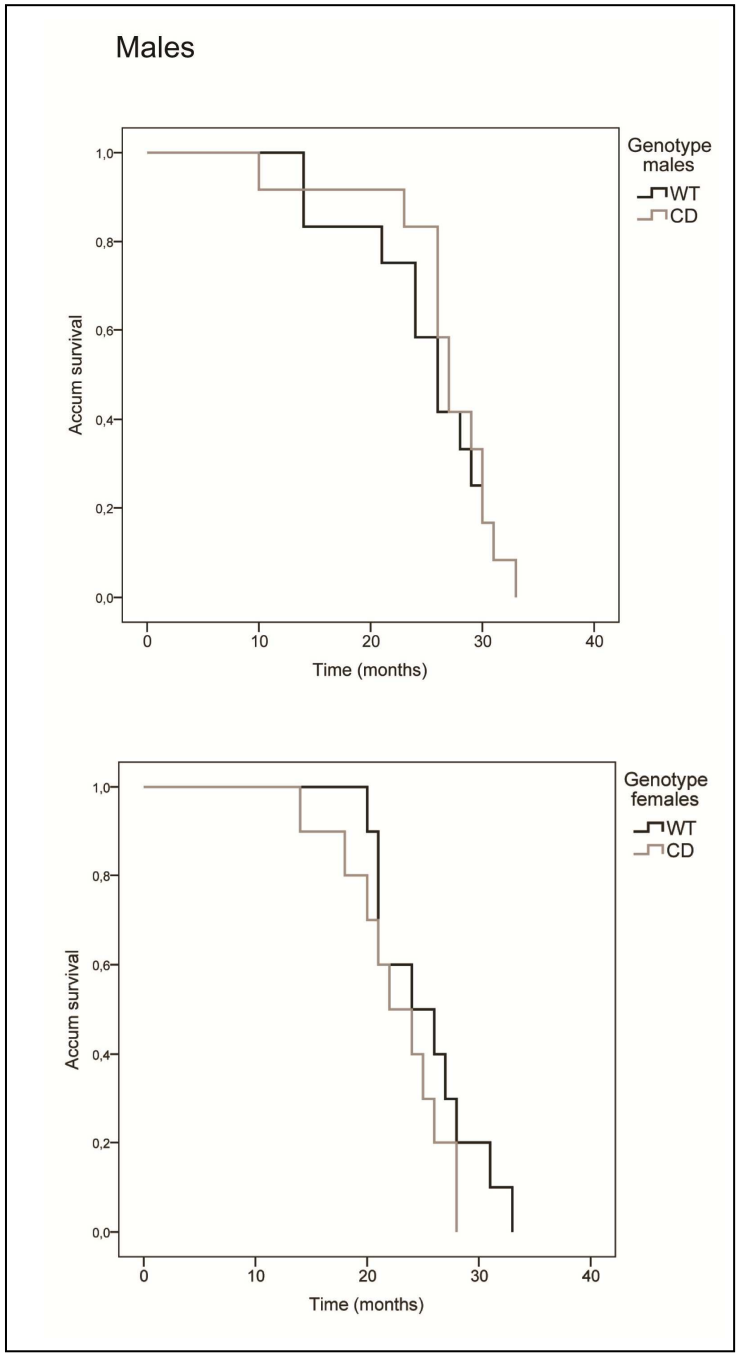

Supplemental figure 2. Acumulated survival representation for males and females. (n=10 males and 12 females per group). In males the two genotypes are superimposed from 30th month. Log rank, Breslow and Tarone-Ware analysis showed no significant differences among genotypes.

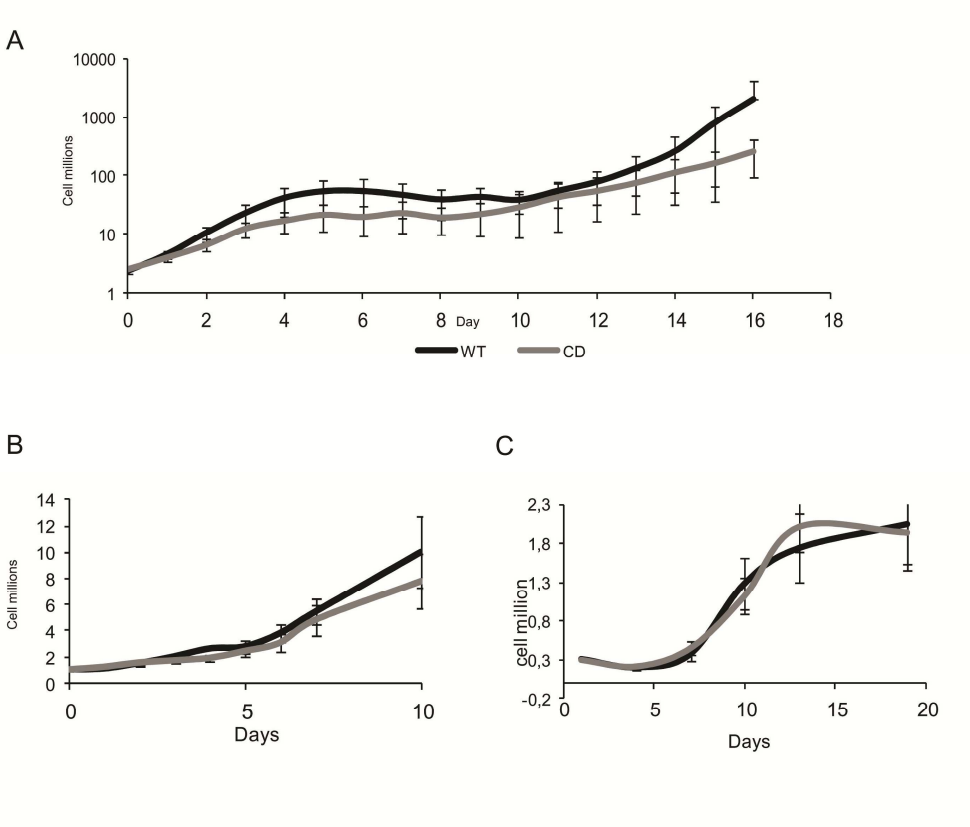

Supplemental figure 3. Mouse embryonic fibroblast characterization. A: Immortalization curve. B: Growth curve. C: Saturation curve. No differences among genotypes are found in any of the analysis. N=10

p-value	Pathway
0.00014	Smooth Muscle Contraction
0.00043	Muscle contraction
0.00046	Focal adhesion
0.00057	ECM-receptor interaction
0.00058	Dilated cardiomyopathy
0.00065	Hypertrophic cardiomyopathy (HCM)
0.00074	Protein digestion and absorption
0.00104	Superpathway of serine and glycine biosynthesis I
0.00137	Platelet degranulation
0.00146	Hemostasis
0.00208	Fanconi anemia pathway
0.00278	Integrin cell surface interactions
0.00320	Response to elevated platelet cytosolic Ca2+
0.003471	Arrhythmogenic right ventricular cardiomyopathy (ARVC)
0.004269	Aminoacyl-tRNA biosynthesis
0.00443	Amoebiasis
0.00493	Colorectal cancer
0.00493	Vascular smooth muscle contraction
0.00503	Alpha-Linolenic acid metabolism
0.00656	Toxoplasmosis
0.00723	Cell surface interactions at the vascular wall
0.00728	Serine biosynthesis
0.00804	Lysine degradation II
0.00806	Platelet activation, signaling and aggregation
0.00846	tRNA charging pathway
0.00846	Pathways in cancer
0.00938	Pyruvate metabolism
0.01049	Aldosterone-regulated sodium reabsorption
0.01049	Tetrapyrrole biosynthesis II
0.0118	Basigin interactions
0.0118	Fatty acid β-oxidation I
0.0118	PPAR signaling pathway
0.01208	Repair synthesis of patch ~27-30 bases long by DNA polymerase
0.01246	Repair synthesis for gap-filling by DNA polymerase in TC-NER
0.01246	Histidine degradation III
0.01384	Vitamin D (calciferol) metabolism
0.01629	PRPP biosynthesis I

p-value	Pathway
0.01701	Glycerophospholipid metabolism
0.01959	Gap-filling DNA repair synthesis and ligation in GG-NER
0.02031	Gap-filling DNA repair synthesis and ligation in TC-NER
0.02041	Lipid digestion, mobilization, and transport
0.02130	Type I hemidesmosome assembly
0.02306	Fatty acid β-oxidation II (core pathway)
0.02536	Proximal tubule bicarbonate reclamation
0.02650	Ether lipid metabolism
0.02687	Glycerolipid metabolism
0.02687	Vitamin B6 metabolism
0.02855	Metabolic pathways
0.02998	Telomere C-strand (Lagging Strand) Synthesis
0.03120	Glycine, serine and threonine metabolism
0.03194	Heme biosynthesis
0.03194	Heme biosynthesis II
0.03295	Metabolism of porphyrins
0.03477	Axon guidance
0.03553	tRNA Aminoacylation
0.03553	Extension of Telomeres
0.03812	Sema4D induced cell migration and growth-cone collapse
0.03909	(deoxy)ribose phosphate degradation
0.03909	Developmental Biology
0.03932	Biosynthesis of unsaturated fatty acids
0.03950	Cytosolic tRNA aminoacylation
0.03950	TGF-beta signaling pathway
0.04363	Telomere Maintenance
0.04424	Chromosome Maintenance
0.04650	Striated Muscle Contraction
0.04650	Hormone-sensitive lipase (HSL)-mediated triacylglycerol hydrolysis
0.04650	folate transformations I
0.04749	Semaphorin interactions
0.04749	Metabolism of lipids and lipoproteins
0.04984	Regulation of KIT signaling
0.04650	Bile salt and organic anion SLC transporters
0.04650	CDP-diacylglycerol biosynthesis II
0.04749	Homologous recombination
0.04749	NCAM1 interactions
0.04984	Regulation of actin cytoskeleton

Supplemental table 1. Complete list of deregulated pathways in the over-representation analysis of the CPDB software.

Tumors	CD (15)	WT (7)	% CD	% WT
Lymphoma	13	6	87	86
Hepatocellular Adenoma	1	2	7	29
Angiosarcoma	1	0	7	0
Lung Carcinoma / Adenoma	2	0	13	0
Myeloproliferation	2	0	13	0
Histiocytic sarcoma	2	0	13	0
Glioblastoma	0	1	0	14

Other	CD (15)	WT (7)	% CD	% WT
Enlarged endocrine islets	4	3	27	43
Arteritis	1	1	7	14
Steatosis	7	2	47	29
Chronic nephropathy	5	2	33	29
Degenerative cardiomyocytes	6	4	40	57
Distended ventricles	4	2	27	29

Supplemental table 2. Pathological analysis of the survival curve animals.

Animals	%Heart weight/ Body weight	p value
WT young (n=16)	0,6062 ± 0,045	0,9100
CD young (n=14)	0,6012 ± 0,06	
WT old (n=25)	0,4829 ± 0,048	0,7400
CD old (n=17)	0,4957 ± 0,051	

Supplemental table 3. Percentage of heart to body ratio in young and old animals. Results represent the mean ± SD in all cases . No significant results were found in the t test.

Motricity tonus strength	WT mean	CD mean	p value
Wire maneuver	0,4 ± 0,2	2,7 ± 0,6	0,001
Hindlimb tone	0,4 ± 0,2	1,3 ± 0,3	0,01

Supplemental table 4. Wire maneuver and hindlimb tone results. Wire maneuver: 0= Grasp 2 HindPaws / 1= Grasp 1 HP / 2=Fall >15s / 3= Fall >5s / 4=Fall <5s / 5=Unable to grasp. Hindlimb tone: 0=Marked /1=Moderate / 2=Slight / 3=None.

Use	Gene name	Sequence (5'→3')	Amplicon size	Location	Tm
MLPA	Gtf2i L	gggttccctaagggttgga//gaatcatggcccaagtagtgatgtctgcct	101	exon 2	87,08
	Gtf2i R	tgcctgccgaagatgaagagtcttcagag//tctagattggatcttgctggcac		exon 2	85,64
	Cyln L	gggttccctaagggttgga//ctaatccacaaggtcatccgaattggcttccca	111	exon 5	88,22
	Cyln R	tccaccagtccagccaaggccaagaagaccaaacgc//tctagattggatcttgctggcac		exon 5	90,46
	Rfc2 L	gggttccctaagggttgga//gccctcaggagaaccatggaaatctactcgaagacg	116	exon 6	88,96
	Rfc2 R	cttcgcccttgcttgtaatgcttcggataagatcatcg//tctagattggatcttgctggcac		exon 6	86,83
	Baz1b L	gggttccctaagggttgga//gctgaggaaagatacagtgaacgcatttggacgtgtaagag	114	exon 2	87,47
	Baz1b R	ggaagcagtcagctaacacacaaggagctgac//tctagattggatcttgctggca		exon 2	86,19
	Limk1 L	gggttccctaagggttgga//cgagtgcatgaggttgacgctactttgttgcacc	104	exon 1	88,98
	Limk1 R	tggagggaagaacgtatgggagaggaag//tctagattggatcttgctggcac		exon 1	85,61
	Fkbp6 L	gggttccctaagggttgga//ccggcgttatatcaaggccctcttcaggtgtggaca	113	exon 6	90,59
	Fkbp6 R	ggtgagttgagggtagtgggggagatcgcgactgacg//tctagcttccatcttgctggca		intron 6	91,11
	Cutl1 F	gggttccctaagggttgga//caaaggaccattaagcccaatctatgtc	99	exon 24	83,84
	Cutl1 R	gtgttttcaaggaagaaaacggaaatgtg//tctacattggatcttgctggcac		exon 24	83,07
	Wbscr17 L	gggttccctaagggttgga//gatcggggtgttgtttgatggcttcactgaggagagtcaaa	118	exon 1	89,88
	Wbscr17 R	tgttggtgttgaacttgatcgcggttgctgactgtac//tctagattggatcttgctggc		exon 1	86,67
Genotyping CD	Hprt L	ctctgaggcttcaaaggttc	302	cassette	60,6
	Hprt R	aatccagcttgtttgggcta		cassette	63,4
Genotyping PD	UF8497	tccaggagcttatgaatgacc	As used in Li et al, 2009		62,9
	UF8494	tttctgtggggcaaaatgta			62,8
qPCR	Baz1b L	cagaaaacgctaggtgcaaag	99	exon 14	63,7
	Baz1b R	tcagacagaacaggtggaagg		exon 15	64,3
	Eln L	tcccggtggagtctattatcc	92	exon 2	63,8
	Eln R	ctggcttaggtggttttcctc		exon 4	63,7
	Gtf2i L	ccccagttacctggagatca	275	exon 31	63,8
	Gtf2i R	acactggacgaacctggaga		exon 34-35	64,8
	Limk1 L	cctacctccattcgatgaaca	262	exon 12	63,7
	Limk1 R	ccaaaggaaaacacgtccac		exon 14	64,2
	Rfc2 L	gcactgaacaacctgcagtc	241	exon 8	63,6
	Rfc2 R	agtatttcagccatcgggaag		exon 10	62,9
	Gtf2ird1 L	cccagatgacatcccctttc	344	exon 30	64,3
	Gtf2ird1 R	gagatctggttggtggatgc		exon 32	64,5
	Ncf1 L	tccctgcatcctatctggag	169	exon 7	64,1
	Ncf1 R	tccaggagcttatgaatgacc		exon 8	62,8
	Rps28 L	tagggtaaccaaagtgctggg	103	exon 1-2	67,9
	Rps28 R	gacatttcggatgatagagcg		exon 3	66,6

Supplemental table 5. Primers list.

CHAPTER 4

TFII-I regulates target genes in the PI-3K and TGF-β signaling pathways through a novel DNA binding motif

Maria Segura-Puimedon, Luis A Pérez-Jurado, Victoria Campuzano

Submitted to BBA – Gene Regulatory Mechanisms

TFII-I is a transcription factor encoded by the *Gtf2i* gene, which is deleted in Williams-Beuren syndrome, a neurodevelopmental disorder caused by a 1,5Mb deletion at 7a11.23. Studies in patients and mouse models have related *Gtf2i* with the cranial and cognitive abnormalities of the syndrome.

Previous work from the group identified the hippocampus and cortex as affected areas in the *Gtf2i*$^{\Delta ex2}$. We have performed array expression analysis in these affected areas and in ES cells mutant for *Gtf2i*. We have been able to identify new target genes for Gtf2i trough the discovery of a highly conserved binding motif. Genes bearing this motif are implicated in pathways such as PI3K, TGFβ signaling and glycolysis, providing new clues for the implication of *Gtf2i* to WBS phenotype and new target genes for future treatments and studies.
.

TFII-I regulates target genes in the PI-3K and TGF-β signaling pathways through a novel DNA binding motif

Segura-Puimedon M, Pérez-Jurado LA, and Campuzano V

ABSTRACT

BACKGROUND: General transcription factor (TFII-I) is a multi-functional protein involved in the transcriptional regulation of critical developmental genes, encoded by the GTF2I gene located on chromosome 7q11.23. . Haploinsufficiency at *GTF2I* has been shown to play a major role in the neurodevelopmental features of Williams-Beuren syndrome (WBS). Identification of genes regulated by TFII-I is thus critical to detect molecular determinants of WBS as well as to identify potential new targets for specific pharmacological interventions, which are currently absent.

METHODOLOGY / PRINCIPAL FINDINGS: We performed a microarray screening for transcriptional targets of TFII-I in hippocampus, cortex and embryonic cells from Gtf2i mutant and wild-type mice. Candidate genes with altered expression were verified using real-time PCR. A novel motif shared by deregulated genes was found and chromatin immunoprecipitation assays in embryonic fibroblasts were used to document in vitro TFII-I binding to this motif in the promoter regions of deregulated genes. Interestingly, the *PI3K* and *TGFβ* signaling pathways were over-represented among *TFII-I*-modulated genes.

CONCLUSIONS/SIGNIFICANCE: In this study we have found a highly conserved DNA element, common to a set of genes regulated by TFII-I, and identified and validated novel *in vivo* neuronal targets of this protein affecting the PI3K and TGFβ signaling pathways. Overall, our data further contribute to unravel the complexity and variability of the different genetic programs orchestrated by TFII-I.

INTRODUCTION

TFII-I is member of an ubiquitously expressed, multifunctional transcription factor family which operate as a molecular switch to convey signals from multiple pathways and mediate cellular response [1]. TFII-I was originally identified as a protein that binds to the initiator (Inr) core promoter element and was later shown to bind to various upstream elements that include the E box [2], the downstream immunoglobulin control element (DICE) sequence [3] and the consensus BRGATTRBR sequence [4]. Structurally, TFII-I consists of multiple I-repeats, each of which contains a putative helix-loop-helix motif that is potentially important for protein-protein interactions [5]. Growth factor signaling leads to rapid tyrosine phosphorylation, followed by nuclear translocation of TFII-I, and subsequent activation of target genes [5-7]. In addition to its function as a transcription factor, cytosolic TFII-I regulates calcium homeostasis by modulating agonist-induced extracellular Ca^{2+} entry [8-9].

The gene encoding TFII-I, *GTF2I* (Entrez Gene ID 2969), has been mapped to an interval of the human chromosome 7q11.23. The region is commonly deleted in Williams-Beuren syndrome (WBS) (OMIM#194050). WBS is a rare developmental disorder with sporadic occurrence (1/7000-1/20000), characterized by mild intellectual disabilities with a cognitive profile including relatively preserved verbal skills, very deficient visuospatial abilities and a characteristic personality showing high sociability with strangers and increased anxiety [10]. Additional features include craniofacial dysmorphism, growth retardation, odynoacusis, as well as cardiovascular, endocrine and connective tissue abnormalities [11-12]. The implication of

GTF2I haploinsufficiency in the origin of this disorder is extensively documented but the concrete pathways and pathogenic mechanisms remain unclear [13-15]. In mouse, the *Gtf2i* gene (Entrez Gene ID 14886, MGI 1202722) is located on chromosome 5G2. *Gtf2i* expression is important for embryonic development, as heterozygous knockout mice featured anomalies similar to those observed in WBS: retarded growth, microcephaly, craniofacial and skeletal defects, odynacusis and hypersociability [13, 16-17].

The mechanisms whereby decreased TFII-I can promote anomalies similar to those observed in WBS have been subject to exhaustive cellular and biochemical studies [5, 18-20]. Transcriptomic profiles resulting from changes in TFII-I dosage have been already defined in cell lines and tissues [16, 21]. So far, involvement of TFII-I in gene regulation has been validated for 20 direct target genes involved in transcriptional regulation, chromatin remodeling, cell cycle, muscle development and neurogenesis [4, 22-23]. Herein, we have extended these observations by comparative transcriptome analysis of brain tissues and ES cells from mutants of TFII-I. Our data unveil the existence of a new consensus binding domain that increases the number of distinct transcriptional networks that depend on the TFII-I signals further endorsing the concept of the function domains as key regulator of the biochemical, genetic and biological outcomes of TFII-I.

RESULTS

Identification of deregulated genes in *Gtf2i* mutant mouse brain and ES cell line

In our effort to elucidate the role of TFII-I in the cognitive phenotype of WBS also observed in different mouse models [24-25], we searched for differentially expressed genes (DEG) by gene expression microarray analysis of heterozygous *Gtf2i* mutant mice (*Gtf2i*$^{+/-exon2}$). Therefore, our analysis was performed using two brain areas that have been reported to be altered in WBS patients, hippocampus and cortex.

Previous studies of dissected brain regions had noticed considerable random variation among individual samples. To reduce the false positives due to this random noise, cDNA was prepared from pools (five mice per pool), extracted from*Gtf2i*$^{+/-exon2}$ and WT mice. After a restrictive statistical analysis, a total of 16026 probes could be analyzed in cortex, and 16719 probes in hippocampus. DEG were selected in each comparison for $B>0$ and/or $p<0.05$. Around 1% of probes were identified as deregulated in hippocampus and 10% in cortex, and the magnitudes of these changes was generally small, ranking between -3.27 to 2.5-fold. Among the concordant probes between cortex and hippocampus, the 84,2% were deregulated in both tissues, and only 9 probes were specifically deregulated in hippocampus and not in cortex. In order to validate the microarray results we carried out qRT-PCR analysis in a subset of selected DEG both in cortex and hippocampus. The results confirmed the microarray data in magnitude for 10 of the 11 genes tested (Fig 1A).

On the other hand, it is well established that undifferentiated stem cells are a very interesting tool for gene expression studies as they express most genes in the organism, including many important for development. To identify genes already deregulated in early developmental stages, we also studied the embryonic stem (ES) cell line XS0353 with the *Gtf2i*$^{+/-exon2}$genotype. After different corrections and quality controls of the results from two replicates, we discriminated 12402 cDNA clones. DEG were selected in each comparison for $B>0$ and $p<0.01$. Only 19% of the DEG found in the brain tissues were also deregulated in the undifferentiated XS0353 cell line. Verification of array data was performed by qRT-PCR using 14 randomly chosen genes, and all of them were found to be deregulated in the same direction and magnitude (100% validation) (Fig 1B). Taken together, we found a very

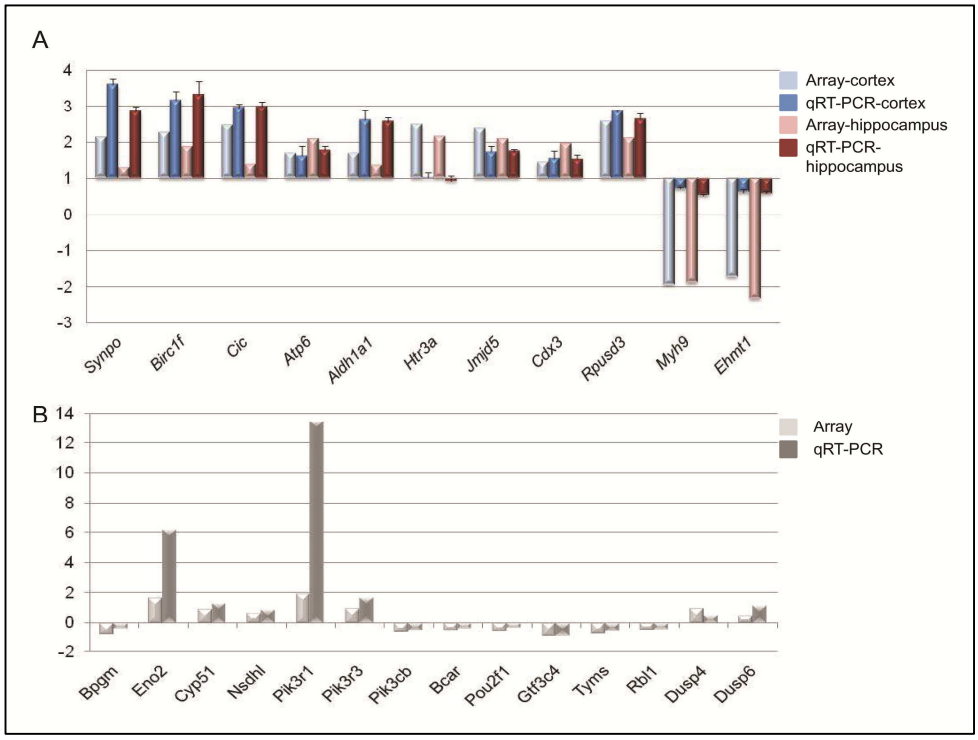

Figure 1: qRT-PCR array validation. Deregulated genes have been validated by qRT-PCR comparing relative expression of *Gtf2i*$^{+/-\Delta exon2}$ versus WT for cortex and hippocampus **(A)** and XS0353 versus AB2.2 cell line **(B)**.

high correlation of microarray data with qRT-PCR results.

Recruitment of TFII-I to the proximal promoter of target genes

To identify potential direct target genes of TFII-I among the candidate DEG, we first searched the consensus TFII-I binding site BRGATTRBR on positive strands within 1kb (–1000 to +1) from the transcription start site of each locus in the mouse genome [4]. The consensus binding motif was found in the promoter of ≈17% of DEG (both cell line and tissue DEGs), which is not significantly enriched with respect to the entire data set (DBTSS) [26].

A set of 27genes commonly deregulated in brain tissues with no BRGATTRBR binding motif were subjected to an *in silico* analysis with the MEME program [27]. After manual curation, a single novel motif with a high degree of significance in multiple DEG (p= $1.49x10^{12}$-$1.72x10^{-7}$) was identified and selected. Phylogenetic footprints were generated by aligning the motifs in the context of flanking upstream sequences of selected genes (Fig 2). A core conserved site containing the sequence 5'-CAGCCWG-3' was identified with strong evidence of further conservation in flanking sequences. Similar to the BRGATTRBR motif, the consensus CAGCCWG motif was found in ≈17% of annotated promoters of the DEGs, which is not significantly enriched with respect to the entire data set.

Six candidate target genes with the BRGATTRBR consensus binding domain and 10 target genes with the regulatory CAGCCWG element were selected for further analyses. To assess whether TFII-I

```
Naip6       Homo sapiens            gGAGTTtgAGacCAGCCtGG
            Mus musculus            TGAGTTCCAGGACAGCCAGG
                                     *****  **  ***** **
Ptpn1       Homo sapiens            AGTtcGAGaCCAGCCTGG
            Mus musculus            AGTGAGAGGCCAGCCTGG
            Rattus norvergicus      AGTGgGAGGCCAGCCTGG
                                    ***  *** *********
            Takifugu rubripes       gGTG-GA-GCCAGC--GG
                                     **  **  *****  **
Zfp280c     Homo sapiens            gGAGTTcG--AGaCCAGCCTGa
            Mus musculus            TGAGTTTG--AGGCCAGCCTGG
            Rattus norvergicus      TacaTTTGgaAGaaCAGCCaGt
                                        ** *  **  ***** *
            Takifugu rubripes       gcAGcagcttct-CCAGCCaGt
                                                ***** *
Snw1        Homo sapiens            AAA-TTaCtAActtaCAGCCAGG
            Mus musculus            AAAGTTCC-AAGG--CAGCCAGG
            Rattus norvergicus      AtAGTTgC-AAt---CAGCCAGa
                                    * * ** * **    *******
            Takifugu rubripes       tgAGa-CCg-AGac-CAGCaAGc
                                      *    *  *    **** **
Htr3a       Homo sapiens            ccTagg-AGG-CAGCCtGG
            Mus musculus            GGTT-CAAGGACAGCCCGG
            Rattus norvergicus      GGTTTCAAGaACAGCCtGa
                                      *    **  ***** *
            Takifugu rubripes       ctgctgAtGctCAGCCtca
                                          *  *****
Jmjd5       Homo sapiens            TcA-TTataAGctCAGCCcTGt
            Mus musculus            TGAGTTCC-AGGCCAGCC-TGG
            Rattus norvergicus      TGtGccCC-AacCCAGCCtTGG
                                    *        *   ***** **
            Takifugu rubripes        attaTgtttcaCCAGCC-TGt
                                               ***** **

Cnp1        Homo sapiens            gGccCgcccCCAGCCcGc
            Mus musculus            TGTACCAGGCCAGCCTGA
            Rattus norvergicus      TaTACCAGGCCAGCCTGA
                                        *    ****** *
            Takifugu rubripes       cGagCCtGtgCAGCCaGA
                                       *     ***** *
CONSENSUS                                   CAGCCWGR
```

Figure 2: Motif description and conservation. Evolutionary conservation of the motif in different genes and organisms providing the conserved 5'-CAGCCWG-3' sequence. Identical nucleotides are starred. In the Logo picture the height of letters correlates with degree of conservation.

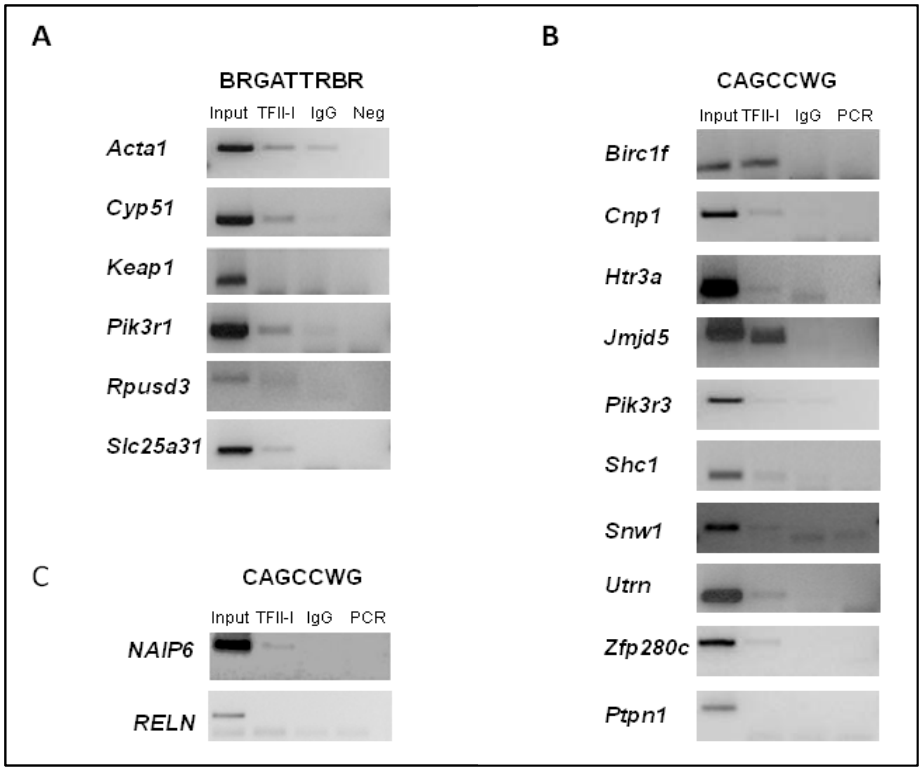

Figure 3: Recruitment of TFII-I to proximal promoters of target genes. A. ChIP analysis of the selected genes containing the BRGATTRBR binding domain in their promoter region**. B.** ChIP analysis of the selected genes containing the CAGCCWG binding domain in their promoter region. **C.** ChIP analysis of the *Birc1f* conserved CAGCCWG motif in HeLA human cell line at the orthologus gene *NAIP6*. *Reln*, is the negative gene control for TFII-I IP in all cases.

can be recruited to promoters of selected target genes we performed chromatin immunoprecipitation (ChIP) analysis in mouse embryonic fibroblast cell lines (MEFs) that endogenously expressed TFII-I proteins. As expected, our ChIP results showed specific enrichment of TFII-I in promoters of 5 of the 6 selected genes containing the BRGATTRBR binding motif (*Acta1, Cyp51, Pik3r1*, *Rpusd3*and *Slc25a31*) (Fig. 3A) and also for 9 of the 10 target genes with the CAGCCWG binding motif (*Birc1f, Cnp1, Htr3a Jmjd5, Pik3r3, Shc1, Snw1, Utrn and Zfp280c)* (Fig 3B).

However, no binding was detected for *Keap1* and *Ptpn1* to the BRGATTRBR and CAGCCWG motifs respectively (Fig 3A and B) in our conditions, despite the presence of the complete consensus binding sequence. Furthermore, ChIP assays in the human HeLa cell line showed an enrichment of TFII-I binding in the human promoter of *NAIP6 (Birc1f* orthologous) (Fig 3C) confirming the *in vivo* functional relevance of this motif under our basal cell culture conditions.

The CAGCBVG motif is necessary for correct binding by TFII-I

To better define the relevant sites of CAGCCWG for TFII-I binding, we performed additional ChIP analyses in five genes containing similar domains in their promoters with small variations with respect

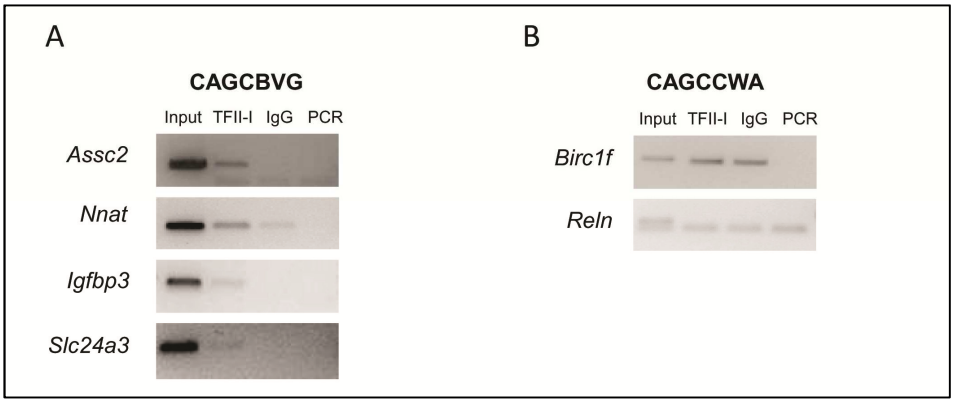

Figure 4: Variability of the CAGCCWG conserved sequence. A. ChIP analysis of target genes containing variations in the conserved motifs, where the presence of CAGCBVG is enough for binding. **B**. Mutagenesis experiment of the conserved 3' guanine changed by an adenine where binding of TFII-I to the *Birc1f* promoter is no longer present.

to the consensus. We could observe positive binding in genes that contain a variation of the consensus sequences (CAGCBVG) in their promoters, such as *Ascc2*, *Nnat*, *Slc24a3* and *Igfbp3* (Fig 4A). In addition, we substituted the 3' conserved guanine for adenine by targeted mutagenesis. This mutation was sufficient to abrogate TFII-I binding in the *Birc1f* gene (Fig 4B), demonstrating the importance of this nucleotide and consensus domain in TFII-I binding to DNA.

Deletion of functional TFII-I domains abolishes its binding to the novel motif.

The *Gtf2i*$^{+/\Delta exon2}$mutant mice generated a truncated protein lacking the first 140 amino acids (Δ140TFII-I), then missing the leucine zipper motif (aa 23 to 44) and disrupting the first I-repeat (aa 104 to 176). *In vitro* studies have shown that the deletion of the N-terminal 90 amino acids of a TFII-I-Δ isoform not only affects its DNA binding ability but also the proper homomerization leading to a fail to activate transcription on TFII-I-dependent reporters [28]. Consequently, we decided to examine whether the expression of Δ140TFII-I could also alter transcriptional regulation through the described motifs.

We performed ChIP experiments into the promoters of positive genes in two genetically modified MEFs with either homozygous (*Gtf2i*$^{\Delta exon2/\Delta exon2}$) or heterozygous (*Gtf2i*$^{+/\Delta exon2}$) mutations expressing Δ140TFII-I. No clear binding pattern was found, suggesting that the binding is gene promoter dependent. In some cases (*Rpusd3* for BRGATTRBR, and *Snw1* and *Zfp280c* for CAGCCWG), the presence of wild-type TFII-I in heterozygous animals form was enough for binding (Fig 5A). In the case of *Cyp51*and *Slc25a31* for BRGATTRBR and *Jmjd5* for CAGCCWG, the complete lack of binding in both homo and heterozygous cells suggested that proper TFII-I dimerization could be required for binding (Fig 5B). In the case of *Pik3r1* for BRGATTRBR, no binding was found in the heterozygous cell line, but normal binding in homozygous was present, which would suggest that abnormal stability of the dimmers might interfere with binding (Fig 5C). For genes like *Birc1f* and *Utrn*, the normal binding in both cell lines, indicated that the first 140 amino acids are not required for TFII-I binding (Fig. 5D).

Functional annotation of TFII-I modulated genes

Finally, we analyzed whether genes containing the different motifs shared a functional pathway. Overall, 347 TFII-I modulated genes were shown to bear the

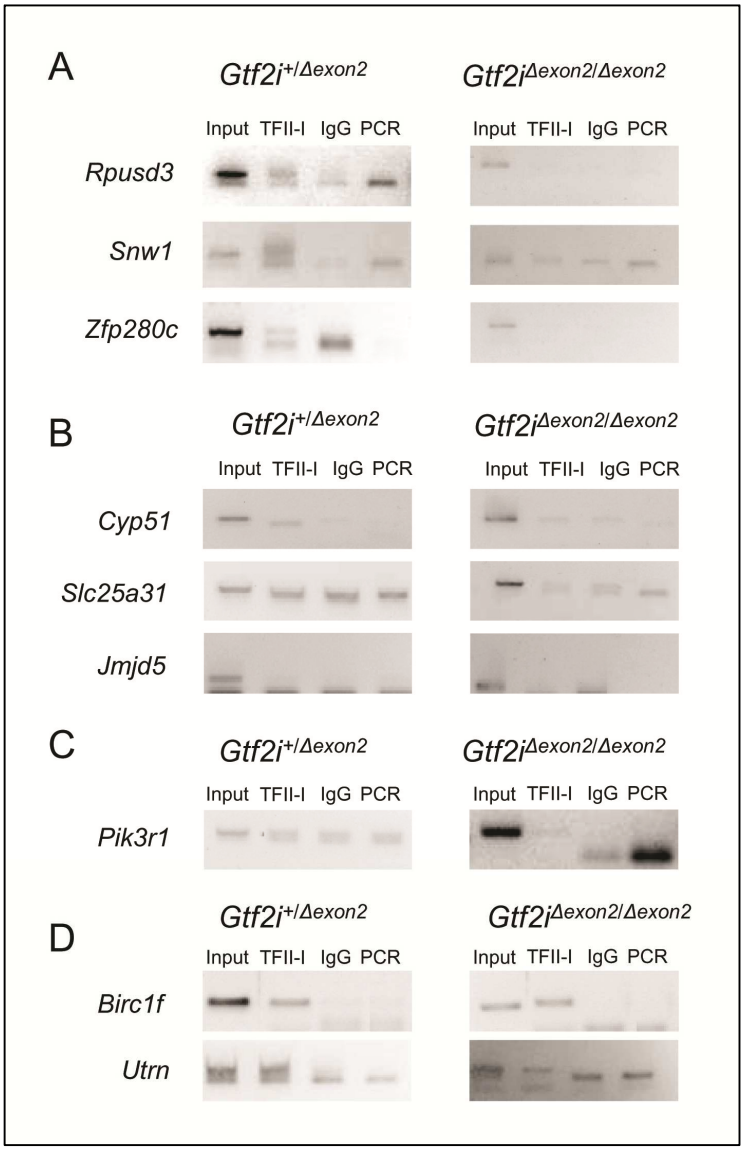

Figure 5: ChIP analysis in *Gtf2i*$^{+/\Delta exon2}$ *and Gtf2i*$^{\Delta exon2/\Delta exon2}$ cell lines. A. ChIP analysis showing that the presence of TFII-I WT form is enough for binding**. B**. ChIP analysis showing no binding is obtained in any of the mutant cell lines. **C**. ChIP analysis showing binding only to the homozygous cell lines. **D**. ChIP analysis showing binding to both mutant cell lines.

two binding motifs in their proximal promoters. CPDB analysis of this set of genes revealed the cell cycle, gene expression and transcription, as the most significant pathways regulated by TFII-I. We could also appreciated significant enrichment ($P<0.03$) for genes involved in EGFR1 signaling, PI3K/AKT activation and TGFβ receptor signaling, among others. These pathways were also significantly enriched in the set of TFII-I modulated genes bearing only one of the motifs. A specific enrichment in the

signaling pathway by NGF was significant only in the set of TFII-I modulated genes bearing the CAGCCWG motif (P=0.0014) (Table 1).

DISCUSSION

Decreased levels of TFII-I protein during development appear to contribute to several relevant features of the WBS phenotype, including craniofacial shape, abnormal sound sensitivity, sensorimotor gating phenotype and altered cognitive profile, as observed in different mouse models[17, 30]. Containing a helix-loop-helix, a DNA binding domain, a leucine zipper (dimerization motif) at the N-terminus and six unique I-repeats with DNA binding properties, TFII-I is capable of partnering with a vast array of both cytoplasmic and nuclear factors, thus affecting diverse signal transduction cascades and modulating the expression of various genes[8, 31-32].

We have studied gene expression profile differences induced by altered TFII-I function in ES cells and adult brain tissues in order to identify deregulated genes and pathways as well as a novel highly conserved DNA binding site for TFII-I. Experimental validation for some of these binding sites in deregulated genes is documented. Conservation of upstream element containing the putative TFII-I-binding site could be observed from humans, with an enrichment of TFII-I binding in the human promoter of *NAIP6,* suggesting a functional role for this sequence. In agreement with our previous results about the *in vivo* relevance of the N-terminal part of TFII-I [25],we provide new experimental data demonstrating the importance of this region to maintain binding capacity of TFII-I to different promoter sequences of various genes and thus, altering its transcriptional activity.

In line with previous reports, pathway classification of TFII-I putative targets showed significant enrichment in genes involved in glycolysis and gluconeogenesis (with experimental validation for Cyp51) and insulin pathways [20] suggesting a possible contribution of *GTF2I* to the glucose intolerance or diabetes present in 75% of adult WBS patients[29]. TFII-I has been previously reported to have a role in thePI3K/AKT pathway [33]. We further demonstrate this relevant function with the experimental validation of direct regulation of the *Pik3r1*gene encoding the 85kD regulatory subunit of phosphatidylinositol 3-kinase (PI3K). Other putative targets of TFII-I include the*Cab39l, Pik3ca, Stk11, Irs1, Gab1, Eif4ebp1, Trib3, Eif4b, Pten* and R*ps6kb2* genes, implicating a significant enrichment of PI3K cascade and *Nup88, Pik3c2a, Nup85, Atp8b1, Plcd4* showed a significant enrichment of the phosphatidylinositol phosphate metabolism. The PI3K/AKT signaling pathway plays a key role in diverse physiologic processes, including dendritic spine formation during development and structural synaptic plasticity.

It has been previously shown that TFII-I proteins play an important role in the regulation of the TGFβ signaling pathway [18, 34]. Here we provide experimental evidence that TFII-I is recruited to the promoter of *Shc1* and *Snw1*, members of the TGFβ signaling pathways.

The 5-hydroxytryptamine (serotonin) receptor 3A gene (*Htr3a*) appears to be another new target of TFII-I. Interactions between the prefrontal cortex and the amygdala are of great interest in the investigation of neural mechanisms underlying part of the WBS phenotype because of their role in anxiety and social cognition. In mouse models with mutations of TFII-I family members, alterations in serotonin 5-HT_{1A} currents have been demonstrated in the prefrontal cortex [35].Our data suggest that TFII-I could participate in these alterations through its direct regulation of *Htr3a*, a gene involved in serotonergic synapse.

Genes	Pathway	Count	*P* value
TFII-I modulated genes with both motifs in their proximal promoters (n=347)	Cell cycle	21	0.0001663
	Gene expression	39	0.0006854
	Insulin signaling	10	0.0014353
	Glucose transport	5	0.0022387
	EGFR1	21	0.0023685
	CDO in myogenesis	4	0.0049139
	Actin organization and cell migration by PI3K	3	0.0066944
	PI3K/AKT activation	4	0.0104319
	Ubiquitin mediated proteolysis	8	0.0148252
	Signaling by VEGFR1 & VEGFR2	5	0.0234935
	TGFβ receptor signaling	4	0.0287998
TFII-I modulated genes with BRGATTRB motif in their proximal promoters (n=542)	DNA replication	18	0.0000078
	Glycolysis and Gluconeogenesis	10	0,0000081
	TNFalpha	20	0,0000369
	EGFR1	29	0.0012183
	VEGFR1 specificsignals	5	0.0033832
	Purine metabolism	5	0.0051766
	Cell cycle	25	0.0005387
	TGFβ receptor signaling	12	0.0193252
	Actin organization and cell migration by PI3K	3	0.0195390
	Insulin signaling	5	0.0225993
	PI3K cascade	6	0.0381539
TFII-I modulated genes with CAGCWG motif in their proximal promoters (n=501)	EGFR1	35	0,0000017
	Cell cycle	28	0,0000279
	DNA replication	14	0.0005531
	Signallingby NGF	7	0.0014121
	TNFR1 signaling	4	0.0018261
	TNFalpha	15	0.0031993
	NCAM signaling for neuriteout-growth	3	0.0045506
	TNFR22 signaling	3	0.0059235
	Pyrimidine metabolism	10	0.0120670
	Purine metabolism	11	0.0180500
	TGFβ signaling	3	0.0253695

Table 1: Pathway involvement of TFII-I modulated genes.

In conclusion, TFII-I is an interesting and unusual transcription factor, particularly in light of its role in the pathogenesisof the neurodevelopmental disorder, WBS. We have expanded the knowledge about TFII-I function by defining a novel regulatory element, CAGCCWG, identifying additional target genes and enriched pathways under TFII-I regulation. The final elucidation of the biological role of TFII-I may facilitate a deeper understanding of relevant molecular mechanisms underlying human development and cognition.

MATERIALS AND METHODS

Sample preparation and cell culture maintenance

Hippocampus and cortex from five animals were immediately dissected from fresh brains and quickly frozen by liquid nitrogen until RNA extractions. Clone XS0353 was obtained from the Sanger Institute Gene Trap Resource (SIGTR) mouse ES cell line collection (http://www.sanger.ac.uk/PostGenomics/genetrap/). aCGH analysis between XS0353 and wild-type cell lines did not shown neither major genomic alterations (deletions or duplications) in chromosome 5 nor in the rest of chromosomes. We found a total of 11 CNVs containing 24 genes. None of them were found deregulated in the expression array analysis (Supplemental Table1). XS0353 cell line was cultured in standard conditions, Knockout DMEM medium (Invitrogen), supplemented with 20% Knockout Serum Replacement for ES cells (Invitrogen),LIF, β-mercaptoethanol, no essential aminoacids and Penicillin/streptomycin. Cells were always cultured in a monolayer of feeder cells and maintained at 37ºC in a humidified 5% CO^2 chamber.

RNA isolation and quantification

Total RNA was extracted from XS0353 cell line and cortex and hippocampus tissues by using TRIZOL reagent (Invitrogen, Carlsbad, CA, USA), followed by a second extraction using RNeasy (Qiagen) in both cases according to the manufacturer's instructions. Quality of all RNA samples was checked using an Agilent 2100 Bioanalyzer (Agilent Technologies). Only those samples with an RNA Integrity Number (RIN) >7 were used for hybridization.

Microarray and Data Analysis

Brain tissues were hybridized to the Agilent 4x44K v1 Mouse Whole Genome chips. All the hybridizations were done in duplicate with direct and dye swap experiments. Fluorescent images were obtained with the Agilent G2565BA Microarray Scanner System (Agilent Technologies) and TIFF images were quantified with the use of the Spot program (http://experimental.act.cmis.csiro.au/Spot/index.php) under the R environment (http://www.r-project.org).The resulting raw values were filtered and an intensity cut-off was applied, selecting those points with a foreground median/background median >3 in at least one channel. A series of programs, collectively packaged as Array File Maker 4.0 (AFM), were use to manipulate and manage DNA microarray data [36].AFM 4.0, Quantarray Data Handler 3.0, and Array Database 1.0 can be downloaded at the Tyers Lab Home Page [http://www.mshri.on.ca/tyers/] and are copyrighted against commercial gain.

ES cells were hybridized using duplicates to the GeneChip Mouse Genome 430 2.0. Array (Affymetrix) microarray images were processed with Microarray Analysis Suite 5.0 (Affymetrix).

All samples demonstrated characteristics of high-quality cRNA (3'/5' ratio of probe sets for glyceraldehyde-3-phosphate dehydrogenase and β-actin of <1.5) and were subjected to subsequent analysis. Raw expression values obtained directly from .CEL files were preprocessed using the RMA method [37], a three-step process which integrates background correction, normalization and summarization of probe values. These normalized values were the

basis for all the analysis. Previous to any analysis, data were submitted to non-specific filtering to remove low signal genes (those genes whose mean signal in each group did not exceed a minimum threshold) and low variability genes (those genes whose standard deviation between all samples did not exceed a minimum threshold).

Statistical analysis

The selection of differentially expressed genes between conditions was based on a linear model analysis with empirical Bayes moderation of the variance estimates following the methodology developed by Smyth [38]. The analysis yields standard tests statistics such as fold changes, (moderated)t or p–values which can be used to rank the genes from most to least differentially expressed. In order to deal with the multiple testing issues derived from the fact that many tests (one per gene) are performed simultaneously, p–values were adjusted to obtain strong control over the false discovery rate using the Benjamini and Hochberg method [39]. The cutoff value for discrimination of positives was at the significance level $P< 0.05$ (corrected P-value) for the brain tissues and $P<0.01$ for ES cell genes.

cDNA obtention, qRT-PCR experiments and data analysis

To validate the expression results obtained in the array analysis, 1μg of the same mRNA used for the array hybridization was used for first-strand cDNA synthesis with Superscript II (Invitrogen). Primers and probes were designed to span an intron in all cases using the Primer3 software Version 0.4.0 [40] (Supplemental Table 2). Real-Time PCR was performed using the SYBR Green Ready Master Mix according to the manufacturer's instructions on the ABI PRISM 7900HT Sequence Detection System (Applied Biosystems). The standard curve method was used for the analysis. The results were normalized respect to a housekeeping gene selected for its stable expression among the different tissues and cell lines. A reagent-only (no DNA) negative control sample was always included in each run. Experiments were performed a minimum of 3 times in 384-well plates with three replicates per sample. Raw data was obtained using SDS 2.4 software (Applied Biosystems).

Chromatin Immunoprecipitation

ChIP experiments were performed using home made MEF cell lines. We selected three wild-type cells lines and two homozygous (*Gtf2i*$^{\Delta ex2/\Delta ex2}$) and two heterozygous (*Gtf2i*$^{\Delta ex2/+}$) cell lines derived from embryos of *Gtf2i*$^{\Delta ex2/+}$ intercrosses. MEFs were crosslinked in 1% formaldehide for 10 minutes, lysed and sonicated to size not bigger than 600bp.To prevent unequal shearing of DNA samples we keep the tip end of the sonicator near the bottom of the sample tubes. Immunoprecipitations were performed overnight at 4ºC with TFII-I antibody[17] and goat anti-mouse IgG (Sc-2028, Santa Cruz Biotechnology) used as negative control. 50μl of the chromatin supernatant were saved as input control. Primers were designed to span the motif region and were located in its close vicinity. All primer sequences are shown in Supplemental Table 2.

Mutagenesis analysis

The sequence of interest of the promoter region of *Birc1f* containing the newly described motif was inserted in a pGem®-T Easy Vector (Promega) and One Shot® TOP10 cells (Life Technologies) were transformed with the vector. 9 clones were analysed for insertion using the *EcoRI* restriction enzyme and three of them contained the desired insert. The recombinant clones were sequenced and correct ones were selected for posterior experiments. Mutagenesis experiment was performed using the QuikChange Kit protocol (Stratagene-An Agilent Technologies Company) following manufacturer's instructions. The conserved

guanine a 3' of the motif was substituted by an adenine. 5 clones were selected and sequenced for correct insertion, obtaining one correct clone. Mutagenesis studies were made in COS7 (a monkey derived cell line) to abolish interference with mouse specific primers. Transfection experiments were performed using the jetPEI® reagent (Poliplus Transfection) following the manufactures recommendations.

Pathway definition
In order to identify which are the affected pathways in the different groups, we used the Consensus Path database release24 (CPDB; http://cpdb.molgen.mpg.de) [41]. Gene information was obtain from Entrez Gene and Ensembl databases.

Accesion number. The accession number for supporting microarray data is: http://www.ncbi.nlm.nih.gov/geo/query/cc.cgi?token=drstlicyasioyroç6acc=GSE23202

Author contributions
Conceived and designed the experiments: VC and LAP-J. Analyzed the results and wrote the manuscript: MS-P, VC and LAPJ. Performed the molecular and cellular biology experiments: MS-P andVC. All authors read and approved the final manuscript.

Acknowledgements
We thank Verena Terrado and q-Genomics for technical assistance. This work was supported by grants from the Spanish Mnistry of Health (FIS 04/0433, to VC), AGAUR (2009 SGR1274) and the VI Framework Prgoramme of the European Union (LSHG-CT-2006-037627, to LAJ-P). MS-P was supported by CIBERER and UPF. VC is a FIS investigator.

REFERENCES

1. Roy, A.L., *Biochemistry and biology of the inducible multifunctional transcription factor TFII-I.* Gene, 2001. **274**(1-2): p. 1-13.
2. Roy, A.L., et al., *Cloning of an inr- and E-box-binding protein, TFII-I, that interacts physically and functionally with USF1.* Embo J, 1997. **16**(23): p. 7091-104.
3. Tantin, D., et al., *Regulation of immunoglobulin promoter activity by TFII-I class transcription factors.* J Biol Chem, 2004. **279**(7): p. 5460-9.
4. Chimge, N.O., et al., *Identification of the TFII-I family target genes in the vertebrate genome.* Proc Natl Acad Sci U S A, 2008. **105**(26): p. 9006-10.
5. Roy, A.L., *Signal-induced functions of the transcription factor TFII-I.* Biochim Biophys Acta, 2007. **1769**(11-12): p. 613-21.
6. Misra, U.K., F. Wang, and S.V. Pizzo, *Transcription factor TFII-I causes transcriptional upregulation of GRP78 synthesis in prostate cancer cells.* J Cell Biochem, 2009. **106**(3): p. 381-9.
7. Parker, R., et al., *Identification of TFII-I as the endoplasmic reticulum stress response element binding factor ERSF: its autoregulation by stress and interaction with ATF6.* Mol Cell Biol, 2001. **21**(9): p. 3220-33.
8. Caraveo, G., et al., *Action of TFII-I outside the nucleus as an inhibitor of agonist-induced calcium entry.* Science, 2006. **314**(5796): p. 122-5.
9. Patterson, R.L., et al., *Phospholipase C-gamma is required for agonist-induced Ca2+ entry.* Cell, 2002. **111**(4): p. 529-41.
10. Morris, C.A., *The behavioral phenotype of Williams syndrome: A recognizable pattern of neurodevelopment.* Am J Med Genet C Semin Med Genet, 2010. **154C**(4): p. 427-31.
11. Morris, C.A., et al., *Natural history of Williams syndrome: physical characteristics.* J Pediatr, 1988. **113**(2): p. 318-26.
12. Tassabehji, M., *Williams-Beuren syndrome: a challenge for genotype-phenotype correlations.* Hum Mol Genet, 2003. **12 Spec No 2**: p. R229-37.
13. Sakurai, T., et al., *Haploinsufficiency of Gtf2i, a gene deleted in Williams Syndrome, leads to increases in social interactions.* Autism Res, 2010.
14. Antonell, A., et al., *Partial 7q11.23 deletions further implicate GTF2I and GTF2IRD1 as the main genes responsible for the*

Williams-Beuren syndrome neurocognitive profile. J Med Genet, 2010. **47**(5): p. 312-20.
15. Ferrero, G.B., et al., *An atypical 7q11.23 deletion in a normal IQ Williams-Beuren syndrome patient.* Eur J Hum Genet, 2010. **18**(1): p. 33-8.
16. Enkhmandakh, B., et al., *Essential functions of the Williams-Beuren syndrome-associated TFII-I genes in embryonic development.* Proc Natl Acad Sci U S A, 2009. **106**(1): p. 181-6.
17. Lucena, J., et al., *Essential role of the N-terminal region of TFII-I in viability and behavior.* BMC Med Genet, 2010. **11**(1): p. 61.
18. Stasyk, T., et al., *Phosphoproteome profiling of transforming growth factor (TGF)-beta signaling: abrogation of TGFbeta1-dependent phosphorylation of transcription factor-II-I (TFII-I) enhances cooperation of TFII-I and Smad3 in transcription.* Mol Biol Cell, 2005. **16**(10): p. 4765-80.
19. Dai, L., et al., *Is it Williams syndrome? GTF2IRD1 implicated in visual-spatial construction and GTF2I in sociability revealed by high resolution arrays.* Am J Med Genet A, 2009. **149A**(3): p. 302-14.
20. Antonell, A., M. Vilardell, and L.A. Perez Jurado, *Transcriptome profile in Williams-Beuren syndrome lymphoblast cells reveals gene pathways implicated in glucose intolerance and visuospatial construction deficits.* Hum Genet, 2010.
21. Chimge, N.O., et al., *Gene expression analysis of TFII-I modulated genes in mouse embryonic fibroblasts.* J Exp Zool B Mol Dev Evol, 2007. **308**(3): p. 225-35.
22. Makeyev, A. and D. Bayarsaihan, *Molecular Basis of Williams-Beuren Syndrome: TFII-I Regulated Targets Involved in the Craniofacial Development.* Cleft Palate Craniofac J, 2010.
23. Lazebnik, M.B., et al., *Williams-Beuren syndrome-associated transcription factor TFII-I regulates osteogenic marker genes.* J Biol Chem, 2009. **284**(52): p. 36234-9.
24. Li, H.H., et al., *Induced chromosome deletions cause hypersociability and other features of Williams-Beuren syndrome in mice.* EMBO Mol Med, 2009. **1**(1): p. 50-65.
25. Lucena, J., et al., *Essential role of the N-terminal region of TFII-I in viability and behavior.* BMC Med Genet, 2010. **11**: p. 61.
26. Wakaguri, H., et al., *DBTSS: database of transcription start sites, progress report 2008.* Nucleic Acids Res, 2008. **36**(Database issue): p. D97-101.
27. Bailey, T.L. and C. Elkan, *Fitting a mixture model by expectation maximization to discover motifs in biopolymers.* Proc Int Conf Intell Syst Mol Biol, 1994. **2**: p. 28-36.
28. Cheriyath, V. and A.L. Roy, *Structure-function analysis of TFII-I. Roles of the N-terminal end, basic region, and I-repeats.* J Biol Chem, 2001. **276**(11): p. 8377-83.
29. Pober, B.R., *Williams-Beuren syndrome.* N Engl J Med, 2010. **362**(3): p. 239-52.
30. Li, H.H., et al., *Induced chromosome deletions cause hypersociability and other features of Williams-Beuren Syndrome in Mice.* EMBO Molecular Medicine, 2009. **1**: p. 50-65.
31. Ashworth, T. and A.L. Roy, *Cutting Edge: TFII-I controls B cell proliferation via regulating NF-kappaB.* J Immunol, 2007. **178**(5): p. 2631-5.
32. Ogura, Y., et al., *TFII-I down-regulates a subset of estrogen-responsive genes through its interaction with an initiator element and estrogen receptor alpha.* Genes Cells, 2006. **11**(4): p. 373-81.
33. Chimge, N.O., et al., *PI3K/Akt-dependent functions of TFII-I transcription factors in mouse embryonic stem cells.* J Cell Biochem, 2012. **113**(4): p. 1122-31.
34. Ku, M., et al., *Positive and negative regulation of the transforming growth factor beta/activin target gene goosecoid by the TFII-I family of transcription factors.* Mol Cell Biol, 2005. **25**(16): p. 7144-57.
35. Proulx, E., et al., *Enhanced prefrontal serotonin 5-HT(1A) currents in a mouse model of Williams-Beuren syndrome with low innate anxiety.* J Neurodev Disord, 2010. **2**(2): p. 99-108.
36. Breitkreutz, B.J., et al., *AFM 4.0: a toolbox for DNA microarray analysis.* Genome Biol, 2001. **2**(8): p. SOFTWARE0001.
37. Irizarry, R.A., et al., *Exploration, normalization, and summaries of high density*

oligonucleotide array probe level data. Biostatistics, 2003. **4**(2): p. 249-64.
38. Smyth, G.K., *Linear models and empirical bayes methods for assessing differential expression in microarray experiments.* Stat Appl Genet Mol Biol, 2004. **3**: p. Article3.
39. Benjamini Y., H.Y., *Controlling the false discovery rate: A practical and powerful approach to multiple testing.* Journal of the Royal Statistical Society. Series B (Methodological), 1995. **57**(1): p. 289-300.
40. Rozen, S. and H. Skaletsky, *Primer3 on the WWW for general users and for biologist programmers.* Methods Mol Biol, 2000. **132**: p. 365-86.
41. Kamburov, A., et al., *ConsensusPathDB--a database for integrating human functional interaction networks.* Nucleic Acids Res, 2009. **37**(Database issue): p. D623-8.

Aberration Algorithm: ADM-2
Threshold: 6.0
Centralization: ON
Bin Size: 10
Centralization Threshold: 6.0
Fuzzy Zero: ON
Combine Replicates (Intra Array): ON
Combine Replicates (Inter Array): OFF
Genome: mm9
Aberration Filters: minProbes = 4 AND minAvgAbsLogRatio = 0.4 AND maxAberrations = 100 AND percentPenetrance = 0

Chr	Cytoband	Start	Stop	#Probes	Amplifica	Deletion	pval	Gene
chr4	qB3	62157765	62182694	8	0,9999	0	1.683e-33	Bspry, Hdhd3, Alad
chr4	qD1	111771911	112279051	41	0	-1,0081	8.543e-17	9530098N22Rik, A430090E18Rik, A030013N09Rik
chr5	qC3.1	69875194	69920724	6	0,6826	0	1.411e-11	Yipf7
chr5	qG3	149854076	150188792	40	0	-0,5111	9.838e-42	Hmgb1, Uspl1,Alox5ap
chr6	qC1	72583546	72616927	6	0,8795	0	8.747e-18	Tcf3
chr7	qB4	54576434	55130466	37	0,9665	0	1.299e-67	Mrgpra1,Mrgpra2,Mrgpra3
chr7	qD3	93087809	93156007	4	0	-1,0301	1.358e-16	Vmn2r74
chr7	qF2	124957604	125258602	16	0	-0,5043	9.145e-18	Rps15a
chr12	qC1	56190963	56363773	29	0,8416	0	2.045e-80	Srp54a,1700047I17Rik2, Srp54b,Srp54c
chrX	qA5	50318750	50352511	6	1,796	0	5.237e-36	Hprt1
chrX	qF5	166413386	166440609	5	0	-1,9029	5.979e-46	Mid1

Supplemental table 1. Genes contained in the CNVs of the XS0353 cell lines. None of them is deregulated in the array analysis.

XS0353 Validation	Sequence (5'→3')	Amplicon size	Location	Tm
Bpgm	ACCGGAGGTACAAAGTGTGC	248	Exon 2	60,04
	CTCCAGCAGAATCGGAACTC		Exon 3	59,95
Eno2	ATGGCAAGGATGCCACTAAC	228	Exon 7	59,96
	GCTGGTCCCCAGTGATGTAT		Exon 8	59,81
Cyp51	TGGCCTTAACATAGCCCACT	225	Exon 4	59,59
	TGGGTAAAACCTCCATCCAG		Exon 5	59,78
Nsdhl	CAGCAGTGCCAGTGTTGTCT	241	Exon 5	60,1
	TTTGCCCTTTCTAGCTGCAT		Exon 6	59,98
Pik3r1	TGGCTGGGGAATGAAAATAC	179	Exon 8	59,76
	CAGCCCTGCTTACTGCTCTC		Exon 9	60,3
Pik3r3	TCTGAGCCCCTGACGTTTAC	187	Exon 4	60,25
	GAGAGTGGAACTCCTGCAGAT		Exon 5	58,48
Pik3cb	GGATCGACTGGCTAAAGCAC	234	Exon 5	59,84
	AGTCACAGGGGCTAGCTTCA		Exon 6	60,01
Bcar1	TATGACGTGCCCCCTAGTGT	189	Exon 4	60,4
	AGCAAGGATCAGTGGGTGTC		Exon 5	60,12
Pou2f1	CACTTCCACAGAGCCAGTCA	188	Exon 9	60,02
	GGTGGTTTGGCTGAAGTCAT		Exon 10	59,97
Gtf3c4	CAAACAGACCTTCCCTGAGC	165	Exon 3	59,84
	ATGCTGTCATGGAGCAAACA		Exon 4	60,27
Tyms	AATCATCATGTGTGCCTGGA	165	Exon 4	59,93
	GCATAGCTGGCAATGTTGAA		Exon 5	59,84
Rbl1	GGAGATTGGAACACCTCGAA	182	Exon 8	60,05
	AAGCTACAGGCGTGGTGACT		Exon 9	59,94
Dusp4	GCCTCTACTCGGCTGTCATC	191	Exon 1	59,98
	GGCCTTGGTTTTAGAGCAGA		Exon 2	59,45
Dusp6	TTGAATGTCACCCCCAATTT	247	Exon 2	60,03
	CATCGTTCATGGACAGGTTG		Exon 3	59,96

Tissues Validation	Sequence (5'→3')	Amplicon size	Location	Tm
Gusb	CAATGAGCCTTCCTCTGCTC	219	Exon 8	64
	TTCAGCAGAGGCAGAATCAC		Exon 10	64,1
Tubb4	TCTTTCGGCCAGACAACTTT	223	Exon 3	63,6
	TCCTCTCGGATCTTGCTGAT		Exon 4	63,8
Synpo	CAAGCCATGACTGGGATGT	254	Exon 1	59,49
	GCTCTCCAAGGTGAACTCGT		Exon 2	59,45
Birc1f	AAGTGGTTCCCCAAATGTGA	254	Exon 3	60,21
	CCTGCTTTGACCAGAGCTTC		Exon 6	59,95
Cic	CTGCTCCGGACCATGTACTC	255	Exon 1	60,68
	AGCAACAGCAGCAGACTCAG		Exon 3	59,52
Mt-Atp6	CGCCTAATCAACAACCGTCT	366	Exon 1	60,13
	TGCTAATGCCATTGGTTGAA		Exon 1	60,07
Aldh1a1	GGGCTGACAAGATTCATGGT	205	Exon 4	63,9
	TGAAGAGCCGTGAGAGGAGT		Exon 6	64,1
Htr3a	TGTTCCTTTCCATGCTGACA	113	Exon 1	60,24
	GTTAGCCAGGAGGTGGTCTG		Exon 2	59,72
Jmjd5	CAGTCCTCCAGACACACCAG	131	Exon 2	59,27
	GGGTACCATCCGCTCTAACA		Exon 3	59,96
Chx3	TGATGATAGCAAATCGAAGAAGA	111	Exon 4	58,98
	AACTCTCCGCTGCTGTCTGT		Exon 5	60,21
Myh9	TTCTCCAAGGTGGAGGACAT	131	Exon 2	59,51
	GGGTTGATGACCACACAGAA		Exon 3	59,37
Ehmt1	CATGCCGAAGTCCATCTTG	121	Exon 3	60,21
	AAGCTGCTGTCGTCCACATT		Exon 4	60,86

ChIP	Sequence (5'→3')	Amplicon size	Location	Tm
Acta1	GAATCCTCGACCCTCTCACA	108	BRGATTRBR	62,6
	CACCACACACACCACAGCTA			64
Cyp51	CAGCAGCACACCAAACAACT	113	BRGATTRBR	63,5
	AACCTGGAGGGTGAGACCAT			65,3
Keap1	CTGGAACTGCCTCTGCGTA	103	BRGATTRBR	64
	CCCGGGTGTCTCTGTAGGT			64,7
Pik3r1	CCTCAGTAGGGCTCTGAGCTA	150	BRGATTRBR	63,5
	CAGGAACCCATCTCATTGCT			65
Slc25a31	CAGGCTAGTGTCTGCACCTG	129	BRGATTRBR	63,7
	ACCAACCCGGTGATTAACTG			63,5
Rpusd3	AGAAATCCGCCTGCCTCT	112	BRGATTRBR	63,9
	CGGGCGTAAAATGAAACAA			63,3
Assc2	CAGCCGCTTAACATCTCTCC	148	CAGCCWG	63,8
	TGCTGGTGCAGCCTGTAA			64,5
Birc1f	GGGCTAAGTGTGGCATCCT	139	CAGCCWG	60,09
	GGCAAGCTTTCTCTGTGTGG			61,3
BIRC1F human	GATGTGGTGGTCATGCCTA	161	CAGCCWG	63,5
	TTTTGTTTCTGTTGTTTTTGATACA			63,4
Cnp1	GCAACTGCCTCCTGTTTTAAG	150	CAGCCWG	59,03
	GGAACTCACTATGTAGCCCTGA			58,34
Htr3a	TCAGGAGGAGCAGAAGTTCAA	102	CAGCCWG	64
	TGCTTTGTTTTGCTTTCTTTTT			64,1
Igfbp3	CAAATTGGCTGGGAGTCATT	100	CAGCCWG	63,2
	TATCAGGGCCACCTCTTCAC			63,2
Jmjd5	GTGGGGACAAGTAGTTCGATT	100	CAGCCWG	61,8
	GTCTGCCTCTGCCTCCAG			64
Lynx1	GACAGGGTTCCTCCGTGTAA	72	CAGCCWG	63,2
	AGGAGTAGGAGCTGGGAGGT			63,2
Nnat	CAAAGCACGCCAATCCTT	103	CAGCCWG	63,8
	CGGTAGTGGCTGCGATCC			66,9
Pik3r3	CAGCCTGACGCGAATAGAG	100	CAGCCWG	63,7
	AGGCTTGAAAAGGGGTTTG			62,9
Ptpn1	AAGAACGGAGCCCGAAGT	100	CAGCCWG	63,2
	TCTTGGTTTTTCCAGACAGG			63,2
Reln	ACCACTCCAGGTGGCAATC	113	negative control	65,1
	CGAGCCCTTTCCAGTCAG			63,7
RELN human	AGCCGGCTCAGACAAAGAA	92	negative control	65
	AGTGTGCCCTGTTTTTCCTG			64
Shc1	CCGGCCAACTCTAAGTTCC	113	CAGCCWG	63,5
	CAAGGAATTACCGGGGAGTG			65,3
Slc24a3	TAAGGCAACGGATGGAAGAG	150	CAGCCWG	64,5
	CTAGGCGGGATGTGGATAGA			62,7
Snw1	GAGGCAGTGTCAAGCTGATG	142	CAGCCWG	63,8
	TGGAGCTGAAGTAGGACTGAGA			63,1
Utm	TGTGGCTGGAGATGGCTTA	111	CAGCCWG	64,5
	CTCACATCCCACGTGCTG			64,4
Zfp280c	CTCAGGCAGGGCAGTGAT	145	CAGCCWG	64,3
	CCCCTGACACAGGGTTTCT			64

Supplemental table 2. Primers list.

CHAPTER 5

Transcriptome profile in embryonic stem cells implicates the N-terminal region of *Gtf2i* in endocrinological, cardiovascular and neural WBS phenotypes

Maria Segura-Puimedon, Luis A Pérez-Jurado, Victoria Campuzano

In preparation

TFII-I is a multi-functional transcription factor encoded by the *Gtf2i* gene that has been demonstrated to regulate the transcription of genes critical for development. Moreover, it has been implicated in Williams-Beuren syndrome neurodeveopmental features. For these reasons, developing knowledge about the expression profile of *Gtf2i* in development is critical to the study of the broad range of targets for this transcription factor.

We have used mouse embryonic stem (ES) cells as tool to identify the transcriptome differences in two *Gtf2i*-mutated and WBS ES cell lines against wild types. With this analysis, we have uncovered the complexity and variability of the multiple genetic programs orchestrated by TFII-I and the essential role of the N-terminal region of the protein in all these programs. This knowledge should help to shed light on the molecular determinants of Williams-Beuren syndrome mostly caused by happloinsufficiency for TFII-I.

Transcriptome profile in embryonic stem cells implicates the N-terminal region of *Gtf2i* in endocrinological, cardiovascular and neural WBS phenotypes

Segura-Puimedon M, Pérez-Jurado LA, Campuzano V

ABSTRACT

General transcription factor II-I (TFII-I) is a multi-functional transcription factor encoded by the *Gtf2i* gene that has been demonstrated to regulate transcription of genes critical for development. Due to its relevant regulatory functions and established role in the neurodevelopmental disorder Williams-Beuren syndrome (WBS), developing a comprehensive expression profile is critical to the study of the broad range of targets for this transcription factor. Mouse embryonic stem (ES) cells provide interesting tools for transcriptome analysis as they express most of the genes in the organism. Microarray-based global gene expression studies were carried out in *Gtf2i*-mutated and WBS ES cell lines against wild types. Overall, our data reveal the complexity and variability of the multiple genetic programs orchestrated by TFII-I and the essential role of the N-terminal region of the protein in all these programs. This knowledge about pathways regulated by TFII-I should help to shed light on the molecular determinants of Williams-Beuren syndrome mostly caused by happloinsufficiency for TFII-I.

INTRODUCTION

TFII-I is a member of a multifunctional transcription factor family implicated in multiple pathways and that mediates various cellular responses [1]. TFII-I has been linked to multiple functions and pathways, such as transcription, cell cycle and DNA repair and its expression is especially high during development [2-6]. Structurally, the TFII-I protein comprises several domains that define its biological function, including a putative leuzine zipper at the N-terminal end, six I-repeats (R1-R6) and a basic region preceding R2 [1]. *GTF2I* gene (Entrez Gene ID 2969) has been mapped to the human chromosome 7q11.23 [7], inside the commonly deleted region of Williams-Beuren syndrome (WBS). WBS is a neurodevelopmental disorder caused by the deletion of 26 to 28 contiguous genes [8-10] and is characterized by intellectual disability, a dysmorphic face, a characteristic cognitive profile, cardiovascular abnormalities including supravalvular aortic stenosis and hypertension and glucose disturbances [11-17].

The implication of the loss of *GTF2I* in several neurodevelopmental features of WBS is documented by studies in patients, which have linked the happloinsufficient loss of the gene to behavioural sociability alterations, visuospatial processing deficits and intellectual disability [18-22]. In mouse, the *Gtf2i* gene (Entrez Gene ID 14886, MGI 1202722) is located on chromosome 5qG2 (chr5:134,713,704-134,790,616) [23]. Experimentally generated mutant mice heterozygous for *Gtf2i* feature anomalies similar to those observed in WBS: retarded growth, microcephaly, craniofacial and skeletal defects and behavioural alterations linked to WBS. The homozygous loss of G*tf2i* causes embryonic lethality in mouse models [24-26].

Gene expression is normally disturbed in most of the disorders that imply loss of one copy of one or various genes. This deregulation in gene expression can also affect nearby genes and genes all along the genome. The study of gene expression in these disorders could provide new understanding of the molecular causes of

Genes inside the WBS deletion	X503/AB22			G6/R1		
	adj.P.Val	B	Fold Chg	adj.P.Val	B	Fold Chg
Gtf2i	1,13E-06	7,366	-1,185	9,68E-05	2,619	0,640
Limk1	0,01389	-4,667	0,382	0,09627	-6,090	0,237
Rfc2	1,55E-06	6,924	-0,847	0,00016	1,864	0,471
Gtf2ird1	0,01894	-5,010	-0,185	2,09E-05	5,117	0,712
Fkbp6	4,23E-06	5,514	-0,880	0,0496	-5,373	0,168
Baz1b	0,20803	-7,470	-0,249	9,97E-05	2,576	0,573
Tbl2	1,38E-05	3,855	-0,877	0,00024	1,268	0,601
Wbscr22	7,36E-06	4,735	-0,755	0,35338	-7,354	-0,068
Wbscr27	7,12E-05	1,641	-0,700	5,91E-05	3,382	0,816
Cldn3	0,00075	-1,299	-0,687	0,08302	-5,931	0,262
Cldn4	9,43E-07	7,628	-1,820	0,00021	1,437	0,822
Eln	0,07747	-6,505	0,282	0,00026	1,183	-0,974
Mlxipl	1,63E-05	3,623	-1,550	0,00619	-2,950	0,600
Abhd11	0,00015	0,649	-0,432	0,01115	-3,656	0,214

Table 1. Expression of the WBSCR represented genes in the *Gtf2i* mutant cell lines. In dark grey the significantly DEG.

the phenotype and also new therapy targets. The development of DNA microarray technologies has allowed the performance of genome-wide analyses of the alterations in gene expression profiles resulting from changes in TFII-I dosage. Extensive data have been accumulated on the transcriptional networks associated to the expression profiles resulting from the ablation and over-expression of TFII-I in murine fibroblasts [24, 27]. Mouse embryonic stem cells are a very interesting tool for gene expression studies as they express most of the genes in the organism.

To better understand the influence of *Gtf2i* regulated pathways in WBS phenotype we performed expression arrays in 3 mutated embryonic stem cells lines: a gene trap for *Gtf2i* (XS0353), a cell line with the loss of the first 140 aminoacids of TFII-I (G6) and a cell line with the complete WBS deletion (ESSP9). Some characteristic phenotypes of WBS patients are already deregulated from the very beginning and a main role in these is played by *Gtf2i* with the important contribution of the N-ternimal region, for which involved deregulated genes are direct targets.

RESULTS

Effect of *Gtf2i* deregulation on WBSCR and contiguous region

Transcriptomic microarray analysis was performed in two *Gtf2i*-mutant cells lines. In the gene-trap XS0353, the expression of *Gtf2i* is reduced 1.2-fold (P=1.13·10^{-6}, B=7,36) and in the gene-targeted G6 is increased by 0.64-fold (P=9.7x10^{-5}, B=2.61). The WBS critical region (WBSCR) includes 26 to 28 genes and, out of the 12402 probes included in the analysis, 15 WBSCR genes were represented and 53% were found to be deregulated in both strains. Four genes (*Cldn4, Rfc2, Tbl2*, and *Wbscr27*) were significantly deregulated in the same direction as *Gtf2i* in both cells lines. Other four genes (*Fkbp6, Mlxipl*, *Abhd11* and *Gtf2ird1*) were significantly deregulated in one of the ES cells and with *p*-values minor than 0.05 in the other (Table 1). The effect of *Gtf2i* deregulation in the genes located near the WBS breakpoints was also analyzed. We analyzed ten genes at the centromeric (expanding 5Mb due to lower gene density), the telomeric (expanding 1.5 Mb) and two external control regions. We could remark a general deregulation, down for XS0353

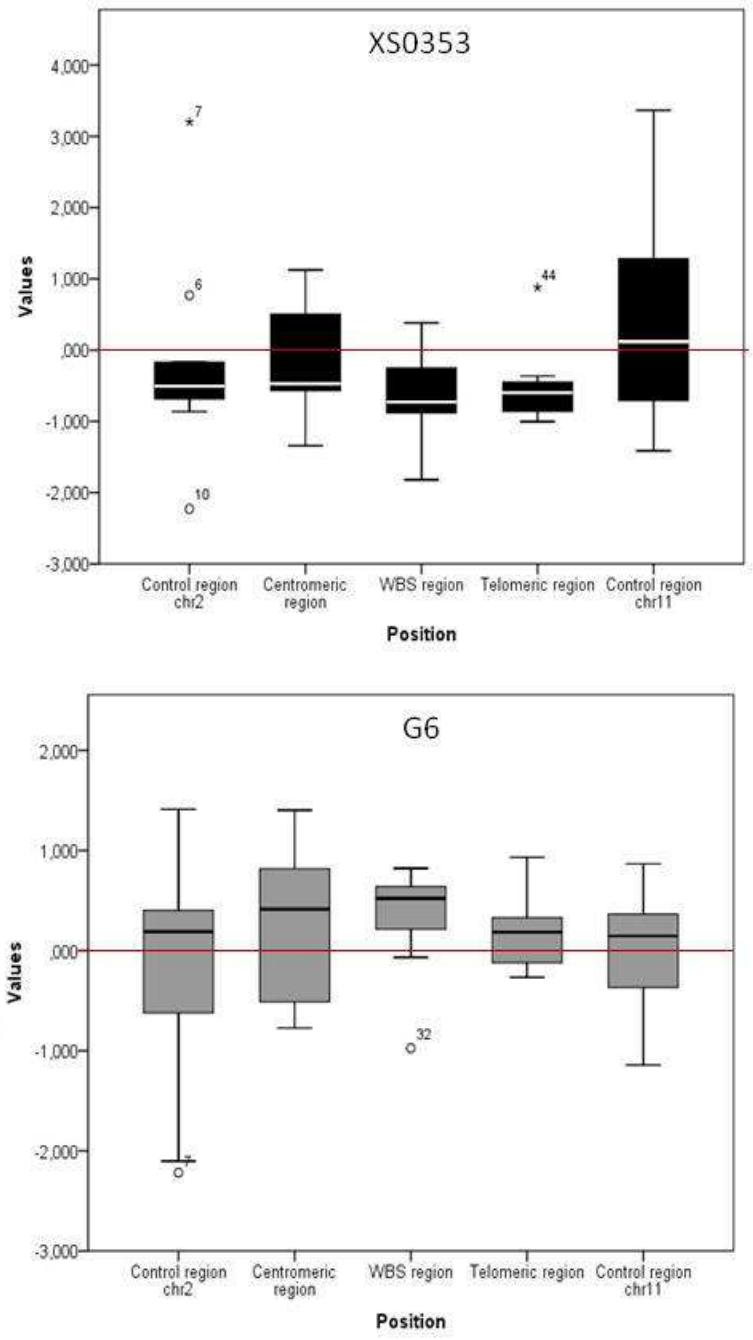

Figure 1: Gene expression profile in WBSCR and flanking regions. Box plots representing array expression in different regions for XS0353 and G6 cell line. Two external control regions in chromosomes 2 and 11 are used. Centromeric and telomeric regions to the WBSCR are analyzed as well as the deleted region.

p value	Involved pathway
3.55e-05	Nfat and hypertrophy of the heart
6.46e-05	Steroid Biosynthesis
0.002	Oxidative stress induced gene expression via nrf2
0.0024	Vegf hypoxia and angiogenesis
0.0045	Erk and pi-3 kinase are necessary for collagen binding in corneal epithelia
0.0085	NGF signalling via TRKA from the plasma membrane
0.0088	Sema3A PAK dependent Axon repulsion
0.0123	Signaling by NOTCH
0.0165	Transport of glucose and other sugars, bile salts and organic acids…
0.0174	Heart development
0.0259	Insulin signaling pathway
0.0495	Glycolysis / Gluconeogenesis - Homo sapiens (human)

Table 2. Altered pathways in the G-WBS group.

and up for G6 cell lines respectively (Fig 1) (Supplemental table 1). This fact suggests a global effect of *Gtf2i* on overall transcription, as expected for a general transcription factor.

Transcriptomal deregulation among *Gtf2i* and WBS mutant cell lines

First, we performed a transcriptomic comparison of XS0353 and ESSP9, a cell line containing the most common deletion of WBS, to determine the role of complete *Gtf2i* loss in the deregulation occurring in WBS. This comparison included 456 deregulaled genes (DEG), establishing the G-WBS group. The degree of concordance with a previous report of WBS human lymphoblastoid cell lines was studied [19]. Only three genes in common (*Msrb2, Bxdc2* and *Cenpj*) were found with the list of 92 genes deregulated in all patients and none was found in common with the 47 DEG of classical WBS patients. This little concordance may be attributable to differences in various factors including tissue expression, time expression and organism differences.

A functional enrichment analysis was performed for the commonly deregulated genes using the Consensus Path DataBase (CPDB). Interestingly, a pathway related to cardiovascular problems, concretely *Nfat* and hypertrophy of the heart was the most significantly deregulated (p=3.55e-05), including some interesting genes such as *Edn1*, *Nfatc1* or *Shc1*, which could be related to the WBS phenotypes. In agreement with previous reports and despite the absence of common DEG, we found two deregulated pathways in the G-WBS group which were already described: angiogenesis [24] and glycolysis [19] (Table 2 and Supplemental table 2).

The role of N-terminal region of *Gtf2i* in *WBS*

To study the role of the N-terminal region of *Gtf2i* in the context of a *Gtf2i* loss, we analyzed the XS0353.G6 comparison, establishing the N-*Gtf2i* group. The final number of DEG was 700.

p value	Involved pathway
0.0001	Amino acid synthesis and interconversion (transamination)
0.0011	BCR signaling pathway
0.0016	IL-6 signaling pathway
0.0020	Cyclin A:Cdk2-associated events at S phase entry
0.0028	eNOS activation and regulation
0.0029	TGF_beta_Receptor
0.0065	Cyclin E associated events during G1/S transition
0.0066	VEGFR3 signaling in lymphatic endothelium
0.0072	ErbB2/ErbB3 signaling events
0.0077	RNA Polymerase I, RNA Polymerase III, and Mitochondrial Transcription
0.0084	Notch
0.0088	Superpathway of serine and glycine biosynthesis I
0.0112	Galactose metabolism - Homo sapiens (human)
0.0119	The igf-1 receptor and longevity
0.0127	MAPK targets/ Nuclear events mediated by MAP kinases
0.0127	VEGFR1 specific signals
0.0141	Cholesterol Biosynthesis
0.0141	Role of nicotinic acetylcholine receptors in the regulation of apoptosis
0.0154	Glucose metabolism
0.0181	FGF signaling pathway
0.0253	SHC1 events in ERBB4 signaling
0.0359	Cyclin A/B1 associated events during G2/M transition
0.0359	Transcription
0.0362	Aldosterone-regulated sodium reabsorption - Homo sapiens (human)
0.0400	Signalling to RAS
0.0436	Angiogenesis overview
0.0442	RNA Polymerase I Transcription Initiation
0.0452	Nfat and hypertrophy of the heart

Table 3. Altered pathways in the N-*Gtf2i* group.

The degree of concordance with previous reports was studied. The comparison with the set of 150 genes deregulated in embryonic fibroblasts of other *Gtf2i* mutant mice found only 1.14% of common genes [28]. Similarly, 5.57% of the DEG genes were common with a set of 1616 DEG in brain tissues of mice derived from the G6 cell line [25] (Segura-Puimedon, Chapter 4), indicating very little concordance of our data with previous reports (Supplemental table 3).

After the initial comparison, a functional enrichment analysis was performed for the commonly deregulated genes using the Consensus Path DataBase (CPDB). The most significant pathway obtained was amino acid synthesis and interconversion (p=0.001). Pathways related to cell cycle, various signaling pathways, glycolysis, VEGFR and heart hypertrophy were also found (Table 3) (Supplemental table 4). Interesting genes include *Mapk1* or *Calm1* in the VEGFR pathway and *Shc1* and *Pik3r1* in the hypertrophy of the heart.

A final step was taken in order to discern the role of the N-terminal region of the TFII-I in Williams-Beuren syndrome. For this reason, we compared the G-WBS and the N-*Gtf2i* groups from the two previous comparisons, obtaining 223 common genes, establishing the N-WBS group. 48.9% genes were found in common with the XS0353.ESSP9, indicating an important role of the N-terminal region in the WBS deregulation by *Gtf2i*. The over-representation analysis showed a pathway related to cholesterol biosynthesis as the most significant (p=0.0008) and also VEGFR, cardiac related pathways and several signaling pathways (Table 4 and Supplemental table 5).

DISCUSSION

Originally described as an activator of the transcription through binding to Inr and upstream elements of several promoters, the TFII-I family members also interact with histone deacetylases (HDACs) and serve as negative regulators of transcription [2-4]. In addition, a role of TFII-I has been documented in cell cycle and DNA repair, as well as in the cytoplasm through the regulation of TRPC3 [5]. A deficit of TFII-I has been shown to cause abnormal sound sensitivity and sensorimotor gating phenotype in two different mouse models, mimicking some of the features of the WBS phenotype in humans [25, 29].

In an attempt to better define the developmental pathways altered by TFII-I depletion and its relation with WBS, we have analyzed the gene expression profiles of three murine ES cell lines, XS0353, a gene trap with no TFII-I expression, G6, expressing truncated TFII-I protein lacking the first 140 aminoacids and ESSP9, expressing the common WBS deletion [25] (Segura-Puimedon, Chapter 3). We have applied restrictive parameters of significance for data processing along with algorithms to minimize background noise and maximize the statistical power. The relevance of the findings is further reinforced by the very high consistency among replicates and additional experimental validation with qRT-PCR.

Our results show that TFII-I may regulate the expression of an important amount of genes in the context of WBS syndrome, as the number of deregulated genes is 456 in the XS0353.ESSP9 hybridization, very similar to the 599 DEG in the ESSP9 cell line when compared to the wild type (Segura-Puimedon, Chapter 3), indicating the possible existence of a compensatory role to cover the loss of 26 to 28 genes in the WBS deletion.

The deregulation of *Gtf2i* has an important effect in the expression regulation of the other genes in the WBSCR. In both *Gtf2i* mutant cell lines, there is the significant deregulation of 8 genes out of the 15 analyzed genes. Moreover, *Gtf2i* deregulation of the WBS is greater than the deregulation provoked by the heterozygous loss of all the genes in the region in the ESSP9 cell lines, were only 6 genes were significantly deregulated (Segura-Puimedon, Chapter 3). Moreover, we could also see an important downregulation of the expression at both ends of the WBSCR in the XS0353 as well as in one of the control cell lines, indicating a global downregulation effect as a consequence of the *Gtf2i* gene-trap.

p value	Involved pathway
0.0008	Cholesterol Biosynthesis
0.0025	VEGFR3 signaling in lymphatic endothelium
0.0035	IL3-mediated signaling events
0.0041	Regulation of map kinase pathways through dual specificity phosphatases
0.0075	Insulin signaling pathway
0.0102	Keap1-Nrf2 Pathway
0.0111	Actions of nitric oxide in the heart
0.0127	Nfat and hypertrophy of the heart
0.0166	Nerve growth factor pathway (ngf)
0.0204	Ras signaling pathway
0.0204	Egf signaling pathway
0.0287	Growth hormone signaling pathway
0.0334	Oxidative stress induced gene expression via nrf2
0.0358	Transcription factor creb and its extracellular signals
0.0383	Role of erk5 in neuronal survival pathway
0.0408	Galactose metabolism - Homo sapiens (human)
0.0411	TGF beta Signaling Pathway

Table 4. Altered pathways in the G-WBS group.

Relevant altered pathways related to the role of *Gtf2i*

A role of TFII-I in cell cycle and DNA repair has been previously demonstrated [5]. As a consequence, pathways related to cell cycle and transcription are present in the N-Gtf2i group, providing clues for a role of the N-terminal region of *Gtf2i* in some of these functions, such as in cyclin events during cell cycle checkpoints or in RNA polymerase transcription initiation.

A pathway related to the TGFβ receptor has been obtained in the N-*Gtf2i* and N-WBS, including an important number of deregulated genes. This result of *Gtf2i* playing a role in the TFGβ signaling pathway is reinforced by the fact that this pathway has been also identified as over-represented in a study of genes bearing a new binding motif for *Gtf2i* binding to the promoter region (Segura-Puimedon, Chapter 4) and one of the genes present in the pathway, *Mapk1* directly interacts with *Gtf2i* [30].

Relevant altered pathways related to the WBS phenotype

Potential TFII-I targets implicated in some of the WBS features have been reported, including osteogenic marker genes for the craniofacial development or neuronal cytoskeletal genes for the neurobehavioral phenotype [28, 31-32]. Moreover, and as said before, we have obtained several over-represented pathways which have been already reported, for example the lipid metabolism, with steroid and cholesterol metabolism. Cholesterol is the precursor of vitamin D, essential in the calcium metabolism. Both vitamin D and lipid metabolism are found to be deregulated in a previous study comparing ESSP9 with the wild-type (Segura-Puimedon, Chapter 3). Consequently, the deregulation of the lipid metabolism with a role of *Gtf2i* could be implicated in the hypercalcaemia phenotype present in a percentage of young WBS patients. Moreover, it could

indicate deregulation in the lipid and cholesterol levels in patients, but no studies have been performed so far in this aspect.

In addition, the glycolisis and angiogenesis pathways have also been reported in WBS and other new described pathways can be linked to a relevant role of *Gtf2i* in WBS phenotypes.

Glycolisis. About 75% of WBS adult patients show abnormal glucose tolerance on standard testing and are at risk of developing diabetes [17]. A previous study showed deregulation of glycolysis in WBS patients, but not in patients with small deletions excluding *GTF2I* [19]. The glycolysis pathway is over represented in a group of potential target genes of *Gtf2i* identified by a new binding motif (Segura-Puimedon, Chapter 4).

In our study, the glycolysis pathway is present in the three studied groups, confirming that *Gtf2i* may be, at least in part, responsible of the glucose abnormalities present in WBS patients and a partial role of the N-terminal region in the deregulation. As previously suggested, the alteration of this pathway could contribute to brain dysfunction and mental retardation in WBS, as shown in other hereditary abnormalities of glucose metabolism [33]. *Mlxipl*, a gene in the WBS deleted region, could also contribute to the glucose phenotype as it is significantly downregulated in the XS0353 cell line, where there is the loss of *Gtf2i*. This gene is a transcription factor with a relevant role as a carbohydrate responsive element binding protein and has been related to glucose and lipid metabolism [34].

Glucose transport, with several *Slc* transporters genes present, is altered in the G-WBS group, indicating a role of *Gtf2i* in the pathway without the contribution of the N-terminal region of the protein. Other found pathways can be related to the phenotype, as the deregulation of the insulin signaling pathway. In this case it would be mediated by the N-terminal region of the protein, as it appears deregulated in the N-WBS group. The *Pik3r1* gene is a regulatory subunit of the Pi3k and in the WBS cell line there is an upregulation of the expression of the protein, which could have an important role in the pathway as attenuation of *Pik3r1* expression has been reported to prevent insulin resistance and we would have here the contrary situation [35].

The galactose pathway, a molecule that can enter the glycolysis pathway being converted to glucose-1-phosphate, is represented in the N-*Gtf2i* and N-WBS groups, indicating a role of the N-terminal part of *Gtf2i* in this pathway regulation.

Taken together, these results demonstrate a role of *Gtf2i* in the regulation of the glucose, galactose and insulin metabolism in WBS, which may be related to the described endocrine abnormalities.

Vasculogenesis and angiogenesis. Developmental anomalies in mutant mice have suggested a major role of TFII-I in vasculogenesis at midgestation [24]. The embryonic lethality of homozygous *Gtf2i* knockout mice has been attributed to vascular problems secondary to downregulation of the VEGFR2 signal transduction cascade [24], while the lethality of homozygous *Gtf2i* mice truncated at the 5'prime occurs so early that no vascular phenotype can be appreciated [25]. TFII-I is expressed in developing lung, heart and gut structures and has been also related to angiogenesis [36-38]. In agreement with this role, we have found pathways related to Vegf or Vegfr in the three studied groups and Tie2 signaling in the common DEG. *Tie2* is a family member of receptor tyrosine kinases involved in vasculogenesis and angiogenesis. Its main role is to stabilize, maintain, and facilitate the structural adaptation of the vasculature during embryonic development. To further

document this relation, *Gtf2i* is reported to interact with *VEGFR2* increasing its transcription [38], and previous ChIP experiments have shown that at least two genes present in these pathways, *Shc1* and *Pik3r1* are direct TFII-I targets (Segura-Puimedon, Chapter 4). *Gtf2i* also interacts with *Calm1*, present in the Vegfr3 pathway of the N-*Gtf2i* group [39].

Notch signaling has been described to have an essential role in vascular morphogenesis and remodeling using knockout mouse models [40-41]. Moreover, *Vegf* regulates *Notch1* trough the PI3K /Akt signaling, also related to *Gtf2i* [42], providing a relation among the pathways and a role for notch signaling in angiogenesis [43]. Notch signaling is present in the N-*Gtf2i* and G-WBS DEG groups, indicating a role of the *Gtf2i* gene in the deregulation of the pathway in WBS. However, this role is not exert trough the N-terminal region of the protein, as the pathway is not present in the N-WBS group.

Cardiovascular phenotype and oxidative stress. An interesting feature of WBS individuals is their cardiovascular phenotype. Most infants are first diagnosed as WBS patients by the presence of supravalvular aortic stenosis. Elastin happloinsufficiency gene has been established as the main cause for the SVAS [44]. In contribution to the cardiovascular phenotype 40% of the patients develop hypertension [45]. Hypertension is caused by an angiotensin II mediated oxidative stress and it was shown that hemizygosity at the *NCF1* gene decreased the risk of hypertension in WBS patients [46-47]. Despite the normal expression of Elastin in the ESSP9 and XS0353 cell lines, several significantly altered pathways present in our analysis can be linked to the cardiovascular disease.

The pathway *Nfat* and hypertrophy of the heart is present in the three groups, with the genes *Shc1*, *Pik3r1* and *Atp2a3* in common and several only appearing in one of the groups. *Shc1* and *Pik3r1* are present in several of the studied pathways as they are part of the PI3K/Akt signaling pathway, with important roles in various signaling cascades. *Atp2a3* encodes for one of the SERCA ATPases (*Serca3*) which catalyzes the hydrolysis of ATP coupled with the translocation of calcium from the cytosol to the sarcoplasmic reticulum lumen in muscle cells. Knockout mice for *Serca3* show normal blood pressure and cardiovascular performance, indicating it does not play an important role on pressure control [48].

The most important number of genes is present in the G-WBS group with the global role of *Gtf2i* in WBS. Endothelin 1 (*Edn1*) is an adrenergic agonist that promotes vasoconstriction and has been implicated in hypertension and hypertrophy induction. *Edn1* binds to G-protein coupled receptor (GPCR) and activates the MAPK pathway, which finally activates the calcineurin-NFAT pathway [49-50]. Changes of *Edn1* and *Nfatc1* expression could contribute to the activation of transcriptional factors such as Gata-4 and thus, lead to cardiac hypertrophy [51-52]**.** *Hdac9* is a type II histone deacetylase and acts as a suppressor of cardiac hypertrophy in response to stress signal. Other hypertrophy related genes found deregulated in the analysis are also part of this signaling pathway. The role of *Gtf2i* in this deregulation is reinforced by the fact that other members of the HDAC family interact with *Gtf2i,* like *Hdac2* and 3. Also, genes of the MAPK pathway like *ERK* interact with *Gtf2i* and the MAPK signaling pathway was found deregulated in our analysis in all the groups [30, 53-54].

Oxidative stress has been linked to WBS as the production mechanism of the hypertension, with an increase in reactive oxygen species due to the increase in the NADPH-oxidase complex [47]. *Gtf2i* may

be playing a role in the oxidative stress via induced expression of NRF2 protein. The deregulated genes in the G-WBS group are *Hmox1, Mafk, Keap1 and Nfe2l2*. *Nfe2l2* encodes for the NRF2 protein, identified as one of the transcription factors acting on the antioxidant response element (ARE) of human NADPH to activate gene transcription [55]. NRF2 is inactive and targeted for ubiquitination by binding to *Keap1*. One of the targets of NRF2 is *Hmox1* which has a cytoprotective and anti-inflammatory role in response to oxidative stress. *Mafk* binds to NRF2 and avoids its transcriptional activation activity. The deregulation of the pathway could have a role in the oxidative stress mediated hypertension found in patients as they are not able to respond adequately to oxidative stress via NRF2 [56].

Neural phenotype. WBS patients have a concrete neural phenotype including mental retardation and a defined cognitive profile with deficient visuospatial abilities and relatively good preserved verbal skills [16]. Several pathways could be related to neural regulation and signaling. The nerve growth factor (NGF) pathway appears over-represented in the G-WBS and the N-WBS DEG groups, indicating a role of *Gtf2i* trough the N-terminal region of the protein in the pathway regulation. In G-WBS most of the genes present in the pathway are downregulated in ESSP9, indicating a role of *Gtf2i* in the upregulation of the pathway that is lost when all the genes of the WBSCR are deleted. This fact implies a downregulation of the NGF signaling pathway in the WBS ES cell pointing to problems in the development of peripheral sympathetic and sensory neurons as NGF controls cell growth, neurite production and elongation, and selective cell death or survival during the prenatal stage [57]. WBS children and adolescents patients have shown elevated levels of NGF in serum which may induce abnormal nerve function, sympathetic hypertrophy and immunological alterations. The study also reports a potential link between NGF and hypertension, as changes in circulating NGF levels seem to be implicated in the pathogenesis of hypertension [57].

Moreover, in the G-WBS DEG, the *Sema3A d*ependent axon repulsion pathway appears, including the *Limk1* gene, deleted in WBS. *Limk1* has been already identified as implicated in the dynamic aspects of the cytoskeleton via the actin filaments [19] and semaphoring related pathways have been identified as deregulated in a study with the ESSP9 cell line (Segura-Puimedon, Chapter 3). Our results would link *Gtf2i* to the deregulation of the pathway and the axon guidance and establishment in WBS.

In summary, the array analysis had high reproducibility among the samples in each cell line and results were validated by qRT-PCR experiments. This report reveals the complexity of the genetic programs and pathways orchestrated by the general transcription factor TFII-I during development after analysing transcriptome profiles in ES cells of *Gtf2i* mutants and a cell line of WBS deletion. Comparative transcriptome analysis provides new insight into the major pathogenic mechanisms for some of the multisystemic features of WBS. Dysfunction of the glycolysis pathway is likely associated with the impaired glucose tolerance, while altered *Nfat* and hypertrophy of the hearth together with altered oxidative stress could contribute to the cardiovascular phenotype development by the WBS since the early infancy. Vasculogenesis pathways and lipid metabolism are also deregulated and could be related with unknown WBS phenotypes. *In vivo* binding of TFII-I to promoter regions of some relevant deregulated genes confirmed the direct involvement of TFII-I in this process. Further analyses of the genes and pathways affected in WBS in other tissues as well as in mouse models are warranted

to better define the networks disturbed in the physiopathology of the WBS phenotype and help in the identification of therapeutic targets.

MATERIALS AND METHODS

ES cell line genotyping and cell culture. Clone XS0353 ES (embryonic stem cells) carries an insertion of the gene trap vector pGT101xf in exon 2 of the *Gtf2i* gene. The insertion completely abolishes the expression of the corresponding *Gtf2i* allele. Clone XS0353 and AB22 were obtained from the Sanger Institute Gene Trap Resource (SIGTR) mouse ES cell line collection (http://www.sanger.ac.uk/PostGenomics /genetrap/). G6 ES cell line was obtained as previously reported.[25] Briefly, replacement of *Gtf2i* genomic sequences integrated by exon2 and flanked intronic sequences by a PGK-*neo* cassette, generated a TFII-I isoform losing the first 140 aminoacid. ESSP9 was obtained as previously reported (Segura-Puimedon, Chapter 3). Briefly, a *loxP* site and a PKG-*hygro* cassette were introduced at intron 5 of the *Fkbp6* genes in the G6 cell line. 2loxP clones in cis were electroporated with a vector containing Cre-recombinase gene and *Puromicin* resistance gene, obtaining a cell line with the WBS common deletion. ES Cell lines were cultured in standard conditions. Penicillin/streptomycin, LIF, no essential aminoacids and β-mercaptoethanol were also added to the medium. Cells were always cultured in a monolayer of feeder cells and maintained at 37ºC in a humidified 5% CO2 chamber.

mRNA preparations and microarray hybridizations. mRNA was extracted from tissues and cell lines by using TRIZOL reagent (Invitrogen, Carlsbad, CA, USA), followed by a second extraction using RNeasy (Qiagen), in both cases according to the manufacturer's instructions. Quality of all RNA samples was checked using an Agilent 2100 Bioanalyzer (Agilent Technologies). Only those samples with an RNA Integrity Number (RIN) >7 were used for hybridization. Samples of 500ng/μl were used to perform an Affymetric mouse 430_2 expression array. Images were processed with Microarray Analysis Suite 5.0 (Affymetrix). All samples demonstrated characteristics of high-quality cRNA (3'/5' ratio of probe sets for glyceraldehyde-3-phosphate dehydrogenase and beta-actin of <1.5) and were subjected to subsequent analysis. Raw expression values obtained directly from .CEL files were preprocessed using the RMA method [58], a three-step process which integrates background correction, normalization and summarization of probe values. These normalized values were the basis for all the analysis. Previous to any analysis, data were submitted to non-specific filtering to remove low signal genes (those genes whose mean signal in each group did not exceed a minimum threshold) and low variability genes (those genes whose standard deviation between all samples did not exceed a minimum threshold).

Statistical analyses. The selection of differentially expressed genes between conditions was based on a linear model analysis with empirical Bayes moderation of the variance estimates following the methodology developed by Smyth [59]. The method extends traditional linear model analysis using empirical Bayes methods to combine information from the whole array and every individual gene in order to obtain improved error estimates which are very useful in microarray data analysis where sample sizes are often small what can lead to erratic error estimates and, in consequence, to untrustful *p*-values. The analysis yields standard tests statistics such as fold changes, (moderated)-t or p–values which can be used to rank the genes from most to least differentially expressed. In order to deal with the multiple testing issues derived

from the fact that many tests (one per gene) are performed simultaneously, *p*–values were adjusted to obtain strong control over the false discovery rate using the Benjamini and Hochberg method [60]. After different corrections, we discriminated 12402 cDNA clones with the correct quality to be analyzed. Differentially expressed genes were selected in each comparison for B>0 and p<0.01.

Pathway definition. In order to identify the affected pathways in the different groups, we used the Consensus Path database version 24 (CPDB; http://cpdb.molgen.mpg.de/) [61], which contains functional molecular interactions obtained from 30 publicly available resources. When a pathway was present in more than one database, the one with lower p value was selected. Gene information was obtained from Entrez Gene (http://www.ncbi.nlm.nih.gov/gene) and Ensembl databases (www.ensembl.org).

cDNA obtention, qPCR experiments and data analysis. To validate the expression results obtained in the array analysis, 2 μg of the same mRNA used for the array hybridization were used for first-strand cDNA synthesis with Superscript II (Invitrogen). Primers and probes were designed to span an intron in all cases using the Primer3 software Version 0.4.0 and are available upon request [62]. Verification of the array data by qRT-PCR was previously performed for XS0353 (Segura-Puimedon, motif) and for ESSP9 (Segura-Puimedon, model), obtaining high levels of validation in both cell lines. The validation was performed for the G6 ES clone compared to the respective wild type clone, R1. All 7 randomly chosen genes were found to be deregulated in the same direction and magnitude, confirming the microarray data (100%) (Supplemental figure 1). Real-Time PCR was performed using the SYBR Green Ready Master Mix according to the manufacturer's instructions in an ABI PRISM 7900HT Sequence Detection System (Applied Biosystems). The standard curve method was used for the analysis. The results were normalized respect to a housekeeping gene selected for its stable expression among the different cell lines. A reagent-only (no DNA) negative control sample was always included in each run. Experiments were performed a minimum of 3 times in 384-well plates with three replicates per sample. Raw data was obtained using SDS 2.1 software (Applied Biosystems).

Accesion number. The accession number for supporting microarray data is: http://www.ncbi.nlm.nih.gov/geo/query/acc.cgi?token=drstlicyasoiyro&acc=GSE23202

AUTHOR CONTRIBUTIONS

Conceived and designed the experiments: VC and LAP-J. Analyzed the results and wrote the manuscript: MS-P, VC and LAP-J. Performed the experiments: MS-P, VC. All authors read and approved the final manuscript.

ACKNOWLEDGEMENTS

We thank Verena Terrado for technical assistance. This work was supported by grants from the Spanish Ministry of Health (FIS 04/0433, to VC), and the VI Framework Programme of the European Union (LSHG-CT-2006-037627, to LAP-J). MS-P was supported by CIBERER and UPF Fellowships. VC is a FIS Investigator.

REFERENCES

1. Roy, A.L., *Biochemistry and biology of the inducible multifunctional transcription factor TFII-I*. Gene, 2001. **274**(1-2): p. 1-13.
2. Ogura, Y., et al., *TFII-I down-regulates a subset of estrogen-responsive genes through its*

interaction with an initiator element and estrogen receptor alpha. Genes Cells, 2006. **11**(4): p. 373-81.
3. Stasyk, T., et al., *Phosphoproteome profiling of transforming growth factor (TGF)-beta signaling: abrogation of TGFbeta1-dependent phosphorylation of transcription factor-II-I (TFII-I) enhances cooperation of TFII-I and Smad3 in transcription.* Mol Biol Cell, 2005. **16**(10): p. 4765-80.
4. Tussie-Luna, M.I., et al., *Physical and functional interactions of histone deacetylase 3 with TFII-I family proteins and PIASxbeta.* Proc Natl Acad Sci U S A, 2002. **99**(20): p. 12807-12.
5. Desgranges, Z.P. and A.L. Roy, *TFII-I: connecting mitogenic signals to cell cycle regulation.* Cell Cycle, 2006. **5**(4): p. 356-9.
6. Roy, A.L., *Signal-induced functions of the transcription factor TFII-I.* Biochim Biophys Acta, 2007. **1769**(11-12): p. 613-21.
7. Perez Jurado, L.A., et al., *A duplicated gene in the breakpoint regions of the 7q11.23 Williams-Beuren syndrome deletion encodes the initiator binding protein TFII-I and BAP-135, a phosphorylation target of BTK.* Hum Mol Genet, 1998. **7**(3): p. 325-34.
8. Francke, U., *Williams-Beuren syndrome: genes and mechanisms.* Hum Mol Genet, 1999. **8**(10): p. 1947-54.
9. Stromme, P., P.G. Bjornstad, and K. Ramstad, *Prevalence estimation of Williams syndrome.* J Child Neurol, 2002. **17**(4): p. 269-71.
10. Schubert, C., *The genomic basis of the Williams-Beuren syndrome.* Cell Mol Life Sci, 2009. **66**(7): p. 1178-97.
11. Morris, C.A., et al., *Natural history of Williams syndrome: physical characteristics.* J Pediatr, 1988. **113**(2): p. 318-26.
12. Tassabehji, M., *Williams-Beuren syndrome: a challenge for genotype-phenotype correlations.* Hum Mol Genet, 2003. **12 Spec No 2**: p. R229-37.
13. Karnik, S.K., et al., *A critical role for elastin signaling in vascular morphogenesis and disease.* Development, 2003. **130**(2): p. 411-23.
14. Li, D.Y., et al., *Elastin is an essential determinant of arterial morphogenesis.* Nature, 1998. **393**(6682): p. 276-80.
15. Pober, B.R., M. Johnson, and Z. Urban, *Mechanisms and treatment of cardiovascular disease in Williams-Beuren syndrome.* J Clin Invest, 2008. **118**(5): p. 1606-15.
16. Pober, B.R., *Williams-Beuren syndrome.* N Engl J Med, 2010. **362**(3): p. 239-52.
17. Cherniske, E.M., et al., *Multisystem study of 20 older adults with Williams syndrome.* Am J Med Genet A, 2004. **131**(3): p. 255-64.
18. Dai, L., et al., *Is it Williams syndrome? GTF2IRD1 implicated in visual-spatial construction and GTF2I in sociability revealed by high resolution arrays.* Am J Med Genet A, 2009. **149A**(3): p. 302-14.
19. Antonell, A., M. Vilardell, and L.A. Perez Jurado, *Transcriptome profile in Williams-Beuren syndrome lymphoblast cells reveals gene pathways implicated in glucose intolerance and visuospatial construction deficits.* Hum Genet, 2010.
20. Danoff, S.K., et al., *TFII-I, a candidate gene for Williams syndrome cognitive profile: parallels between regional expression in mouse brain and human phenotype.* Neuroscience, 2004. **123**(4): p. 931-8.
21. Hirota, H., et al., *Williams syndrome deficits in visual spatial processing linked to GTF2IRD1 and GTF2I on chromosome 7q11.23.* Genet Med, 2003. **5**(4): p. 311-21.
22. Morris, C.A., et al., *GTF2I hemizygosity implicated in mental retardation in Williams syndrome: genotype-phenotype analysis of five families with deletions in the Williams syndrome region.* Am J Med Genet A, 2003. **123A**(1): p. 45-59.
23. Valero, M.C., et al., *Fine-scale comparative mapping of the human 7q11.23 region and the orthologous region on mouse chromosome 5G: the low-copy repeats that flank the Williams-Beuren syndrome deletion arose at breakpoint sites of an evolutionary inversion(s).* Genomics, 2000. **69**(1): p. 1-13.
24. Enkhmandakh, B., et al., *Essential functions of the Williams-Beuren syndrome-associated TFII-I genes in embryonic development.*

Proc Natl Acad Sci U S A, 2009. **106**(1): p. 181-6.
25. Lucena, J., et al., *Essential role of the N-terminal region of TFII-I in viability and behavior.* BMC Med Genet, 2010. **11**(1): p. 61.
26. Sakurai, T., et al., *Haploinsufficiency of Gtf2i, a gene deleted in Williams Syndrome, leads to increases in social interactions.* Autism Res, 2010.
27. Chimge, N.O., et al., *Gene expression analysis of TFII-I modulated genes in mouse embryonic fibroblasts.* J Exp Zool B Mol Dev Evol, 2007. **308**(3): p. 225-35.
28. Chimge, N.O., et al., *Identification of the TFII-I family target genes in the vertebrate genome.* Proc Natl Acad Sci U S A, 2008. **105**(26): p. 9006-10.
29. Li, H.H., et al., *Induced chromosome deletions cause hypersociability and other features of Williams-Beuren Syndrome in Mice.* EMBO Molecular Medicine, 2009. **1**: p. 50-65.
30. Kim, D.W. and B.H. Cochran, *JAK2 activates TFII-I and regulates its interaction with extracellular signal-regulated kinase.* Mol Cell Biol, 2001. **21**(10): p. 3387-97.
31. Lazebnik, M.B., et al., *Williams-Beuren syndrome-associated transcription factor TFII-I regulates osteogenic marker genes.* J Biol Chem, 2009. **284**(52): p. 36234-9.
32. Makeyev, A. and D. Bayarsaihan, *Molecular Basis of Williams-Beuren Syndrome: TFII-I Regulated Targets Involved in the Craniofacial Development.* Cleft Palate Craniofac J, 2010.
33. Blass, J.P., R.K. Sheu, and J.M. Cedarbaum, *Energy metabolism in disorders of the nervous system.* Rev Neurol (Paris), 1988. **144**(10): p. 543-63.
34. Merla, G., et al., *The subcellular localization of the ChoRE-binding protein, encoded by the Williams-Beuren syndrome critical region gene 14, is regulated by 14-3-3.* Hum Mol Genet, 2004. **13**(14): p. 1505-14.
35. McCurdy, C.E., et al., *Attenuated Pik3r1 Expression Prevents Insulin Resistance and Adipose Tissue Macrophage Accumulation in Diet-Induced Obese Mice.* Diabetes, 2012.
36. Fijalkowska, I., et al., *Expression of the transcription factor, TFII-I, during post-implantation mouse embryonic development.* BMC Res Notes, 2010. **3**: p. 203.
37. Mammoto, A., et al., *A mechanosensitive transcriptional mechanism that controls angiogenesis.* Nature, 2009. **457**(7233): p. 1103-8.
38. Jackson, T.A., et al., *Vascular endothelial growth factor receptor-2: counter-regulation by the transcription factors, TFII-I and TFII-IRD1.* J Biol Chem, 2005. **280**(33): p. 29856-63.
39. Shen, X., et al., *Scanning the human proteome for calmodulin-binding proteins.* Proc Natl Acad Sci U S A, 2005. **102**(17): p. 5969-74.
40. Huppert, S.S., et al., *Embryonic lethality in mice homozygous for a processing-deficient allele of Notch1.* Nature, 2000. **405**(6789): p. 966-70.
41. Krebs, L.T., et al., *Notch signaling is essential for vascular morphogenesis in mice.* Genes Dev, 2000. **14**(11): p. 1343-52.
42. Chimge, N.O., et al., *PI3K/Akt-dependent functions of TFII-I transcription factors in mouse embryonic stem cells.* J Cell Biochem, 2012. **113**(4): p. 1122-31.
43. Liu, Z.J., et al., *Regulation of Notch1 and Dll4 by vascular endothelial growth factor in arterial endothelial cells: implications for modulating arteriogenesis and angiogenesis.* Mol Cell Biol, 2003. **23**(1): p. 14-25.
44. Li, D.Y., et al., *Novel arterial pathology in mice and humans hemizygous for elastin.* J Clin Invest, 1998. **102**(10): p. 1783-7.
45. Broder, K., et al., *Elevated ambulatory blood pressure in 20 subjects with Williams syndrome.* Am J Med Genet, 1999. **83**(5): p. 356-60.
46. Del Campo, M., et al., *Hemizygosity at the NCF1 gene in patients with Williams-Beuren syndrome decreases their risk of hypertension.* Am J Hum Genet, 2006. **78**(4): p. 533-42.
47. Campuzano, V., et al., *Reduction of NADPH-oxidase activity ameliorates the cardiovascular phenotype in a mouse model of Williams-Beuren Syndrome.* PLoS Genet, 2012. **8**(2): p. e1002458.
48. Dally, S., et al., *Multiple and diverse coexpression, location, and regulation of additional SERCA2 and SERCA3 isoforms in*

nonfailing and failing human heart. J Mol Cell Cardiol, 2010. **48**(4): p. 633-44.
49. Palacin, M., et al., *Lack of association between endothelin-1 gene variants and myocardial infarction.* J Atheroscler Thromb, 2009. **16**(4): p. 388-95.
50. Cullen, J.P., et al., *Use of A-192621 to provide evidence for involvement of endothelin ET(B)-receptors in endothelin-1-mediated cardiomyocyte hypertrophy.* Eur J Pharmacol, 2001. **417**(3): p. 157-68.
51. Rohini, A., et al., *Molecular targets and regulators of cardiac hypertrophy.* Pharmacol Res, 2010. **61**(4): p. 269-80.
52. Barry, S.P., S.M. Davidson, and P.A. Townsend, *Molecular regulation of cardiac hypertrophy.* Int J Biochem Cell Biol, 2008. **40**(10): p. 2023-39.
53. Crusselle-Davis, V.J., et al., *Recruitment of coregulator complexes to the beta-globin gene locus by TFII-I and upstream stimulatory factor.* FEBS J, 2007. **274**(23): p. 6065-73.
54. Hakimi, M.A., et al., *A candidate X-linked mental retardation gene is a component of a new family of histone deacetylase-containing complexes.* J Biol Chem, 2003. **278**(9): p. 7234-9.
55. Nguyen, T., P. Nioi, and C.B. Pickett, *The Nrf2-antioxidant response element signaling pathway and its activation by oxidative stress.* J Biol Chem, 2009. **284**(20): p. 13291-5.
56. Kaspar, J.W., S.K. Niture, and A.K. Jaiswal, *Nrf2:INrf2 (Keap1) signaling in oxidative stress.* Free Radic Biol Med, 2009. **47**(9): p. 1304-9.
57. Calamandrei, G., et al., *Serum NGF levels in children and adolescents with either Williams syndrome or Down syndrome.* Dev Med Child Neurol, 2000. **42**(11): p. 746-50.
58. Irizarry, R.A., et al., *Exploration, normalization, and summaries of high density oligonucleotide array probe level data.* Biostatistics, 2003. **4**(2): p. 249-64.
59. Smyth, G.K., *Linear models and empirical bayes methods for assessing differential expression in microarray experiments.* Stat Appl Genet Mol Biol, 2004. **3**: p. Article3.
60. Benjamini Y., H.Y., *Controlling the false discovery rate: A practical and powerful approach to multiple testing.* Journal of the Royal Statistical Society. Series B (Methodological), 1995. **57**(1): p. 289-300.
61. Kamburov, A., et al., *ConsensusPathDB--a database for integrating human functional interaction networks.* Nucleic Acids Res, 2009. **37**(Database issue): p. D623-8.
62. Rozen, S. and H. Skaletsky, *Primer3 on the WWW for general users and for biologist programmers.* Methods Mol Biol, 2000. **132**: p. 365-86.

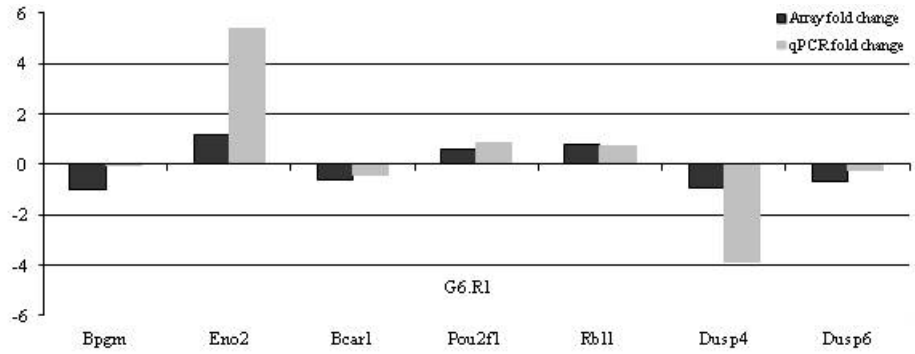

Figure S1: Array validation for the G6 cell line. Deregulated genes were validated by qRT-PCR comparing fold change values in G6 versus R1 cell lines. 100% of the genes were validated in both cell lines. All qRT-PCR analyses were done in triplicate.

Centromeric region		X503/AB22			G6/R1		
Genes	Position	adj.P.Val	B	Fold Chg	adj.P.Val	B	Fold Chg
Gats	5 G2	2,40E-06	6,312	1,125	0,00048	0,331	-0,512
Auts2	5 G2	0,00032	-0,246	0,503	1,93E-05	5,278	0,935
Tyw1	5 G2	0,00038	-0,462	-0,631	0,00035	0,733	0,690
Asl	5 G2	0,00020	0,303	-0,488	0,00087	-0,476	0,411
Gusb	5 G2	0,00035	-0,370	0,605	0,00014	2,058	-0,773
Psph	5 G2	1,10E-07	10,599	-1,343	8,66E-06	6,726	0,818
Gbas	5 G2	7,00E-05	1,662	-0,519	0,00043	0,473	0,419
Sfrs8	5 G2	0,02121	-5,134	-0,454	0,0001	2,536	-0,673
Gpr133	5 G2	0,12625	-6,995	-0,336	0,00023	1,322	1,402
Piwil1	5 G2	0,00553	-3,633	-0,568	0,67618	-7,826	0,070

Telomeric region		X503/AB22			G6/R1		
Genes	Position	adj.P.Val	B	Fold Chg	adj.P.Val	B	Fold Chg
Hip1	5 G2	0,00031	-0,217	-0,858	0,41722	-7,491	0,124
Nsun5	5 G2	2,87E-06	6,053	-1,005	0,03388	-4,948	0,187
Pom121	5 G2	8,91E-06	4,458	-0,931	0,20555	-6,860	-0,120
Srcrb4d	5 G2	0,00587	-3,698	-0,366	4,84E-05	3,694	0,932
Zp3	5 G2	0,00115	-1,805	-0,448	0,00791	-3,250	0,330
Dtx2	5 G2	2,34E-05	3,121	-0,692	0,02421	-4,564	0,181
Lrwd1	5 G2	2,89E-05	2,833	-0,592	0,00211	-1,612	0,268
Alkbh4	5 G2	5,90E-05	1,883	-0,591	0,00531	-2,764	-0,267
Prkrip1	5 G2	9,20E-06	4,410	-0,605	0,0001	2,446	0,450
Orai2	5 G2	0,00024	0,091	0,878	0,3137	-7,250	-0,152

Control region 1		X503/AB22			G6/R1		
Genes	Position	adj.P.Val	B	Fold Chg	adj.P.Val	B	Fold Chg
Ryr3	2 E3	0,00012	0,949	-0,864	1,71E-05	5,485	1,412
Rasgrp1	2 E5	0,17559	-7,312	-0,171	6,56E-05	3,216	1,037
Slc12a6	2 E3	0,04307	-5,898	-0,521	0,44564	-7,543	0,183
Nola3	2 E3	0,00016	0,578	-0,501	0,27706	-7,139	0,088
Meis2	2 E4	0,00046	-0,706	-0,512	0,01651	-4,118	0,349
Spred1	2 E5	0,00217	-2,558	0,769	0,24165	-7,013	0,197
Thbs1	2 E5	3,94E-09	15,315	3,202	4,75E-07	12,395	-2,218
Zfp770	2 E4	4,14E-05	2,355	-0,687	0,00161	-1,258	0,401
Actc1	2 E4	0,10193	-6,784	-0,309	0,0077	-3,218	-0,621
Fmn1	2 E4	4,29E-07	8,735	-2,227	1,51E-06	10,082	-2,103

Control region 2		X503/AB22			G6/R1		
Genes	Position	adj.P.Val	B	Fold Chg	adj.P.Val	B	Fold Chg
Gas7	11 B3	1,91E-06	6,629	1,281	1,22E-05	6,087	-1,142
Ntn1	11 B3	1,19E-09	17,115	3,364	0,00565	-2,838	-0,274
Myh10	11 B3	0,00012	0,892	0,422	0,00047	0,365	-0,369
Myh3	11 B3	1,45E-06	7,012	-1,414	0,00212	-1,616	0,454
Ndel1	11 B3	0,00281	-2,860	0,386	0,00012	2,228	-0,718
Rangrf	11 B3	0,05632	-6,177	-0,146	0,00198	-1,530	0,317
Pfas	11 B3	1,62E-06	6,861	-0,926	0,00075	-0,270	0,365
Aurkb	11 B3	1,27E-05	3,967	-0,708	0,59697	-7,753	0,040
Cntrob	11 B3	0,0002	0,310	-0,555	3,10E-05	4,427	0,867
Chd3	11 B3	2,96E-06	6,011	1,424	0,00316	-2,118	0,251

Supplemental table 1. P, B and fold change values of the WBSCR, centromeric and telomeric regions and external control regions. In dark grey the significantly DEG.

p value	Involved pathway	Genes included
3.55e-05	Nfat and hypertrophy of the heart	NFATC1; ACTA1; SHC1; ATP2A3; HDAC9; PIK3R1; EDN1
6.46e-05	Steroid Biosynthesis	MVK; SOAT1; MVD; SQLE; NSDHL
0.002	Oxidative stress induced gene expression via nrf2	NFE2L2; MAFK; HMOX1; KEAP1
0.0024	Vegf hypoxia and angiogenesis	ACTA1; BCAR1; SHC1; PIK3R1
0.0045	Erk and pi-3 kinase are necessary for collagen binding in corneal epithelia	ACTA1; BCAR1; CAPN1; PIK3R1
0.0085	NGF signalling via TRKA from the plasma membrane	RALGDS; FRS2; RALA; PIK3R1; DUSP4; DUSP6; SHC1; SH3GL2
0,0088	Sema3A PAK dependent Axon repulsion	LIMK1; NRP1
0.0123	Signaling by NOTCH	MOV10; TBL1XR1; ST3GAL4; HDAC9; RBPJ; NOTCH4
0.0165	Transport of glucose and other sugars, bile salts and organic acids, metal ions and amine compounds	SLC6A1; SLC6A6; SLC16A1; SLC22A5; SLC5A3; SLC47A1
0,0174	Heart development	CTNNB1; GATA6; PITX2; NFATC1
0.0259	Insulin signaling pathway	SHC1; PIK3R1
0.0495	Glycolysis / Gluconeogenesis - Homo sapiens (human)	ACSS2; ENO2; BPGM; ADH4

Supplemental table 2. List of representative over-represented pathways and genes in G-WBS group.

Common genes (8)	Common genes (39)	
mll3	Actr1b	Id2
ankrd1	Aldoc	Itga4
atp2a3	Ap3m2	Lrch1
col23a1	Arhgap5	Mafb
hmox1	Asns	Mospd1
rprm	Baiap2	Napa
tubb3	Bcor	Pik3r1
nrp1	Camta1	Ptk2b
	D1Ertd622e	Ramp2
	Derl1	Rap2b
	Ehd1	Rps9
	Elmo2	Slc25a17
	Etv1	Slc6a8
	Fbxo42	Slc7a3
	Fut9	Sp4
	Hs3st1	Tax1bp1
	Hspa12a	Tpcn1
	Hspa2	Tsga14
	Hspa8	Ulk1
		Zfp445

Supplemental table 3. List of the common DEG with previous published studies for the N-Gtf2i group.

p value	Involved pathway	Genes included
0.0001	Amino acid synthesis and interconversion (transamination)	PYCR1; ALDH18A1; GLS2; ASNS; PHGDH
0.0011	BCR signaling pathway	SHC1; CALM1; MAPK1; PIK3R1; LYN; PPP3CC; MALT1; BLNK
0.0016	IL-6 signaling pathway	NCOA1; SHC1; MAPK1; PRDM1; PIK3R1; A2M
0.0020	Cyclin A:Cdk2-associated events at S phase entry	CDKN1B; MNAT1; CDK7
0.0028	eNOS activation and regulation	DHFR; ZDHHC21; CALM1; GCHFR
0.0029	TGF_beta_Receptor	KLF10; RBL1; NCOA1; HSPA8; KAT2B; MAPK1; SKIL; PIK3R1; RBX1; DAB2; LEF1; AR; ATF2
0.0065	Cyclin E associated events during G1/S transition	CDKN1B; MNAT1; CDK7
0.0066	VEGFR3 signaling in lymphatic endothelium	MAPK1; ITGA4; SHC1; PIK3R1
0.0072	ErbB2/ErbB3 signaling events	NRG1; MAPK1; SHC1; PIK3R1; CHRNA1
0.0077	RNA Polymerase I, RNA Polymerase III, and Mitochondrial Transcription	MBD2; HIST1H4I; HIST1H4H; KAT2B; POLR3D; HIST1H3F; H3F3B; CDK7; MNAT1; POU2F1
0.0084	Notch	RBPJ; KAT2B; MAPK1; PIK3R1; RBX1; LEF1
0.0088	Superpathway of serine and glycine biosynthesis I	SHMT2; PHGDH
0.0112	Galactose metabolism - Homo sapiens (human)	GLA; PFKL; PGM2; GALK2
0.0119	The igf-1 receptor and longevity	SHC1; PIK3R1; SOD1
0.0127	MAPK targets/ Nuclear events mediated by MAP kinases	DUSP4; MAPK1; DUSP6; ATF2
0.0127	VEGFR1 specific signals	MAPK1; NRP1; PIK3R1; CALM1
0.0141	Cholesterol Biosynthesis	MVD; SQLE; NSDHL
0.0141	Role of nicotinic acetylcholine receptors in the regulation of apoptosis	PTK2B; PIK3R1; RAPSN
0.0154	Glucose metabolism	PCK2; CALM1; PGM2; PFKL; ALDOA; ALDOC
0.0181	FGF signaling pathway	PTK2B; MAPK1; SHC1; PIK3R1; IL17RD
0.0253	SHC1 events in ERBB4 signaling	NRG1; MAPK1; SHC1
0.0359	Cyclin A/B1 associated events during G2/M transition	MNAT1; CDK7
0.0359	Transcription	MNAT1; CDK7
0.0362	Aldosterone-regulated sodium reabsorption - Homo sapiens (human)	ATP1B2; MAPK1; PIK3R3; PIK3R1
0.0400	Signalling to RAS	MAPK1; RALGDS; SHC1
0.0436	Angiogenesis overview	PTK2B; MAPK1; ATF2; NRP1; SHC1
0.0442	RNA Polymerase I Transcription Initiation	MNAT1; KAT2B; CDK7
0.0452	Nfat and hypertrophy of the heart	PPP3CC; SHC1; PIK3R1; ATP2A3

Supplemental table 4. List of representative deregulated pathways and genes in the *N-Gtf2i* group.

p value	Involved pathway	Genes included
0.0008	Cholesterol Biosynthesis	MVD; SQLE; NSDHL
0.0025	VEGFR3 signaling in lymphatic endothelium	ITGA4; SHC1; PIK3R1
0.0035	IL3-mediated signaling events	SHC1; PIK3R1; PIM1
0.0041	Regulation of map kinase pathways through dual specificity phosphatases	DUSP4; DUSP6
0.0075	Insulin signaling pathway	SHC1; PIK3R1
0.0102	Keap1-Nrf2 Pathway	NFE2L2; HMOX1
0.0111	Actions of nitric oxide in the heart	CHRNA1; PIK3R1; SLC7A1
0.0127	Nfat and hypertrophy of the heart	SHC1; PIK3R1; ATP2A3
0.0166	Nerve growth factor pathway (ngf)	SHC1; PIK3R1
0.0204	Ras signaling pathway	RALGDS; PIK3R1
0.0204	Egf signaling pathway	SHC1; PIK3R1
0.0287	Growth hormone signaling pathway	SHC1; PIK3R1
0.0334	Oxidative stress induced gene expression via nrf2	NFE2L2; HMOX1
0.0358	Transcription factor creb and its extracellular signals	SHC1; PIK3R1
0.0383	Role of erk5 in neuronal survival pathway	SHC1; PIK3R1
0.0408	Galactose metabolism - Homo sapiens (human)	GLA; GALK2
0,0411	TGF beta Signaling Pathway	KLF10; SKIL; PIK3R1; SHC1

Supplemental table 5. List of representative deregulated pathways and genes in N-WBS group.

DISCUSSION

Use of mouse models to establish genotype-phenotype correlations in WBS

WBS is a complex neurodevelopmental disorder caused by the heterozygous loss of 26 to 28 genes. Although WBS has been widely studied for the specific combination of physiological and cognitive deficits, the nature of its molecular basis with most patients carrying almost identical deletions has hindered the establishment of genotype-phenotype correlations to implicate specific genes in the phenotype. The only success is the case of the elastin gene, responsible of the cardiovascular phenotype with supravalvular aortic stenosis, as well as other connective tissue abnormalities.

In this thesis project we have centered the study in the creation and use of mouse models, cells and tissues to obtain a greater knowledge about the syndrome, to establish genotype-phenotype correlations, to define new possible targets for treatment and to analyze the efficacy of two treatments for hypertension.

A total of 5 mouse models have been used in this project, carrying the loss of one or various genes on the WBS critical region or flanking regions (Figure 10). Besides the ES lines from which the various models were derived, we have also generated and characterized mouse embryonic fibroblasts (MEFs) of primary and immortalized lines.

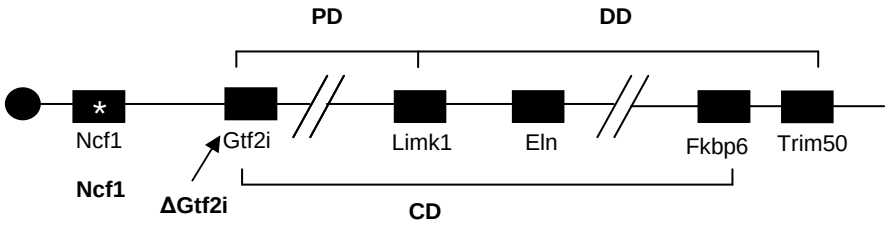

Figure 10. Schematic map of the genomic structure of the orthologous region to the WBS locus in mouse and the rearrangements present in the different mouse models used in this study. In bold the names of the different used mouse models. * symbolizes a point mutation in the *Ncf1* model disrupting the expression of the gene. Modified from [129].

Creation of the G6 cell line and the *Gtf2i*$^{\Delta ex2}$ mouse model

We have generated the G6 cell line, with the loss of the first 140 amino acids of *Gtf2i* as a previous step of the creation of the *Gtf2i*$^{\Delta ex2}$ mouse model, which has also been accomplished.

The expression of the G6 cell line has been analysed and a slightly up-regulation of the *Gtf2i* expression is present. The array expression analysis of genes in the WBSCR shows the upregulation of 8 genes in the region and a slight non significant increase of flanking regions, pointing to an important role of *Gtf2i* in the regulation of genes in the WBSCR. This fact is reinforced by the results of the XS0353 cell line, a gene trap for *Gtf2i*, where there is a downregulation of *Gtf2i* gene and also a significant downregulation of 8 genes in the WBSCR.

Reduced viability is found in the *Gtf2i*$^{\Delta ex2/\Delta ex2}$ mouse model pointing to early lethality. The analysis of decidual swellings at 9.5-12.5 days post coitum shows highly disorganized embryos, although no increased apoptosis is found. Moreover, reduced fertility is found in the surviving animals. The *Gtf2i*$^{+/\Delta ex2}$ model is viable and fertile.

Creation of the ESPP9 cell line and the CD mouse model and effect on gene expression

Using genetic engineering and Cre-recombinase technology, we have created for the first time, a mouse model that mimics the most common deletion present in WBS patients, an almost complete deletion model (CD), with the heterozygous loss of 24 genes, from *Gtf2i* to *Limk1* (Figure 10).

Both the ES cell line (ESSP9) and the CD animal have been analyzed to confirm the reduction of one copy of the genes inside the deletion using MLPA technology. The correlation with a reduction in the expression has been also analyzed obtaining a reduction of the expression in 12 out of 14 genes in the ES cell line and in all seven analyzed genes in different tissues in the mouse model.

There is some controversy on whether the common WBSCR deletion may or not affect the expression of neighboring genes. In expression studies performed in fibroblasts from WBS patients, Merla et al. reported a position

effect on neighboring gene expression [130]. Animal models do not show that influence. In our data, generated from ES cells, as well as in brain tissues no differences in expression for genes in the centromeric or the telomeric ends of the deletion were found with respect to two external control regions [73]. Moreover, no changes in expression were found in these flanking regions in lymphoblastoid cell lines derived from human patients [120].

The CD mouse model, with the heterozygous loss of the genes in the WBSCR region, is viable and fertile and has a reduction in the body weight until the 6th month of age, in concordance with the DD, PD and D/P mouse models [73]. No homozygous mice have been obtained indicating early embryonic lethality. The survival of the CD model is similar to the wild-type littermates and the most frequent death cause is lymphoma, according to the reported causes for C57BL/6 background. However, the model presents some specificities that, although not significant, might have a relation with the phenotype, such as a higher variety of tumours, less enlarged endocrine islets and increased hepatic steatosis.

Mouse embryonic fibroblasts (MEFs)

The characterization of the MEFs has been performed in cell lines derived from CD, Gtf2i$^{+/\Delta ex2}$ and Gtf2i$^{\Delta ex2/\Delta ex2}$ embryos. No cell lines with the homozygous loss of the WBSCR were obtained due to early lethality. In the immortalization study, no differences are observed in the CD or the Gtf2i$^{+/\Delta ex2}$, but Gtf2i$^{\Delta ex2/\Delta ex2}$ cell lines immortalize earlier. The CD model and the Gtf2i$^{\Delta ex2/\Delta ex2}$ do not present differences in the growth or saturation, but slower growth is observed in the Gtf2i$^{+/\Delta ex2}$, indicating a signaling defect as a consequence of an abnormal composition of the TFII-I complexes.

Cardiovascular phenotype

The great majority of WBS patients suffer from cardiovascular symptoms, being the most frequent arteriopathy consisting in stenosis of medium and large-sized arteries. The stenosis is caused by the thickening of the vascular media by smooth muscle overgrowth, normally present as supravalvular aortic stenosis [12]. Hypertension is present in approximately 50% of the patients [13]. Several molecules have been proposed as a treatment for the cardiovascular disease such as the ones that promote elastin biosynthesis or

suppress vascular smooth muscle cell differentiation, but none of them have shown to be clinically effective yet [131-132]. So far, β-adrenergic blocker and calcium channel blocker group have been used but no specific drug has been recommended for the therapy of hypertension [13].

We have performed a complete cardiovascular phenotype characterization in the DD and the CD mouse models. Both models have only one copy of the elastin gene, correlating with a reduction in the expression. The heterozygous mouse model for the elastin gene presents an increase in the number of the elastic lamellae and is hypertensive [69, 80].

DD mice develop a full cardiovascular phenotype including increased aortic wall thickness and disorganized elastin fibers which lead to hypertension and heart hypertrophy correlating with an increase in the volume of the cardiomyocytes. The consequence is the appearance hypertension in these animals from the 8th week of life and through all life.

In the CD model we have analyze the same cardiovascular parameters and, no significant changes are found in the aortic wall thickness, no increase in the elastin sheet fibers, no heart hypertrophy and no hypertension, although a tendency to an increase is present in all the parameters, for example with a 17% increase in the mean blood pressure. The data is in accordance with the absence of hypertension or elastin fibers increase in the D/P mouse model [74].

In WBS patients, the deletion of one functional copy of *NCF1* is present in some patients depending on the deletion breakpoints and a 4-fold decreased risk of hypertension is reported in patients with *NCF1* hemizygosity [58, 66]. We have analyzed the expression of *Ncf1* in both DD and CD models and a significant increase in the levels of *Ncf1* expression is found in DD model and levels comparable to the wild-type in the CD model. The difference in *Ncf1* expression could explain the presence and absence of cardiovascular phenotype in the DD and CD models respectively. These results suggest the existence of a regulator of the expression of *Ncf1* in the proximal part of the WBS deletion, most probably in the most proximal part, next to *Ncf1* locus. The loss of the regulator could cause the reduction of *Ncf1* expression seen in the CD and the D/P models but not in the DD model. This hypothesis is in disagreement with the one raised by Goergen et al, who suggested the unlikeliness of *Ncf1* implication in the cardiovascular phenotype in mice as

the gene in not deleted in any of the studied DD, PD or C/D models [74]. More investigations are needed to identify the possible existence and situation of this regulator, probably in conserved regions of the non coding region of the proximal deletion area.

In the DD model we have analyzed the possible origin of the hypertension and have concluded that it is an angII mediated hypertension as we see increased levels of angII and also increased expression of several NADPH-oxidase (NOX) complex molecules as well as increased oxidative stress. An increased activity of the NADPH complex was detected in spontaneously hypertensive rats (SHR) producing higher amount of O_2^- and an increased expression of some NOX molecules in several vascular tissues was reported in the same SHR rats, providing a link between the NADPH activity and the development of hypertension [83]. To further prove the hypothesis of *Ncf1* being the main cause of differences in the phenotype, we generated a DD/*Ncf1*$^{+/-}$ model, with the loss of one functional copy of the gene. *Ncf1* hemizygosity in DD model reduces the blood pressure levels, the oxidative stress and the expression of NOX molecules in the model and partially restores other parameters such as the angII levels or the heart hypertrophy.

Global results point to the possibility of NOX as a therapeutic target for the cardiovascular phenotype in WBS. We have used the DD model, as it is the one showing cardiovascular phenotype, to analyze the efficacy and safety of two different pharmacological treatments, losartan, which is an AT1R blocker [133] and apocynin, an inhibitor of the NAPDH oxidase assembly preventing the p47phox phosphorylation [134]. Both treatments are effective in preventing the cardiovascular anomalies both in the prenatal and postnatal administration and in most cases can reduce the expression of NOX molecules. Many reports pointed to a malignant effect of losartan in pregnancy and we have verified this fact as prenatal losartan administration is associated with an increase of fetal and postnatal premature deaths, fact that did not occur in the apoxynin prenatal administration [135-136].

We have also used transcriptome analysis to discover deregulated pathways in WBS which could be related to the cardiovascular phenotype. A comparison of the differentially expressed genes (DEG) in ESSP9, XS0353 a gene-trap derived ES cells with the loss of *Gtf2i* expression and G6, an ES cell with the loss of the first 140 amino acids of *Gtf2i*, provided several

deregulated pathways related to cardiac development and disease. We have performed various comparisons among the cell lines.

The comparison of XS0353 and ESSP9, to identify differences among the loss of *Gtf2i* and the loss of the whole WBSCR, identifies the deregulated pathways Nfat and hypertrophy of the heart and oxidative stress induced gene expression via Nrf2. These pathways are also present when studying the role of the N-terminal part of Gtf2i in the WBS deletion, indicating a role of this region in the deregulation of the pathways. The present DEG in these pathways such as *Edn1* and *Nfatc1* could contribute to the activation of the transcriptional factors such as *Gata-4* and lead to hypertrophy [137-138]. Moreover, the deregulation of the oxidative stress pathway could have a role in the oxidative stress mediated hypertension found in patients as they are not able to respond adequately to oxidative stress via NRF2 [139].

Pathways related to *Vegf* and *Tie2* signaling, which were previously reported as implicated in the vascular problems causing the embryonic lethality in a mouse model for *Gtf2i,* are also present in the different groups [88]. This reinforces the role of TFII-I and implicates the N-terminal part of the protein in the regulation of angiogenesis and vasculogenesis.

In conclusion, we have been able to characterize the cardiovascular phenotype in two of our mouse models and to identify the mechanism of production of the hypertension, as well as to confirm the role of *Ncf1* as the most important modifier for this phenotype. Moreover, we have proven the efficacy of two treatments in preventing the cardiovascular anomalies in WBS in mice and we consider that the validation of apocynin for human use would be of great interest as a possible treatment in human cardiovascular disease. Finally, we have identified important deregulated genes and pathways in three different ES cell lines related to WBS which can provide target genes for posterior study and treatment options in human patients.

Endocrinological phenotype

WBS is also characterized by an endocrinological phenotype, characterized by the presence of glucose intolerance or diabetes in 75% of patients [19-20]. To discern the endocrinological phenotype in the mouse models, we have performed glucose tolerance test, an analysis of the Langerhans islet area and

we have also discovered some deregulated pathways using the ES cell analysis.

Our analysis of the glucose tolerance test in the CD, PD and DD models shows no significant differences in any of the different time points. However, regarding the basal glucose levels, a nearly significant increase is observed in the DD and the PD models, but not in the CD. Historically, the endocrinological phenotype has been linked to the distal part of the deletion, by results in two genes, *Mlxipl* and *Stx1a* [123, 126-127] . Our results, however, suggest that genes in both parts of the deletion could play a role in the increased basal glucose levels and that a compensation effects occurs in the CD model, losing the increased basal levels. In the DD part, the role could be attributed to the known genes.

In the PD model, a possible insight comes from the obtained results in the ES cells, as glycolysis is importantly deregulated in the comparison of the two mutant cell lines of *Gtf2i*. Moreover, the glycolysis is also deregulated in the comparison among the *Gtf2i* mutants and the WBS mutant. These results suggest a role of the TFII-I protein in the endocrinological phenotype of WBS, and this role is reinforced by results in lymphoblastic cell lines presenting a deregulation of glycolysis in WBS derived cell lines but not in cell lines from patients with partial deletion without the deletion of *Gtf2i* [120].

Regarding the Langerhans islet size, CD animals present a reduced size of the islets compared to the WT animals. This reduction is maintained trough life as the pathological analysis of the animals shows less enlarged endocrine islets in the CD model. The same reduction in the islet area has been seen in diabetes type 2 patients compared to non diabetic subjects [140-141]. A deregulation of the insulin signaling pathways is also found in the transcriptome analysis and this could have a relation with the obtained results in the CD model, although no glucose intolerance is found in the model.

Craniofacial phenotype

WBS patients present a characteristic facial and cranial appearance, including a retrognathic or micrognathic mandible [6, 47-48]. The craniofacial phenotype has been studied in the CD mouse model and also in the *Gtf2i*^{tm1ex2}

and compared with the results obtained in the PD, DD and D/P models, with an already published craniofacial characterization [73].

The CD model presents global differences in the mandible, with a reduction of the size, a characteristic also present in human patients. No global differences are observed in the size of the skull of the CD model neither in the shape of the skull or the mandible, although smaller ratios are present in the nose size. In the heterozygous *Gtf2i*$^{+/ex2}$ model, there is a shorter nose and wider nasal bridge, and a midface hypoplasia.

These results in the CD model differ from the previous results obtained in the DD, PD and D/P models where the most important reductions are observed in the cranial bases [73]. Differences between the CD and the D/P models could be attributed to the lack of *Limk1* gene in the D/P mouse model, as well as to *in cis* effects in our model that are not acting in the D/P model and could compensate the phenotype.

The results in the *Gtf2i*$^{+/ex2}$ model are in accordance with previous results from other TFII-I family mouse models, where cranial abnormalities are found [92-93]. Moreover, *Gtf2i* has been related with the regulation of osteogenic markers, being a potential negative regulator of osteoclast differentiation [97]. The PD model, including the deletion of the TFII-I family genes, presents an increase of the skull size, meaning that there could be another gene in the proximal deleted region implicated in the cranial phenotype.

Neurological phenotype

The neurological phenotype in WBS has been studied as a consequence of the characteristic cognitive profile present in patients, including moderate intellectual disability, visuospatial defects and a relative preservation of the language [25]. Moreover, coordination difficulties and signs of cerebellar dysfunction, resulting in difficulties with balance, tool use and motor planning have also been described [22].

The complete study of the neurological phenotype has been performed in the CD and PD model, as *Gtf2i* and *Gtf2ird1* have been more related to the cognitive profile of patients [70, 88, 142]. In *Gtf2i*$^{+/ex2}$ only a partial analysis has been performed. Some contributions to genotype-phenotype correlations

can be also extracted from the study in the ES cell lines. The CD model presents a reduction in the brain weight with an 11% decrease in males and 8% in females, correlating with the post-mortem results in human patients [31-32]. No differences in brain weight are found in the *Gtf2i*$^{\Delta ex2}$ model. Three different brain regions have been studied in CD and PD models regarding volume and number of cells due to its implication in the visuospacial deficits, hippocampus, or the social phenotype, amygdala and orbitofrontal cortex. Additionally, several structural and functional abnormalities have been described in these regions [33, 37-38, 143].

Consistent with the brain weight, a non significant reduction of the studied brain areas is present in the CD mice, while an increase was found in the PD consistent with the previously reported increase in skull size [73].

The volume and cell number analysis reveals anomalies in all the studied areas. Amygdala has its central role in emotional processing and fear motivated learning [144]. The reduced number of cells found in the basolateral area of the CD model respect the PD model, and nearly significant with the WT, could have a role in an impaired function of the amygdala, specially regarding the acquisition and expression of fear-related behaviours, where the basolateral complex plays a key role. No studies regarding the concrete areas of the amygdala have been performed in human patients, although preservation or increase of the global volume has been reported as well as increase in the reactivity [33, 37].

The orbitofrontal cortex has important connexions with the amygdala and along with it, they have been reported to play a role in the social phenotype of WBS human patients [37]. Reductions in the grey matter and changes in the volume have been described, [38, 42-43]. The reduced volume found in the layer I of the CD model could have a relation with functional abnormalities in the region.

The hippocampus is crucial for declarative memory and for processing of spatial navigation information, which could be related to the visuospatial difficulties found in human patients [145]. Actually, several anomalies have been reported in human patients, including functional and structural anomalies [145]. No anomalies have been found in the hippocampus of the *Gtf2i*$^{\Delta ex2}$ model, discarding a role for the N-terminal part of the protein in the hippocampus formation.

We have found anomalies in the dentate gyrus and also in the CA3 region of the hippocampus, in this last case regarding both volumes and number of cells. In general, a significant decreased volume and number of cells is found in the CD model respect the PD model and nearly significant decrease in the case of CD to WT. However, when we analyze the number of doublecortin positive cells, a marker for immature neurons, we find an increased density in the CD respect the other two models in the superior area of the subgranular zone, and a reduced length and number of neurons in the inferior region, conserving the density. The increased neurogenesis and reduced total number of cells point to a structural problem in the hippocampus of the CD model, where neurogenesis in the subgranular zone does not imply a higher or maintained number of neurons, pointing to a possible increase in apoptosis of cells in the area. *Fzd9* knock out mouse model, a gene in the DD region, shows increased apoptotic cell deaths and increased precursor proliferation during hippocampal development [112]. *Fzd9* could be playing a role in our findings in the CD model as it is deleted in the CD model but not in the PD model, where no changes in density are observed. However, more studies regarding neuron morphology will be needed to further define the phenotypes in these cerebral regions.

The studies with cell lines have also given us some insight in the deregulated pathways as a consequence of the loss of the WBSCR. In the comparison of the ESSP9 and its wild type cell line, one of the deregulated pathways is axon guidance, which could be related to neural problems present in the CD model. *Sema4d,* a member of the semaphoring family is one of the up-regulated genes and its cascade leads to the inhibition of microtubule assembly and axon elongation [146]. Moreover, previous experiments showed axonal growth cone collapse when exposing rat hippocampal neurons to *Sema4d* [147]. In fact, a previous report on a transcriptome analysis also identified genes involved in axon guidance, neurogenesis and cytoskeleton regulation in neurons as deregulated in WBS patients [120], pointing to some of these deregulated genes as possible future targets in treatment. Moreover, a neural phenotype is also seen when comparing the two mutant cell lines for *Gtf2i* and the ESSP9 cell line. Several pathways could be related to neural regulation and signaling. The nerve growth factor pathway appeared deregulated indicating a role of *Gtf2i* in the regulation of the pathway and this result is in accordance with a previous study showing elevated levels of NGF in serum which may induce abnormal nerve function, sympathetic hypertrophy and immunological alterations [148].

Behavioral phenotype

The behavioral characterization of two of the mouse models has been performed to analyze the similarities with the human phenotype, which present a cognitive and behavioral characteristic phenotype including intellectual disability, visuospatial difficulties, increased anxiety, motor problems and hyperacusia [149].

In both the CD and the *Gtf2i*$^{+/\Delta ex2}$ models the characterization included general characteristics, motor, anxiety, and learning and attention tests. In the motor tests, the CD model presents an impaired performance in the Rotarod test. Together with an impairment in the wire maneuver, these results directed us to a coordination problem in the model, in accordance with the D/P model and the motor problems found in human patients [73]. In the *Gtf2i*$^{+/\Delta ex2}$, no impaired motor coordination is found. Other models for WBS genes showing motor problems point to a role of Gtf2ird1 in this phenotype [73, 93] but there must be the contribution of one or more genes of the DD region, as the DD and the PD models do not present motor abnormalities [73].

Regarding anxiety, no differences were found in the CD model, but increased anxiety was found in the *Gtf2i*$^{+/\Delta ex2}$ model, which correlated with previous studies in models from the TFII-I family and from the PD model, pointing to a role of these genes in the PD region to the anxiety phenotype [73, 94].

The learning and attention tests show interesting tendencies in the CD model. The object recognition test points to a tendency to show greater interest in novel object in the CD mice and the water maze test shows a more direct thigmotaxic strategy in the CD model, which could be related to the inhibited behavior in humans.

Other observed results are a tendency to a reduction of freezing in the fear conditioning test, similar to the results in the D/P model. In this behavior a compensatory role of the PD region may exist, as the DD model showed significant differences [73]. Regarding the auditory response, the *Gtf2i*$^{+/\Delta ex2}$ model presents a lower threshold for sound intolerance and, in the CD model, a tendency to an increased response is seen at 120 dB, the same result as the D/P model [73].

Globally, the *Gtf2i*$^{+/\Delta ex2}$ model shows decreased exploratory activity, higher anxiety and a lower threshold for sound intolerance and the CD model presents motor problems and tendencies to present a greater interest in novel objects and an inhibited behavior. All of these behaviors have its correspondence in human patients and present these models as useful tools for future tests.

New binding motif for *Gtf2i*

Gtf2i is a member of the TFII-I family and has been implicated in several of the cognitive and physical anomalies of WBS, turning it to one of the essential genes contributing to the phenotype.

In an attempt to increase the knowledge about this transcription factor and discover new targets which could have a relation with WBS, we have used transcriptomic analysis of the hippocampus and cortex of the *Gtf2i*$^{+/\Delta ex2}$ model, the most plausible affected areas from the behavioral analysis of the model, to perform an *in silico* analysis to discover new consensus binding sequences for *Gtf2i* to promoter regions.

A new binding motif, CAGCCWG, has been discovered. This motif is evolutionarily conserved in target genes up to takifugu rubripes and binding of *Gtf2i* to the promoter region of these genes has been shown. Abolishment of the binding is present when one of the conserved residues is mutated and the role of the N-terminal part of the protein has been determined as essential for the binding to some of the target genes using *Gtf2i*$^{+/\Delta ex2}$ and *Gtf2i* $^{\Delta ex2/\Delta ex2}$ cell lines. Genes containing the motif in their promoter region have been related to pathways such as glycolysis, where others have documented a role for *Gtf2i* and also our array expression studies in the *Gtf2i* mutant cell lines [120]. The pathway enrichment analysis shows that the DEG containing the new motif are part of the PI3K pathway [150] or the TGFβ signaling pathway [151], both linked to the activity of *Gtf2i*. Direct binding of TFII-I to genes of these pathways is reported indicating a direct regulation role of TFII-I.

Concluding remarks

WBS is a rare disease including different symptoms and phenotypes. For this reason and, as the deletion includes ~26 genes, genotype-phenotype correlations have been historically difficult.

In this thesis project, we have confirmed the role of *Ncf1* as the main modifier of the cardiovascular phenotype in WBS, as changes in the expression among the DD and the CD model explain the lack of cardiovascular phenotype in the latest. Moreover, gene dosage reduction of *Ncf1* in the DD model rescues the cardiovascular phenotype. We have also established the efficacy of two treatments in reducing the altered parameters, one of them with less secondary effects but still not usable in human patients.

We have created two different mouse models presenting a variety of phenotypes also present in human patients. For *Gtf2i* we have established the role of the N-terminal region in behaviour and viability. CD mice are the most appropriate model for the human disease since these mice carry an almost identical genomic deletion to human patients. We have completed a general characterization of the CD phenotype, including cardiovascular, endocrine, craniofacial, neurological and behavioural features. CD mice recapitulate most of the phenotypes of human patients and could be used in future studies to deepen in the physiopathology of each phenotypic feature and to test novel and specific treatments.

Finally, we have used expression array studies to discover a new binding motif for TFII-I and also to identify deregulated genes and pathways using both WBS and *Gtf2i* mutant ES cell lines. Given that TFII-I (encoded by *GTF2I*) is likely to play a major role in most of the neurodevelopmental features of WBS, the identified pathways and target genes could be used as targets for future treatments.

CONCLUSIONS

We have created a complete deletion mouse model mimicking the deletion found in human patients. The CD model is viable and fertile in heterozygosis and presents reduced growth both in males and females. It does not present a cardiovascular phenotype as a consequence of reduced *Ncf1* expression. Multi-systemic phenotypic features include a reduction of the mandible size, decreased brain weight correlating with a non-significant reduction of the amygdala and several changes in volume and cell number of hippocampus, and reduced area of the Langerhans islets. CD mice present motor impairment and tendencies to increased novelty search, disinhibition, reduced freezing and sound intolerance. A contribution to the neurological phenotype is suggested from the expression arrays in the WBS cell line with the deregulation of genes related to axon guidance and neural growth factor.

We have also created a mouse model lacking the N-terminal part of the TFII-I protein. The N-terminal part of the protein is implicated in viability, as *Gtf2i*$^{\Delta ex2/\Delta ex2}$ mice present with reduced viability and fertility and morphologically abnormal decidual swellings. Moreover, TFII-I has a role in craniofacial morphogenesis, as the *Gtf2i*$^{-\Delta ex2}$ model has a shorter nose, wider nasal bridge and midface hypoplasia. Finally, TFII-I is also involved in neurodevelopment since *Gtf2i*$^{\Delta ex2/\Delta ex2}$ mice exhibit a behavioral phenotype including increased anxiety, decreased exploratory activity and a low threshold for sound intolerance. Expression array analysis in *Gtf2i* and WBS mutant cell lines suggests the implication of the N-terminal region of *Gtf2i* in heart hypertrophy, oxidative stress, vascular regulation and neural phenotype.

Transcriptome analysis of the hippocampus and cortex has been studied in the *Gtf2i*$^{-\Delta ex2}$ model leading to the discovery of a new binding evolutionarily conserved motif for TFII-I, CAGCCWG. New targets genes for this motif and for the already described BRGATTRBR motif have been found. We have shown that in some target genes, variation in the conserved sequence is allowed, obtaining binding in CAGCBVG and that the mutagenesis of the 3' guanine of the conserved residues of the motifs is able to disrupt TFII-I binding. The N-terminal part of TFII-I is important to maintain binding capacity to some of the target and the pathway enrichment analysis of deregulated genes with the binding motif implicates TFII-I in the regulation of glycolisis, PI3K cascade, and TGFβ signalling pathway.

We have compared the CD mice with the previously described mouse models. Genes in both the PD and DD regions have a role in the endocrinological phenotype, which is compensated in the CD model. Volume and number of cells increases are under the regulation of genes in the PD region and some enhancer may be deleted in the proximal part of the deletion in the CD mouse lowering *Ncf1* expression compared to the DD model. Genes in both the PD and DD region have a role in the behavioral phenotype.

Ncf1 is the main modifier of the cardiovascular phenotype in WBS. Increased *Ncf1* expression is found in the DD model and normalized expression in the CD model. The reduction of *Ncf1* dosage is able to partially rescue the cardiovascular phenotype in the DD mouse model. The use of losartan or apocynin is highly effective in the prevention of the development of cardiovascular anomalies in the DD model. Apocynin treatment is associated with less secondary effects in the prenatal treatment.

REFERENCES

1. Stromme, P., P.G. Bjornstad, and K. Ramstad, *Prevalence estimation of Williams syndrome.* J Child Neurol, 2002. **17**(4): p. 269-71.
2. Fanconi, G., et al., *[Chronic hyperglycemia, combined with osteosclerosis, hyperazotemia, nanism and congenital malformations].* Helv Paediatr Acta, 1952. **7**(4): p. 314-49.
3. Williams, J.C., B.G. Barratt-Boyes, and J.B. Lowe, *Supravalvular aortic stenosis.* Circulation, 1961. **24**: p. 1311-8.
4. Beuren, A.J., J. Apitz, and D. Harmjanz, *Supravalvular aortic stenosis in association with mental retardation and a certain facial appearance.* Circulation, 1962. **26**: p. 1235-40.
5. Beuren, A.J., et al., *The Syndrome of Supravalvular Aortic Stenosis, Peripheral Pulmonary Stenosis, Mental Retardation and Similar Facial Appearance.* Am J Cardiol, 1964. **13**: p. 471-83.
6. Morris, C.A. and C.B. Mervis, *Williams syndrome and related disorders.* Annu Rev Genomics Hum Genet, 2000. **1**: p. 461-84.
7. Morris, C.A., et al., *Natural history of Williams syndrome: physical characteristics.* J Pediatr, 1988. **113**(2): p. 318-26.
8. Partsch, C.J., et al., *Longitudinal evaluation of growth, puberty, and bone maturation in children with Williams syndrome.* J Pediatr, 1999. **134**(1): p. 82-9.
9. Pober, B.R., *Williams-Beuren syndrome.* N Engl J Med, 2010. **362**(3): p. 239-52.
10. Bruno, E., et al., *Cardiovascular findings, and clinical course, in patients with Williams syndrome.* Cardiol Young, 2003. **13**(6): p. 532-6.
11. Pober, B.R. and C.A. Morris, *Diagnosis and management of medical problems in adults with Williams-Beuren syndrome.* Am J Med Genet C Semin Med Genet, 2007. **145C**(3): p. 280-90.
12. Pober, B.R., M. Johnson, and Z. Urban, *Mechanisms and treatment of cardiovascular disease in Williams-Beuren syndrome.* J Clin Invest, 2008. **118**(5): p. 1606-15.
13. Broder, K., et al., *Elevated ambulatory blood pressure in 20 subjects with Williams syndrome.* Am J Med Genet, 1999. **83**(5): p. 356-60.
14. Wessel, A., et al., *[Arterial hypertension and blood pressure profile in patients with Williams-Beuren syndrome].* Z Kardiol, 1997. **86**(4): p. 251-7.
15. Sadler, L.S., et al., *Differences by sex in cardiovascular disease in Williams syndrome.* J Pediatr, 2001. **139**(6): p. 849-53.
16. Eronen, M., et al., *Cardiovascular manifestations in 75 patients with Williams syndrome.* J Med Genet, 2002. **39**(8): p. 554-8.
17. Wollack, J.B., et al., *Stroke in Williams syndrome.* Stroke, 1996. **27**(1): p. 143-6.
18. Wessel, A., et al., *Risk of sudden death in the Williams-Beuren syndrome.* Am J Med Genet A, 2004. **127A**(3): p. 234-7.
19. Cherniske, E.M., et al., *Multisystem study of 20 older adults with Williams syndrome.* Am J Med Genet A, 2004. **131**(3): p. 255-64.

20. Pober, B.R., et al., *High prevalence of diabetes and pre-diabetes in adults with Williams syndrome.* Am J Med Genet C Semin Med Genet, 2010. **154C**(2): p. 291-8.
21. Bedeschi, M.F., et al., *Clinical follow-up of young adults affected by Williams syndrome: Experience of 45 Italian patients.* Am J Med Genet A, 2011. **155**(2): p. 353-9.
22. Dilts, C.V., C.A. Morris, and C.O. Leonard, *Hypothesis for development of a behavioral phenotype in Williams syndrome.* Am J Med Genet Suppl, 1990. **6**: p. 126-31.
23. Morris, C.A., et al., *Adults with Williams syndrome.* Am J Med Genet Suppl, 1990. **6**: p. 102-7.
24. Gagliardi, C., et al., *Evolution of neurologic features in Williams syndrome.* Pediatr Neurol, 2007. **36**(5): p. 301-6.
25. Martens, M.A., S.J. Wilson, and D.C. Reutens, *Research Review: Williams syndrome: a critical review of the cognitive, behavioral, and neuroanatomical phenotype.* J Child Psychol Psychiatry, 2008. **49**(6): p. 576-608.
26. Mervis, C.B., et al., *The Williams syndrome cognitive profile.* Brain Cogn, 2000. **44**(3): p. 604-28.
27. Mervis, C.B., B.F. Robinson, and J.R. Pani, *Visuospatial construction.* Am J Hum Genet, 1999. **65**(5): p. 1222-9.
28. Dykens, E.M., *Anxiety, fears, and phobias in persons with Williams syndrome.* Dev Neuropsychol, 2003. **23**(1-2): p. 291-316.
29. Woodruff-Borden, J., et al., *Longitudinal course of anxiety in children and adolescents with Williams syndrome.* Am J Med Genet C Semin Med Genet, 2010. **154C**(2): p. 277-90.
30. Jernigan, T.L. and U. Bellugi, *Anomalous brain morphology on magnetic resonance images in Williams syndrome and Down syndrome.* Arch Neurol, 1990. **47**(5): p. 529-33.
31. Galaburda, A.M., et al., *Williams syndrome: neuronal size and neuronal-packing density in primary visual cortex.* Arch Neurol, 2002. **59**(9): p. 1461-7.
32. Reiss, A.L., et al., *An experiment of nature: brain anatomy parallels cognition and behavior in Williams syndrome.* J Neurosci, 2004. **24**(21): p. 5009-15.
33. Capitao, L., et al., *MRI amygdala volume in Williams Syndrome.* Res Dev Disabil, 2011. **32**(6): p. 2767-72.
34. Menghini, D., et al., *Relationship between brain abnormalities and cognitive profile in Williams syndrome.* Behav Genet, 2011. **41**(3): p. 394-402.
35. Reiss, A.L., et al., *IV. Neuroanatomy of Williams syndrome: a high-resolution MRI study.* J Cogn Neurosci, 2000. **12 Suppl 1**: p. 65-73.
36. Schmitt, J.E., et al., *Analysis of cerebral shape in Williams syndrome.* Arch Neurol, 2001. **58**(2): p. 283-7.
37. Jackowski, A.P., et al., *Brain abnormalities in Williams syndrome: a review of structural and functional magnetic resonance imaging findings.* Eur J Paediatr Neurol, 2009. **13**(4): p. 305-16.

38. Chiang, M.C., et al., *3D pattern of brain abnormalities in Williams syndrome visualized using tensor-based morphometry.* Neuroimage, 2007. **36**(4): p. 1096-109.
39. Wang, P.P., et al., *Specific neurobehavioral profile of Williams' syndrome is associated with neocerebellar hemispheric preservation.* Neurology, 1992. **42**(10): p. 1999-2002.
40. Avery, S.N., et al., *White matter integrity deficits in prefrontal-amygdala pathways in Williams syndrome.* Neuroimage, 2012. **59**(2): p. 887-94.
41. Meyer-Lindenberg, A., et al., *Neural correlates of genetically abnormal social cognition in Williams syndrome.* Nat Neurosci, 2005. **8**(8): p. 991-3.
42. Eckert, M.A., et al., *To modulate or not to modulate: differing results in uniquely shaped Williams syndrome brains.* Neuroimage, 2006. **32**(3): p. 1001-7.
43. Meyer-Lindenberg, A., et al., *Neural basis of genetically determined visuospatial construction deficit in Williams syndrome.* Neuron, 2004. **43**(5): p. 623-31.
44. Meyer-Lindenberg, A., C.B. Mervis, and K.F. Berman, *Neural mechanisms in Williams syndrome: a unique window to genetic influences on cognition and behaviour.* Nat Rev Neurosci, 2006. **7**(5): p. 380-93.
45. Jabbi, M., et al., *The Williams syndrome chromosome 7q11.23 hemideletion confers hypersocial, anxious personality coupled with altered insula structure and function.* Proc Natl Acad Sci U S A, 2012. **109**(14): p. E860-6.
46. Mobbs, D., et al., *Reduced parietal and visual cortical activation during global processing in Williams syndrome.* Dev Med Child Neurol, 2007. **49**(6): p. 433-8.
47. Axelsson, S., et al., *Neurocranial morphology and growth in Williams syndrome.* Eur J Orthod, 2005. **27**(1): p. 32-47.
48. Makeyev, A. and D. Bayarsaihan, *Molecular Basis of Williams-Beuren Syndrome: TFII-I Regulated Targets Involved in the Craniofacial Development.* Cleft Palate Craniofac J, 2010.
49. Marler, J.A., et al., *Sensorineural hearing loss in children and adults with Williams syndrome.* Am J Med Genet A, 2005. **138**(4): p. 318-27.
50. Valero, M.C., et al., *Fine-scale comparative mapping of the human 7q11.23 region and the orthologous region on mouse chromosome 5G: the low-copy repeats that flank the Williams-Beuren syndrome deletion arose at breakpoint sites of an evolutionary inversion(s).* Genomics, 2000. **69**(1): p. 1-13.
51. Peoples, R., et al., *A physical map, including a BAC/PAC clone contig, of the Williams-Beuren syndrome--deletion region at 7q11.23.* Am J Hum Genet, 2000. **66**(1): p. 47-68.
52. Stankiewicz, P. and J.R. Lupski, *Structural variation in the human genome and its role in disease.* Annu Rev Med, 2010. **61**: p. 437-55.
53. Schubert, C., *The genomic basis of the Williams-Beuren syndrome.* Cell Mol Life Sci, 2009. **66**(7): p. 1178-97.
54. Merla, G., et al., *Copy number variants at Williams-Beuren syndrome 7q11.23 region.* Hum Genet, 2010. **128**(1): p. 3-26.

55. Perez Jurado, L.A., et al., *Molecular definition of the chromosome 7 deletion in Williams syndrome and parent-of-origin effects on growth.* Am J Hum Genet, 1996. **59**(4): p. 781-92.
56. Morris, C.A., I.T. Thomas, and F. Greenberg, *Williams syndrome: autosomal dominant inheritance.* Am J Med Genet, 1993. **47**(4): p. 478-81.
57. Bayes, M., et al., *Mutational mechanisms of Williams-Beuren syndrome deletions.* Am J Hum Genet, 2003. **73**(1): p. 131-51.
58. Del Campo, M., et al., *Hemizygosity at the NCF1 gene in patients with Williams-Beuren syndrome decreases their risk of hypertension.* Am J Hum Genet, 2006. **78**(4): p. 533-42.
59. Heyworth, P.G., D. Noack, and A.R. Cross, *Identification of a novel NCF-1 (p47-phox) pseudogene not containing the signature GT deletion: significance for A47 degrees chronic granulomatous disease carrier detection.* Blood, 2002. **100**(5): p. 1845-51.
60. Somerville, M.J., et al., *Severe expressive-language delay related to duplication of the Williams-Beuren locus.* N Engl J Med, 2005. **353**(16): p. 1694-701.
61. Osborne, L.R. and C.B. Mervis, *Rearrangements of the Williams-Beuren syndrome locus: molecular basis and implications for speech and language development.* Expert Rev Mol Med, 2007. **9**(15): p. 1-16.
62. Van der Aa, N., et al., *Fourteen new cases contribute to the characterization of the 7q11.23 microduplication syndrome.* Eur J Med Genet, 2009. **52**(2-3): p. 94-100.
63. Beunders, G., et al., *A triplication of the Williams-Beuren syndrome region in a patient with mental retardation, a severe expressive language delay, behavioural problems and dysmorphisms.* J Med Genet, 2010. **47**(4): p. 271-5.
64. Osborne, L.R., et al., *A 1.5 million-base pair inversion polymorphism in families with Williams-Beuren syndrome.* Nat Genet, 2001. **29**(3): p. 321-5.
65. Hobart, H.H., et al., *Inversion of the Williams syndrome region is a common polymorphism found more frequently in parents of children with Williams syndrome.* Am J Med Genet C Semin Med Genet, 2010. **154C**(2): p. 220-8.
66. Cusco, I., et al., *Copy number variation at the 7q11.23 segmental duplications is a susceptibility factor for the Williams-Beuren syndrome deletion.* Genome Res, 2008. **18**(5): p. 683-94.
67. Tassabehji, M., *Williams-Beuren syndrome: a challenge for genotype-phenotype correlations.* Hum Mol Genet, 2003. **12 Spec No 2**: p. R229-37.
68. DeBry, R.W. and M.F. Seldin, *Human/mouse homology relationships.* Genomics, 1996. **33**(3): p. 337-51.
69. Li, D.Y., et al., *Novel arterial pathology in mice and humans hemizygous for elastin.* J Clin Invest, 1998. **102**(10): p. 1783-7.

70. Antonell, A., et al., *Partial 7q11.23 deletions further implicate GTF2I and GTF2IRD1 as the main genes responsible for the Williams-Beuren syndrome neurocognitive profile.* J Med Genet, 2010. **47**(5): p. 312-20.
71. Frangiskakis, J.M., et al., *LIM-kinase1 hemizygosity implicated in impaired visuospatial constructive cognition.* Cell, 1996. **86**(1): p. 59-69.
72. Edelmann, L., et al., *An atypical deletion of the Williams-Beuren syndrome interval implicates genes associated with defective visuospatial processing and autism.* J Med Genet, 2007. **44**(2): p. 136-43.
73. Li, H.H., et al., *Induced chromosome deletions cause hypersociability and other features of Williams-Beuren Syndrome in Mice.* EMBO Molecular Medicine, 2009. **1**: p. 50-65.
74. Goergen, C.J., et al., *Induced Chromosome Deletion in a Williams-Beuren Syndrome Mouse Model Causes Cardiovascular Abnormalities.* J Vasc Res, 2010. **48**(2): p. 119-129.
75. Ewart, A.K., et al., *Hemizygosity at the elastin locus in a developmental disorder, Williams syndrome.* Nat Genet, 1993. **5**(1): p. 11-6.
76. Curran, M.E., et al., *The elastin gene is disrupted by a translocation associated with supravalvular aortic stenosis.* Cell, 1993. **73**(1): p. 159-68.
77. Metcalfe, K., et al., *Elastin: mutational spectrum in supravalvular aortic stenosis.* Eur J Hum Genet, 2000. **8**(12): p. 955-63.
78. Li, D.Y., et al., *Elastin is an essential determinant of arterial morphogenesis.* Nature, 1998. **393**(6682): p. 276-80.
79. Karnik, S.K., et al., *A critical role for elastin signaling in vascular morphogenesis and disease.* Development, 2003. **130**(2): p. 411-23.
80. Faury, G., et al., *Developmental adaptation of the mouse cardiovascular system to elastin haploinsufficiency.* J Clin Invest, 2003. **112**(9): p. 1419-28.
81. Hultqvist, M., et al., *Enhanced autoimmunity, arthritis, and encephalomyelitis in mice with a reduced oxidative burst due to a mutation in the Ncf1 gene.* Proc Natl Acad Sci U S A, 2004. **101**(34): p. 12646-51.
82. Bedard, K. and K.H. Krause, *The NOX family of ROS-generating NADPH oxidases: physiology and pathophysiology.* Physiol Rev, 2007. **87**(1): p. 245-313.
83. Touyz, R.M., *Reactive oxygen species, vascular oxidative stress, and redox signaling in hypertension: what is the clinical significance?* Hypertension, 2004. **44**(3): p. 248-52.
84. Lee, M.Y. and K.K. Griendling, *Redox signaling, vascular function, and hypertension.* Antioxid Redox Signal, 2008. **10**(6): p. 1045-59.
85. Bozhenok, L., P.A. Wade, and P. Varga-Weisz, *WSTF-ISWI chromatin remodeling complex targets heterochromatic replication foci.* EMBO J, 2002. **21**(9): p. 2231-41.
86. Kitagawa, H., et al., *The chromatin-remodeling complex WINAC targets a nuclear receptor to promoters and is impaired in Williams syndrome.* Cell, 2003. **113**(7): p. 905-17.

87. Yoshimura, K., et al., *Distinct function of 2 chromatin remodeling complexes that share a common subunit, Williams syndrome transcription factor (WSTF).* Proc Natl Acad Sci U S A, 2009. **106**(23): p. 9280-5.
88. Enkhmandakh, B., et al., *Essential functions of the Williams-Beuren syndrome-associated TFII-I genes in embryonic development.* Proc Natl Acad Sci U S A, 2009. **106**(1): p. 181-6.
89. Roy, A.L., *Biochemistry and biology of the inducible multifunctional transcription factor TFII-I: 10years later.* Gene, 2012. **492**(1): p. 32-41.
90. Ferrero, G.B., et al., *An atypical 7q11.23 deletion in a normal IQ Williams-Beuren syndrome patient.* Eur J Hum Genet, 2010. **18**(1): p. 33-8.
91. Sakurai, T., et al., *Haploinsufficiency of Gtf2i, a gene deleted in Williams Syndrome, leads to increases in social interactions.* Autism Res, 2010.
92. Tassabehji, M., et al., *GTF2IRD1 in craniofacial development of humans and mice.* Science, 2005. **310**(5751): p. 1184-7.
93. Howard, M.L., et al., *Mutation of Gtf2ird1 from the Williams-Beuren syndrome critical region results in facial dysplasia, motor dysfunction, and altered vocalisations.* Neurobiol Dis, 2011.
94. Schneider, T., et al., *Anxious, hypoactive phenotype combined with motor deficits in Gtf2ird1 null mouse model relevant to Williams syndrome.* Behav Brain Res, 2012. **233**(2): p. 458-73.
95. Danoff, S.K., et al., *TFII-I, a candidate gene for Williams syndrome cognitive profile: parallels between regional expression in mouse brain and human phenotype.* Neuroscience, 2004. **123**(4): p. 931-8.
96. Ohazama, A. and P.T. Sharpe, *TFII-I gene family during tooth development: candidate genes for tooth anomalies in Williams syndrome.* Dev Dyn, 2007. **236**(10): p. 2884-8.
97. Lazebnik, M.B., et al., *Williams-Beuren syndrome-associated transcription factor TFII-I regulates osteogenic marker genes.* J Biol Chem, 2009. **284**(52): p. 36234-9.
98. Roy, A.L., *Biochemistry and biology of the inducible multifunctional transcription factor TFII-I.* Gene, 2001. **274**(1-2): p. 1-13.
99. Chimge, N.O., et al., *Identification of the TFII-I family target genes in the vertebrate genome.* Proc Natl Acad Sci U S A, 2008. **105**(26): p. 9006-10.
100. Makeyev, A.V. and D. Bayarsaihan, *New TFII-I family target genes involved in embryonic development.* Biochem Biophys Res Commun, 2009. **386**(4): p. 554-8.
101. Hoogenraad, C.C., et al., *LIMK1 and CLIP-115: linking cytoskeletal defects to Williams syndrome.* Bioessays, 2004. **26**(2): p. 141-50.
102. Nimchinsky, E.A., B.L. Sabatini, and K. Svoboda, *Structure and function of dendritic spines.* Annu Rev Physiol, 2002. **64**: p. 313-53.
103. Morris, C.A., et al., *GTF2I hemizygosity implicated in mental retardation in Williams syndrome: genotype-phenotype analysis of five families with deletions in*

the Williams syndrome region. Am J Med Genet A, 2003. **123A**(1): p. 45-59.
104. Tassabehji, M., et al., *Williams syndrome: use of chromosomal microdeletions as a tool to dissect cognitive and physical phenotypes.* Am J Hum Genet, 1999. **64**(1): p. 118-25.
105. Karmiloff-Smith, A., et al., *Using case study comparisons to explore genotype-phenotype correlations in Williams-Beuren syndrome.* J Med Genet, 2003. **40**(2): p. 136-40.
106. Gray, V., et al., *In-depth analysis of spatial cognition in Williams syndrome: A critical assessment of the role of the LIMK1 gene.* Neuropsychologia, 2006. **44**(5): p. 679-85.
107. Meng, Y., et al., *Abnormal spine morphology and enhanced LTP in LIMK-1 knockout mice.* Neuron, 2002. **35**(1): p. 121-33.
108. Richter, N.J., et al., *Further biochemical and kinetic characterization of human eukaryotic initiation factor 4H.* J Biol Chem, 1999. **274**(50): p. 35415-24.
109. Capossela, S., et al., *Growth Defects and Impaired Cognitive-Behavioral Abilities in Mice Knockout for Eif4h, a Gene Located in the Mouse Homolog of the Williams-Beuren Syndrome Critical Region.* Am J Pathol, 2012.
110. Wang, Y.K., et al., *A novel human homologue of the Drosophila frizzled wnt receptor gene binds wingless protein and is in the Williams syndrome deletion at 7q11.23.* Hum Mol Genet, 1997. **6**(3): p. 465-72.
111. Botta, A., et al., *Detection of an atypical 7q11.23 deletion in Williams syndrome patients which does not include the STX1A and FZD3 genes.* J Med Genet, 1999. **36**(6): p. 478-80.
112. Zhao, C., et al., *Hippocampal and visuospatial learning defects in mice with a deletion of frizzled 9, a gene in the Williams syndrome deletion interval.* Development, 2005. **132**(12): p. 2917-27.
113. Ranheim, E.A., et al., *Frizzled 9 knock-out mice have abnormal B-cell development.* Blood, 2005. **105**(6): p. 2487-94.
114. Hoogenraad, C.C., et al., *The murine CYLN2 gene: genomic organization, chromosome localization, and comparison to the human gene that is located within the 7q11.23 Williams syndrome critical region.* Genomics, 1998. **53**(3): p. 348-58.
115. De Zeeuw, C.I., et al., *CLIP-115, a novel brain-specific cytoplasmic linker protein, mediates the localization of dendritic lamellar bodies.* Neuron, 1997. **19**(6): p. 1187-99.
116. Gagliardi, C., et al., *Unusual cognitive and behavioural profile in a Williams syndrome patient with atypical 7q11.23 deletion.* J Med Genet, 2003. **40**(7): p. 526-30.
117. Vandeweyer, G., et al., *The Contribution of CLIP2 Haploinsufficiency to the Clinical Manifestations of the Williams-Beuren Syndrome.* Am J Hum Genet, 2012.
118. Hoogenraad, C.C., et al., *Targeted mutation of Cyln2 in the Williams syndrome critical region links CLIP-115 haploinsufficiency to*

neurodevelopmental abnormalities in mice. Nat Genet, 2002. **32**(1): p. 116-27.
119. Ashe, A., et al., *A genome-wide screen for modifiers of transgene variegation identifies genes with critical roles in development.* Genome Biology, 2008. **9**(12).
120. Antonell, A., M. Vilardell, and L.A. Perez Jurado, *Transcriptome profile in Williams-Beuren syndrome lymphoblast cells reveals gene pathways implicated in glucose intolerance and visuospatial construction deficits.* Hum Genet, 2010.
121. Henrichsen, C.N., et al., *Using transcription modules to identify expression clusters perturbed in williams-beuren syndrome.* PLoS Comput Biol, 2011. **7**(1): p. e1001054.
122. Iizuka, K. and Y. Horikawa, *ChREBP: A glucose-activated transcription factor involved in the development of metabolic syndrome.* Endocrine Journal, 2008. **55**(4): p. 617-624.
123. Iizuka, K., et al., *Deficiency of carbohydrate response element-binding protein (ChREBP) reduces lipogenesis as well as glycolysis.* Proc Natl Acad Sci U S A, 2004. **101**(19): p. 7281-6.
124. Zhang, R., A.B. Maksymowych, and L.L. Simpson, *Cloning and sequence analysis of a cDNA encoding human syntaxin 1A, a polypeptide essential for exocytosis.* Gene, 1995. **159**(2): p. 293-4.
125. Yamakawa, T., et al., *Interaction of syntaxin 1A with the N-terminus of Kv4.2 modulates channel surface expression and gating.* Biochemistry, 2007. **46**(38): p. 10942-9.
126. Lam, P.P., et al., *Transgenic mouse overexpressing syntaxin-1A as a diabetes model.* Diabetes, 2005. **54**(9): p. 2744-54.
127. Ohara-Imaizumi, M., et al., *Imaging analysis reveals mechanistic differences between first- and second-phase insulin exocytosis.* J Cell Biol, 2007. **177**(4): p. 695-705.
128. Ashe, A., et al., *A genome-wide screen for modifiers of transgene variegation identifies genes with critical roles in development.* Genome Biol, 2008. **9**(12): p. R182.
129. Campuzano, V., et al., *Reduction of NADPH-oxidase activity ameliorates the cardiovascular phenotype in a mouse model of Williams-Beuren Syndrome.* PLoS Genet, 2012. **8**(2): p. e1002458.
130. Merla, G., et al., *Submicroscopic deletion in patients with Williams-Beuren syndrome influences expression levels of the nonhemizygous flanking genes.* Am J Hum Genet, 2006. **79**(2): p. 332-41.
131. McGowan, S.E., M.M. Doro, and S.K. Jackson, *Endogenous retinoids increase perinatal elastin gene expression in rat lung fibroblasts and fetal explants.* Am J Physiol, 1997. **273**(2 Pt 1): p. L410-6.
132. Tsoporis, J., et al., *Arterial vasodilation and vascular connective tissue changes in spontaneously hypertensive rats.* J Cardiovasc Pharmacol, 1998. **31**(6): p. 960-2.

133. Habashi, J.P., et al., *Losartan, an AT1 antagonist, prevents aortic aneurysm in a mouse model of Marfan syndrome.* Science, 2006. **312**(5770): p. 117-21.
134. Drummond, G.R., et al., *Combating oxidative stress in vascular disease: NADPH oxidases as therapeutic targets.* Nat Rev Drug Discov, 2011. **10**(6): p. 453-71.
135. Quan, A., *Fetopathy associated with exposure to angiotensin converting enzyme inhibitors and angiotensin receptor antagonists.* Early Hum Dev, 2006. **82**(1): p. 23-8.
136. Alwan, S., J.E. Polifka, and J.M. Friedman, *Angiotensin II receptor antagonist treatment during pregnancy.* Birth Defects Res A Clin Mol Teratol, 2005. **73**(2): p. 123-30.
137. Rohini, A., et al., *Molecular targets and regulators of cardiac hypertrophy.* Pharmacol Res, 2010. **61**(4): p. 269-80.
138. Barry, S.P., S.M. Davidson, and P.A. Townsend, *Molecular regulation of cardiac hypertrophy.* Int J Biochem Cell Biol, 2008. **40**(10): p. 2023-39.
139. Kaspar, J.W., S.K. Niture, and A.K. Jaiswal, *Nrf2:INrf2 (Keap1) signaling in oxidative stress.* Free Radic Biol Med, 2009. **47**(9): p. 1304-9.
140. Kilimnik, G., et al., *Altered islet composition and disproportionate loss of large islets in patients with type 2 diabetes.* PLoS One, 2011. **6**(11): p. e27445.
141. Deng, S., et al., *Structural and functional abnormalities in the islets isolated from type 2 diabetic subjects.* Diabetes, 2004. **53**(3): p. 624-32.
142. Lucena, J., et al., *Essential role of the N-terminal region of TFII-I in viability and behavior.* BMC Med Genet, 2010. **11**(1): p. 61.
143. Hocking, D.R., J.L. Bradshaw, and N.J. Rinehart, *Fronto-parietal and cerebellar contributions to motor dysfunction in Williams syndrome: a review and future directions.* Neurosci Biobehav Rev, 2008. **32**(3): p. 497-507.
144. Sah, P., et al., *The amygdaloid complex: anatomy and physiology.* Physiol Rev, 2003. **83**(3): p. 803-34.
145. Meyer-Lindenberg, A., et al., *Functional, structural, and metabolic abnormalities of the hippocampal formation in Williams syndrome.* J Clin Invest, 2005. **115**(7): p. 1888-95.
146. Zhou, Y., R.A. Gunput, and R.J. Pasterkamp, *Semaphorin signaling: progress made and promises ahead.* Trends Biochem Sci, 2008. **33**(4): p. 161-70.
147. Swiercz, J.M., et al., *Plexin-B1 directly interacts with PDZ-RhoGEF/LARG to regulate RhoA and growth cone morphology.* Neuron, 2002. **35**(1): p. 51-63.
148. Calamandrei, G., et al., *Serum NGF levels in children and adolescents with either Williams syndrome or Down syndrome.* Dev Med Child Neurol, 2000. **42**(11): p. 746-50.
149. Morris, C.A., *The behavioral phenotype of Williams syndrome: A recognizable pattern of neurodevelopment.* Am J Med Genet C Semin Med Genet, 2010. **154C**(4): p. 427-31.

150. Chimge, N.O., et al., *PI3K/Akt-dependent functions of TFII-I transcription factors in mouse embryonic stem cells.* J Cell Biochem, 2012. **113**(4): p. 1122-31.
151. Ku, M., et al., *Positive and negative regulation of the transforming growth factor beta/activin target gene goosecoid by the TFII-I family of transcription factors.* Mol Cell Biol, 2005. **25**(16): p. 7144-57.

LIST OF ACRONYMS

CD: Complete Deletion

CV: Cardiovascular Disease

DCX: Doublecortin

DD: Distal Deletion

DEG: Diferentially Expressed Genes

DNA: Deoxyribonucleic Acid

D/P: Distal and Proximal deletion

ID: Identification number

IQ: Intelligence Quotient

LCR: Low Copy Repeats

MLPA: Multiplex Ligation-dependent Probe Amplification

NAHR: Non Allelic Homologous Recombination

NADPH: Nicotinamide Adenin dinucleotide Phosphate

NOX: NADPH Oxidase

PCR: Polymerase Chain Reaction

PD: Proximal Deletion

qRT-PCR: quantitative RT-PCR

RNA: Ribonucleic Acid

ROS: Reactive Oxygen Species

SHR: Spontaneously Hypertensive Rats

SVAS: Supravalvular Aortic Stenoses

WBS: Williams-Beuren Syndrome

WBSCR: Williams-Beuren Syndrome Critical Region

WINAC: *WSTF* Including Nucleosome Assembly Complex

WT: Wild-Type